A. FLUIDIZED BEDS AND FIXED BEDS

A. FLUIDIZED BEDS AND FIXED BEDS

1. Bubble Assemblage Model for Fluidized Bed Catalytic Reactors

1.1 Introduction

Ever since the fluidized bed technique was first applied to the making of synthesis gas from coal by the Winkler generator and to the catalytic cracking of petroleum, fluidized beds have been used for a number of other chemical processes, particulary in catalytic synthesis.

Some of the fluidized bed catalytic processes are the catalytic reforming of naphthas, the phthalic anhydride production, the catalytic oxidation of ethylene, the production of alkyl chlorides, the synthesis of acetonitrile from acetylene and ammonia, etc. just to mention a few.

However, owing to the complex gas flow and solid particle movement within the fluidized bed, design procedure of catalytic fluidized bed reactors has not been well established in spite of the fact that a number of models for fluidized bed reactors have been suggested.

There have been a number of investigations on the gas flow behavior in a fluidized bed. Injecting a tracer gas into the bed and examining the behavior of the tracer gas by high speed photography, comparing the reactant conversion in both the fluidized bed and the fixed bed under the same operating conditions for well defined catalytic reactions, and observing bubbles rising in the bed have been some of the techniques employed to determine the gas flow behavior.

Based on the results of these observations, Kunii and Levenspiel[22,23] recently proposed a gas flow model which they called the "Bubbling Bed Model" for explanation and prediction of fluidized bed behaviors asserting that only the effective size of bubble is needed to supply adequate description of the flow of gas through the bed.

Although the concept developed certainly contributed considerably to the understanding of fluidized bed behavior, to use an effective bubble diameter to represent an assemblage of bubbles of varying sizes seems to be somewhat an oversimplification.

In this chapter we shall present a new model the "Bubble Assemblage Model" based on multiple bubbles of varying sizes for design and scale-up purposes. The "Bubble Assemblage Model" contains essentially no adjustable parameter and is convenient for computer simulations.

The experimental data available in literature on first order catalytic reaction systems in fluidized beds are used to test the validity of the proposed model. Unless specified,the equations appearing in this paper are all based on C. G. S. units.

1.2 Previous Investigations

An attempt to find the gas flow behavior in a fluidized bed using tracer technique was first made by Gilliland and Mason[9] who measured the concentration variation of a tracer gas injected into a fluidized bed. A model, usually the dispersion model or the two phase model, is presupposed in the analysis and the flow behavior is represented in terms of model parameters such as dispersion coefficient or interchange coefficient between the two phases. Table A-1 summarizes the results of investigation using the tracer technique. Since the parameters determined by this manner are in a sense adjustable, unless the model selected can describe flow behavior reasonably accurately, the information obtained is of little use for scale-up purposes. In addition if the model involves more than two parameters, the analysis could become hopelessly difficult.

TABLE A-1 EXPERIMENTAL INVESTIGATION OF MODEL PARAMETERS

i. TRACER METHOD

Authors	Model	Experimental Condtions	Experimental Results
Gilliland Mason(9)	dispersion model	steady state method gas: air tracer: He particle: F.C.C., glass D_R = 2.5 ~ 11.4 cm.	$E_z \propto u_o \rho_p (1 - \bar{\varepsilon})$ E_z is affected by u_{mf} $E_z = 10^2 \sim 10^3$ [cm^2/sec]
Muchi, et al. (33)	dispersion model	steady state method gas: air tracer: NH_3 particle: sand, glass D_R = 5 ~ 15 cm.	$E_z/\nu = 100\{N_{Rep}/1-\varepsilon\}^{0.94}$ at $15 < N_{Rep}/1 - \varepsilon < 50$ $E_z/\nu = 180\{N_{Rep}/1 - \varepsilon\}^{0.8}$ at $50 < N_{Rep}/1 - \varepsilon < 200$
Winter (44)	dispersion model	residence time curve gas: air tracer: He particle: glass D_R = 2.0 ~ 13.5 cm.	$E_z = C^* d_p^{2.2} \exp(-\omega^* d_p^{1.9}/u)$ where $\omega^* = 3.5 \times 10^5$ $C^* = 3.6 \times 10^7$
Kobayashi et al. (19)	two phase model $D_e = 0$ $u_e = u_{mf}$	residence time curve gas: air tracer: He particle: silica, gel D_R = 8.4 cm.	$F_o = 11/D_B$
De Grout (6)	two phase model $D_e = 0$ $u_e = u_{mf}$	residence time curve gas: air tracer: He particle: silica D_R = 10 ~ 150 cm.	$H_K = 0.67 D_R^{0.25} L^{0.5}$ where L = bed height (m) $H_K = u/F_o$; u[m/sec]
Iwasaki, et al. (14)	contact time distribution	residence time curve gas: air, H_2 tracer: H_2, C_2H_4, C_3H_8 particle: silica-alumina D_R = 5.08 ~ 7.63 cm.	conversion of reactant in fluidized bed is expressed by $x=1- \int_o^\infty E(\emptyset)\exp(-k\emptyset W/F)d\emptyset$ contact time distribution $E(\emptyset)$ is obtained from residence time curve of adsorbed and non-adsorbed tracer gas on solid
Kato, et al. (15)	two phase model $u_e = 0$ $D_e = 0.68\left(\frac{u-u_{mf}}{u_{mf}}\right) D_p \varepsilon_p$	residence time curve gas: air, H_2, N_2 tracer: H_2, C_2H_4, C_3H_5 particle: silica-alumina, glass D_R = 10 cm., D_p = 1 ~ 3 cm.	F_o = 5 ~ 3 1/sec. for u/u_{mf} = 2 ~ 30 M = 0.4 ~ 0.2 1/sec. for u/u_{mf} = 2 ~ 30

Another technique useful for the search of flow behavior in a fluidized bed is to compare the conversion obtained in a fluidized bed reactor with that obtainable in a fixed bed reactor under the same operating conditions. This technique initiated by Shen and Johnstone[37] also needs a presupposed model for evaluation of model parameters. Experimental data are used to compute either the interchange coefficient between the two phases or the fraction of catalyst present in the bubble phase. The results of studies using this technique are summarized in Table A-2.

Although the parameters obtained by this technique may satisfactorily represent the individual experimental results, it is doubtful that these parameters have any physical significance under other operating conditions for fluidized beds of complex flow patterns.

So far most of the experimental data on kinetic study in fluidized beds were fitted on the two phase model. A general expression of the two phase model can be given as

$$F \frac{\partial C_b}{\partial t} - F D_b \frac{\partial^2 C_b}{\partial h^2} + F u \frac{\partial C_b}{\partial h} + F_0 (C_b - C_e) + F_s \gamma = 0 \qquad (1)$$

$$f \frac{\partial C_e}{\partial t} - f D_e \frac{\partial^2 C_e}{\partial h^2} + f u_e \frac{\partial C_e}{\partial h} + F_0 (C_e - C_b) + f_s \gamma = 0 \qquad (2)$$

Most of the investigators used a simplified form of the two phase model by either assuming or estimating some of the terms in Equations (1) and/or (2). In Table A-3the results of the theoretical development of the two phase model are summarized.

As has been observed, numerous studies have tried to explain the flow pattern of gas in fluidized beds, the main difficulty seems to

TABLE A-2 EXPERIMENTAL INVESTIGATION OF MODEL PARAMETERS

ii. REACTION METHOD

Authors	Parameter Assumed	Experimental Conditions	Parameter and Experimental Results
Shen Johnstone (37)	$a = 0$ $u_e = u_{mf}$ $D_e = 0$ or ∞	decomposition of nitrous oxide D_R = 11.4 cm., L_{mf}=26 32 cm. d_P = 60 ~ 200 mesh	parameter: F_o k = 0.06 ~ 0.85 (1/sec)
Massimila Johnstone (29)	$a = 0$ $u_e = u_{mf}$ $D_e = 0$	oxidation of NH_3 D_R = 11.4, L_{mf} = 26 ~ 54 cm. d_P = 100 ~ 325 mesh	parameter: F_o k = 0.071 (1/sec)
Mathis Watson(30)	$D_e = 0$ $u_e = u_{mf}$	decomposition of cumene D_R = 5 ~ 10.2 cm.,L_{mf}=10~31 cm. d_P = 100 ~ 200 mesh	parameter: F_o, a k = 0.64 (1/sec)
Lewis,et al. (34)	$u_e = 0$ $D_e = 0$ or ∞	hydrogenation of ethylene D_R = 5.2 cm., L_{mf} = 11 ~ 53 cm. d_P = 0.001 ~ 0.003 cm.	parameter: F_o, a k = 1.1 ~ 15.6 (1/sec) a = 0.05 ~ 0.18,F=0.4~0.8
Orcutt, et al.(34)	$a = 0$ $u_e = 0$	decomposition of ozone D_R = 10 ~ 15 cm.,L_{mf} = 30~60 cm. d_P = 0.001 ~ 0.003 cm.	k = 0.1 ~ 3.0 (1/sec)
Gomezplata Shuster (10)	$a = 0$ $u_e = u_{mf}$ $D_e = 0$	decomposition of cumene D_R = 7.6 L_{mf} = 3.8 ~ 20 cm. d_P = 100 ~ 200 mesh	parameter: F_o, a k = 0.75 (1/sec)
Kobayashi, et al.(20)	$u_e = u_{mf}$ $D_e = 0$	decomposition of ozone D_R = 8.3 cm.,L_{mf} = 10 ~ 100 cm. d_P = 60 ~ 80 mesh	parameter: a k = 0.1 ~ 0.8 1/sec a = 15 (L/L_{mf} - 1)
Kobayashi, et al. (21)	$u_e = u_{mf}$ $D_e = 0$	decomposition of ozone D_R = 20 cm.,L_{mf} = 10 ~ 100 cm. d_P = 60 ~ 80 mesh	parameter: a k = 0.2 ~ 3.5 (1/sec) a = 0.1 ~ 0.3 (--)
Ishii Osberg (13)	dispersion model	packed fluidized bed isomerization of cyclo-propane, D_R = 4.2 ~ 12 cm., L_{mf}=15 ~ 50 cm. d_P = 100 ~ 200 mesh,D_P=1 ~ 2.5 cm.	k = 0.5 ~ 2.1 (1/sec)
Kato(16)	$u_e = u_{mf}$ $D_e = 0$	packed fluidized bed hydrogenation of ethylene D_R = 8.7 cm.,L_{mf} = 10 ~ 30 cm. d_P = 100 ~ 200 mesh,D_P= 1 ~ 3 cm.	parameter: a k = 1.1 ~3.3 (1/sec) a = 0.35 ~ 0.45

TABLE A-3 THEORETICAL STUDY OF THE TWO-PHASE MODEL

Authors	Parameter Assumed	Method	a or F_o	Remarks
Van Deemter (41)	$a = 0$ $u_e = 0$ $D_e = D_s$	a steady-state analysis of gas backmixing and residence time curve and first order reaction by two phase model	$H_k = \frac{F_o L}{u}$ $H_k = 0.5 \sim 2.5 \quad a = 0$	parameter, F_o, is not related to the bubble movement in the bed
Muchi (32)	$u_e = u_{mf}$ $0<D_e<\infty$	a study of effect of F_o, a, D_e, u_e on conversion of a first order reaction		no relation between bubble movement and parameters
Mamuro, Muchi (28)	$u_e = u_{mf}$ $a = 0$	analysis of a first order reaction based on the two-phase cell model	$\frac{F_o}{\phi} = 0.05$ ϕ = shape factor of bubble	
Van Deemter (42)	$D_e = 0$	analysis of back mixing, residence time curve of tracer gas and the first order reactions	$F_o = 0.4 \sim 1.2$ (1/sec)	parameter a, F_o, u_e are not related to the bubble growth in the bed
Kunii, Levenspiel (22)	$u_e = 0$	analysis of various phenomena in fluidized beds by the "bubbling bed model"	$\frac{1}{F_o} = \frac{1}{F_{bc}} + \frac{1}{F_{ce}}$ $F_{bc} = 45(\frac{u_{mf}}{D_B}) + 5.85(\frac{D^{1/2} g^{1/4}}{D_B^{5/4}})$ $F_{ce} = 6.78(\frac{\varepsilon_{mf} D u_b}{D_B})^{1/2}$	parameter: D_B model is characterized by a single effective size of the bubble
Davidson, Harrison (5)	$D_e = 0$ or ∞ $a = 0$	estimation of conversions for a first order reaction	$F_o = \frac{5.85 D^{1/2} g^{1/4}}{D_B^{5/4}} + \frac{4.5 u_{mf}}{D_B}$	parameter: D_B model does not account for bubble growth in the bed
Kobayashi Arai (17)	$u_e = 0$ $D_e = 0$	a study of the effect of k, a, D_e and F_o on conversion of a first order reaction		parameters a, F_o, D_e are not related to the bubble movement

revolve about obtaining a satisfactory flow model which will fit the observed conversion in fluidized beds under a wide range of conditions. Thus a new flow model taking into account the presence of an assemblage of bubbles seems to be needed.

1.3 Bubble Assemblage Model

In developing a model for the flow of gas through a fluidized bed based on an assemblage of bubbles, following simplifying assumptions are made.

(a) A fluidized bed may be represented by "n" numbers of compartments in series. The height of each compartment is equal to the size of each bubble at the corresponding bed height. This assumption not only makes it possible for the introduction of bubbles of multiple sizes into the flow model but also makes it convenient for computer calculations.

(b) Each compartment is considered to consist of the bubble phase and the emulsion phase. The gas flowing through the bubble phase and the emulsion phase is considered to be completely mixed within each phase.

(c) The void space within the emulsion phase is considered to be equal to that of the bed at incipient fluidizing conditions. The upward velocity of the gas in the emulsion phase is at u_e.

(d) The bubble phase is assuemd to consist of spherical bubbles surrounded by spherical clouds. The diameter of the bubbles and that of cloud are given by Davidson[4] as

$$\left(\frac{R_c}{R_b}\right)^3 = \frac{u_b + 2\, u_{mf}/\varepsilon_{mf}}{u_b - u_{mf}/\varepsilon_{mf}} \qquad (3)$$

$$\text{for } u_b \geq u_{mf}/\varepsilon_{mf}$$

Under normal operating conditions, u_b is much larger than u_{mf}/ε_{mf}. In this region cloud formation around the bubble can be observed. However, when large particles are used for fluidization, u_{mf} is correspondingly large and therefore, the bubble velocity can become smaller than u_{mf}/ε_{mf}. The calculation presented here based on the proposed model would not be applicable to this range of operation. The voidage within the cloud is assumed to be the same as that in the emulsion phase.

(e) The total volume of the gas bubbles within the bed may be expressed as $(L - L_{mf})\ S$.

(f) Gas interchange takes place between the two phases. Overall interchange coefficient per unit volume of gas bubbles is given by

$$F_d = F_o + K'M \qquad (4)$$

(g) The bubbles are considered to grow continuously while passing through the bed until they reach the maximum stable size or reach the diameter of the bed column. Harrison, et al.(11) showed that the maximum stable bubble diameter is attained when the upward flowing velocity becomes the terminal velocity of particles. The maximum stable bubble diameter, D_T, can be found from

$$D_T = \left(\frac{u_T}{0.71}\right)^2 \frac{1}{g} \tag{5}$$

(h) Since the effective thermal diffusivity and the heat transfer coefficient (43) in a fluidized bed have been shown to be very large, the bed is assumed to be operating under isothermal conditions. The majority of experimental data reported are also obtained under isothermal conditions.

Bubble Size

The studies on bubble growth are numerous, among them the works of Yasui and Johanson[45], Toei, et al.[39], Hiraki, et al.[12], Kobayashi,et al.[18] and Baugarten and Pigford[2] are noteworthy. Their experimental data are plotted in Fig·A-1 following Kobayashi, et al.[18], in terms of $D_B/\rho_P d_P(u/u_{mf})$ and the bed height, h. In this figure, some additional data were incorporated into the original plot of Kobayshi, et al.[18]. Although some scattering of the data is seen, the bubble diameter and the distance from the distributor can be approximately related by the correlation equation of Kobayashi et al.[18] as

$$D_B = 1.4\ \rho_P d_P \left(\frac{u}{u_{mf}}\right) h \tag{6}$$

Examination of Fig. A-1 reveals that the bubble diameter is not necessarily proportional to the first power of the bed height. In fact several sets of the data indicate the power on the bed height to be somewhat smaller than unity. However, before more accurate measurement of bubble diameter with respect to bed height becomes possible, there is at present no justification of using more sophisticated correlation beyond that of Kobayashi, et al.[18].

Strictly speaking, the bubble diameter also should vary slightly with the bed diameter, D_R under the same fluidization conditions. There is an experimental evidence indicating that the bubble diameters are slightly

smaller when the bed diameter becomes larger. However, the relationship between the bubble velocity and the bubble diameter is also affected by the change in bed diameter. In other words, for a larger bed, the velocity of the bubble having the same diameter will become slightly larger due to the reduced friction along the wall of the bed. Just how great the wall effect on the bubble velocity is not very clear at present. Hence, until additional research is made to provide more refined relationship between the bubble velocity and the bed diameter, Equations (6) and (8) are believed to be most reliable today.

The above correlation is based on the data obtained using porous plates as the distributor. For perforated plates the size of bubbles at the surface of the distributor are substantial and therefore must be taken into consideration.

According to Cooke, et al.[3] the bubble size at the surface of a perforated plate having n_o number of holes, can be calculated from $(6G/\pi)^{0.4}/g^{0.2}$ based on the work of Davidson and Harrison[5] where $G = (u - u_{mf})/n_o$. Therefore, in general, the diameter of bubbles in a fluidized bed can be approximated by

$$D_B = 1.4\ \rho_P d_P\ (\frac{u}{u_{mf}})\ h + D_o \qquad (7)$$

where $D_o = (\frac{6G}{\pi})^{0.4}/g^{0.2}$

The validity of Equation (7) is tested using the experimental data of Cooke, et al.[3] and is shown in Table A-4.

Equation (7) can be used to compute local average bubble diameter along the axis of the fluidized bed.

Voidage Distribution and Bubble Velocity

In developing the gas flow model, it is necessary to know the voidage distribution within the fluidized bed. The study of Bakker[1] and that of Fan, et al.[8] indicate the voidage up to the bed height corresponding

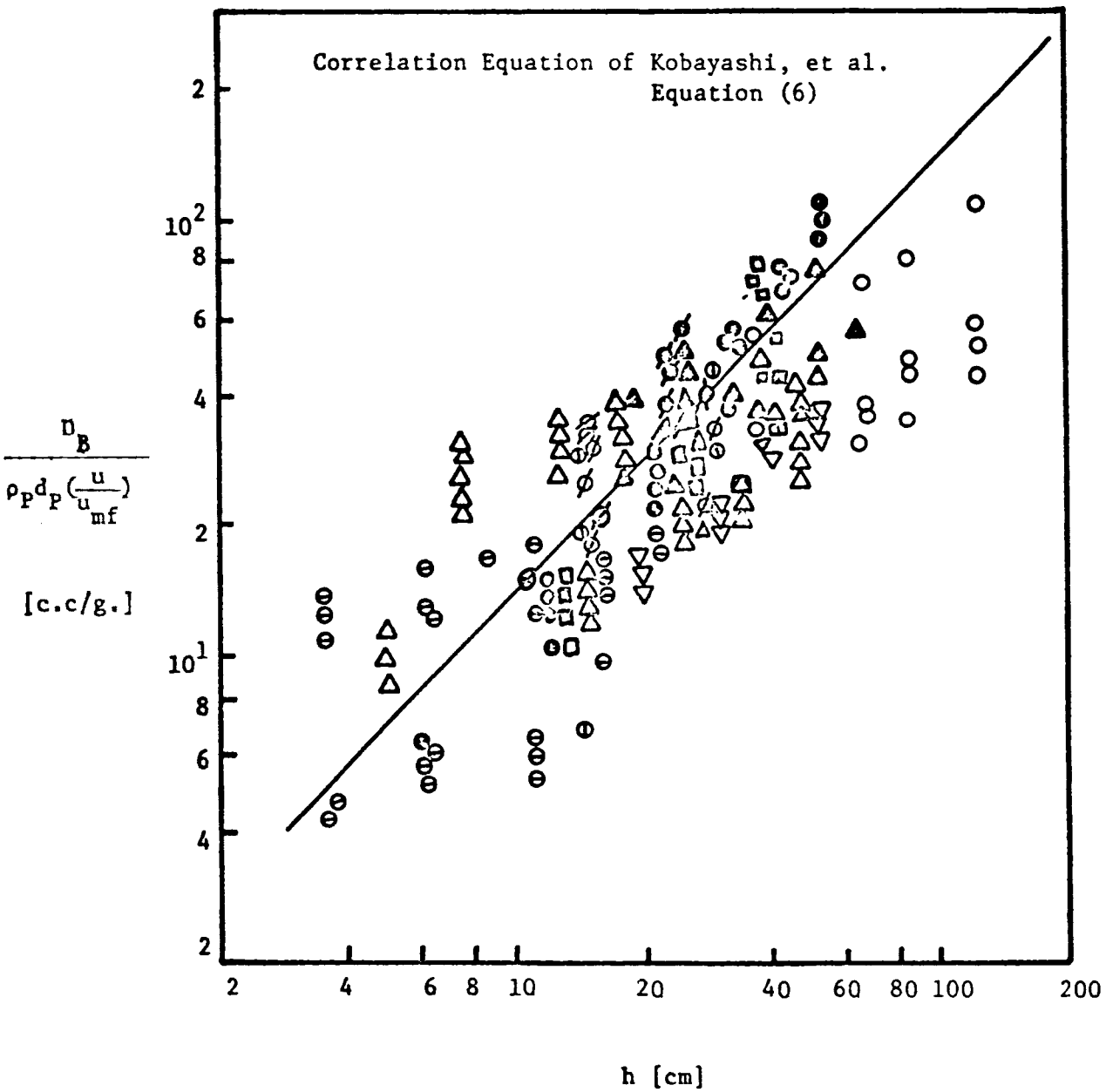

FIGURE A-1 CORRELATION OF BUBBLE DIAMETER ALONG THE BED AXIS FOR CROWD OF BUBBLES

KEY TO FIGURE A-1

		Material	d_p [cm]
O	Hiraki, et al.[12]	F.C.C. catalyst	0.015
●	Kobayashi, et al.[18]	silica gel	0.0194
△	Toei, et al.[39]	glass	0.0137
▲	Yasui and Johnson [45]	glass	0.0041 ~ 0.0267
⊘		olivine	0.0042 ~ 0.015
□		coal	0.0692
▣		magetite	0.0072
▥		V.O.P. catalyst	0.0078
▽	Tanaka [38]	silica gel	0.0213
⊖	Winter[44]	glass	0.011 ~ 0.025
◐	Baugarten and Pigford [2]	glass	0.0074
⌀	Romero[35]	glass	0.0071

TABLE A-4 COMPARISON OF EXPERIMENTAL BUBBLE DIAMETER WITH CALCULATED VALUES USING EQ.(7)

condition	u (cm/sec)	u/u_{mf}	h(cm)	$D_{B\ obs.}$* (cm)	$D_{B\ cal.}$ (cm)
u_{mf} = 5 cm/sec.	36	72	20	15	16.2
	36	72	40	24	27.4
	24	4.8	20	12.5	11.5
ρ_P = 1.4 g/cc	24	4.8	40	21.0	19.3
perforated plate	18	3.6	20	9.8	9.1
$n_o = 0.1/cm^2$	18	3.6	40	16.0	14.8
	18	3.6	60	22	20.4
D_R = 30 cm x 1.2 cm	18	3.6	80	27	26.0

*Based on data from Cooke, et al.[3].

to L_{mf} can be considered approximately uniform and that the voidage above L_{mf} increases along the bed height. For an approximation, it is assumed that above the bed height corresponding to L_{mf}, $(1 - \varepsilon)$ decreases linearly with respect to the bed height. It is further assumed that the average bed height reported in the experiments can be considered as an arithmatic average of the maximum bed height corresponding to $\varepsilon = 1$ and L_{mf}.

Following Davidson and Harrison[5], the velocity of rise of a crowd of bubbles through a fluidized bed can be calculated by

$$u_b = u_o - u_{mf} + 0.711\ (g\ D_B)^{1/2} \tag{8}$$

Now, if the characteristic bubble diameter is taken as that corresponding to the bubble situated at $L_{mf}/2$, from Equations (7) and (8) and assumption 5, the bed expansion ratio can be expressed as

$$(L - L_{mf}) / L_{mf} = (u - u_{mf}) / \{\ 0.711\ (g\ \overline{D}_B)^{1/2}\ \} \tag{9}$$

where $\overline{D}_B$ is an average bubble diameter of the bed given by

$$\overline{D}_B = 1.4 \rho_P d_P \left(\frac{u}{u_{mf}}\right) \frac{L_{mf}}{2} + D_o$$

In Figure A-2 the bed expansions calculated from Equation (9) are compared with the experimental data of Leva, et al.[25], Lewis, et al.[27], and Tanaka[38]. As seen from the figure, the ratios of calculated bed height to experimental bed height are within $\pm$ 10% of 1.0 indicating a favorable agreement. Thus, in model development, Equation (9) may be used to compute the bed height with reasonable accuracy. Once the bed expansion ratio is known, the voidage from the distributor up to a height corresponding to L_{mf} and that from L_{mf} to the top of the bed can be computed, respectively, as

		Material	d_p, [cm]	D_R [cm]
O	Leva, et al.[25]	round sand	0.0063~0.0381	6.35
◐		round and sharp sand	0.00775	6.35 ~ 10.15
△		Fisher-Tropsch.Cat.	0.00705 ~ 0.0385	10.15
◎	Lewis,et al.[27]	glass-beads	0.0102 ~ 0.056	6.35 ~ 11.4
□	Tanaka[38]	silica gel	0.021	20.0

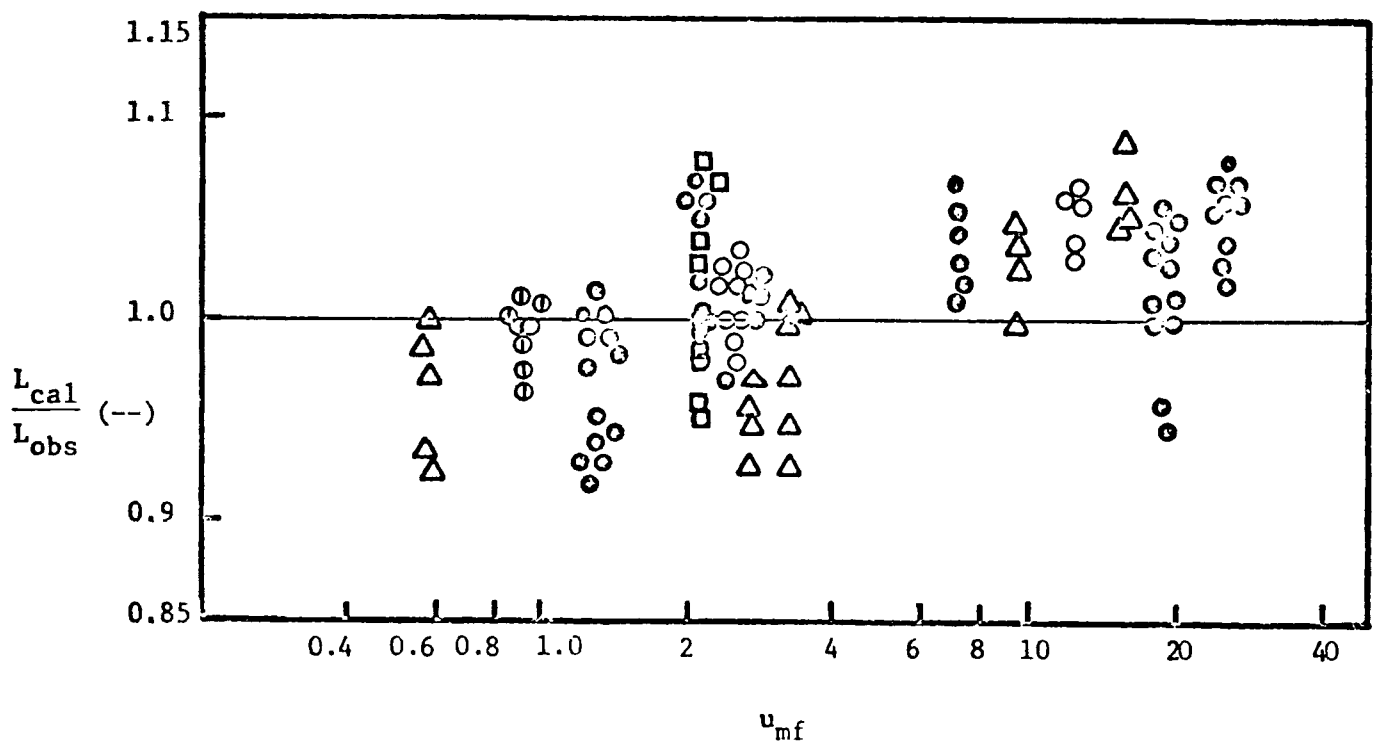

FIGURE A-2 COMPARISON OF EXPERIMENTAL BED EXPANSION WITH CALCULATED BED EXPANSION

$$1 - \varepsilon = \frac{L_{mf}}{L}(1 - \varepsilon_{mf}) \qquad \text{for } h \leq L_{mf} \tag{11}$$

and

$$1 - \varepsilon = \frac{L_{mf}}{L}(1 - \varepsilon_{mf}) - \frac{L_{mf}(1 - \varepsilon_{mf})(h - L_{mf})}{2L(L - L_{mf})} \tag{12}$$

$$\text{for } L_{mf} \leq h \leq L_{mf} + 2(L - L_{mf})$$

Gas Velocity in Emulsion Phase

Since the knowledge of the upward velocity of the gas flowing in the emulsion phase, u_e, is still a controversial subject, we shall assume that for large u/u_{mf}, u_e is negligibly small. This is a reasonable assumption in view of the fact that the experimental findings of May[31] and Kunii and Levenspiel[22] indicate the emulsion gas may reverse its direction in vigorously bubbling beds. According to Kunii and Levenspiel[22], the velocity of gas flowing in the emulsion phase in the axial direction can be expressed as

$$\frac{u_e}{u_{mf}} = 1 - \frac{\varepsilon_{mf}\,\alpha\left(\frac{L - L_{mf}}{L}\right) u_b}{u_{mf}\left\{\left(1 - \left(\frac{L - L_{mf}}{L}\right)\right) - \alpha\left(\frac{L - L_{mf}}{L}\right)\right\}} \tag{13}$$

where α is the ratio of the volume of emulsion transported upward behind a bubble (i.e. volume of wake) to the volume of a bubble. The value of α is approximately 0.2 ~ 0.3 according to the experimental study of Rowe and Partridge[36]. Therefore, under normal experimental conditions, Equation (13) yields $u_e/u_{mf} = 0.5$ for $u/u_{mf} = 3$, and $u_e/u_{mf} = 0$ for $u/u_{mf} = 5 \sim 6$. Latham, et al.[24] also studied using a tracer gas to locate the velocity at which the emulsion gas will reverse its direction ($u_e = 0$) and found that $u_e = 0$ when $u/u_{mf} = 2.7 \sim 6.0$. Based on the above experimental findings and the argument presented by Levenspiel and Kunii[23], it would be reasonable to assume $u_e = 0$ under most of the normal operating conditions.

Interchange Coefficient

The gas interchange between the bubble phase and emulsion phase involves direct interchange of gas in bubbles and in emulsion, and indirect interchange due to adsorbed gas on the surface of interchanging particles. Since no experimental data are available for the particle interchange rate, M, and adsorption equilibrium constant, K', for the reacting gas on particle surfaces, the analysis presented here will neglect gas interchange due to adsorbed gas on interchanging particles. Therefore, Equation (4) is reduced to $F_d = F_o$, As to the direct gas interchange, semi-theoretical studies by Zenz[46], Davidson and Harrison[5] and Kunii and Levenspiel[22] as well as an analysis based on the stimulus-response curve from tracer data using the two phase model by Kobayashi, et al.[19] are available. Most of these studies agree on one point that the interchange coefficient, F_o, is approximately inversely proportional to the bubble diameter. Therefore, the following equation based on the experimental work of Kobayashi, et al.[19] will be used:

$$F_o = 11/D_B \tag{14}$$

In a recent study, Toei, et al.[40] injected a single CO_2 bubble into a fluidized bed and measured the variation of CO_2 concentration within the bubble. They calculated the gas interchange coefficient based on these measurements and found that F_o, which is somewhat affected by the particle diameter, can be approximated by $3/D_B \sim 6/D_B$. Since their study pertains to a single bubble, the effects of bubble collisions and coalesence are not taken into consideration. It is therefore not unreasonable to assume that in a vigorously fluidizing bed, the interchange coefficient is more closely represented by Equation (14).

1.4 Calculation Procedure Based on Bubble Assemblage Model

Let the height of n-th compartment be Δh_n, where n = 1, 2, 3, ... Based on an arithmatic average of bubble size, the height of initial compartment immediately above the distributor becomes

$$\Delta h_1 = \frac{D_o + (m\Delta h_1 + D_o)}{2} \quad \text{or} \quad \Delta h_1 = \frac{D_o}{(1 - \frac{m}{2})}$$

where $m = 1.4\ \rho_p d_p\ (\frac{u}{u_{mf}})$, a proportionality constant relating the bubble diameter for a given operating condition. The height of the second compartment then becomes

$$\Delta h_2 = 2D_o \frac{(2+m)}{(2-m)^2}$$

and that of n-th compartment becomes,

$$\Delta h_n = 2D_o \frac{(2+m)^{n-1}}{(2-m)^n} \tag{15}$$

The number of bubbles in the n-th compartment becomes

$$N = \frac{6S(L - L_{mf})}{\pi\ L(\Delta h_n)^2} \tag{16}$$

The volume of cloud in the n-th compartment can be computed from Equation (3) as,

$$V_{cn} = \frac{N\pi(\Delta h_n)^3}{6} \left(\frac{3u_{mf}/\varepsilon_{mf}}{u_b - u_{mf}/\varepsilon_{mf}}\right) \tag{17}$$

where

$$u_b = 0.711\ (g\Delta h_n)^{1/2}$$

The total volume of the bubble phase and that of the emulsion phase in the n-th compartment are, respectively,

$$V_{bn} = \frac{N\pi(\Delta h_n)^3}{6} \left(\frac{u_b + 2u_{mf}/\varepsilon_{mf}}{u_b - u_{mf}/\varepsilon_{mf}}\right) \tag{18}$$

$$V_{en} = S\Delta h_n - V_{bn} \tag{19}$$

The distance from the distributor to the n-th compartment is

$$h_n = \sum_{i=1}^{n} \Delta h_i \tag{20}$$

The gas interchange coefficient based on unit volume of bubbles from Equation (3) can be shown as

$$F'_{on} = F_{on} \frac{(u_b - u_{mf}/\varepsilon_{mf})}{(u_b + 2u_{mf}/\varepsilon_{mf})} \tag{21}$$

Hence, the material balance for the gaseous reactant around the n-th compartment becomes,

for the bubble phase,

$$(SuC_b)_{n-1} = \{F'_{on} V_b (C_b - C_e)\}_n + (r_b V_c)_n + (SuC_b)_n \tag{22}$$

and for the emulsion phase,

$$\{F'_{on} V_b (C_b - C_e)\}_n = (r_e V_e)_n \tag{23}$$

Where r_b and r_e are the reaction rates per unit volume for the bubble phase and emulsion phase respectively. For example, if the rate of reaction is a first order with respect to reactant gas, they become; $r_b = kC_b$ and $r_e = kC_e$.

The computational procedure for conversion and concentration profile in a fluidized reactor is given below when the operating conditions such as, particle size, d_p, particle density, ρ_p, minimum fluidization velocity, u_{mf}, gas velocity, u, distributor arrangement, column diameter, D_R, incipient bed height, L_{mf}, the reaction rate constant, k, and order of reaction are known. Note that this model requires no adjustable parameter.

First, Equations (8) and (9) are used to calculate the expanded bed height, L. Next, Equation (15) is used to compute the size of the n-th compartment. Using Equations (17), (18), and (19), the volumes of cloud, that of the bubble phase, and the emulsion phase for the n-th compartment are then calculated. C_{bn} and C_{en} are computed from $(C_b)_{n-1}$ and $(C_e)_{n-1}$ using Equations (22) and (23). The calculations are repeated from the distributor until the bed height equivalent to L_{mf} is reached. For bed height above L_{mf}, the voidage is adjusted by Equation (12) and V_{en}, V_{bn}, and V_{en} are obtained using the same procedure as that shown for the height smaller than L_{mf}. The calculation is repeated until the bed height reaches $L_{mf} + 2(L - L_{mf})$. A computer logic diagram based on this procedure is shown in Table A-5.

1.5 Results of Calculations

Since most of the experimental data were obtained using porous plates, the bubble size at the surface is very difficult to estimate. Therefore, the height of initial compartment, Δh_1, is assumed. It becomes necessary to test the effect of size of Δh_1 on the conversion in order to show the soundness of this assumption. For a comparatively small fluidized bed reactor, say column diameter of 5 cm. ~ 20 cm. and bed height of less than 100 cm., we should expect the sizes of bubbles forming on the surface of a porous plate to be quite small. It is therefore logical to assume that the height of the first compartment would be no more than a few centimeters. In Figure A-3 the effect of Δh_1 on conversion is examined for cases where reaction rate is comparatively fast (i.e. for large k). It is quite obvious that for slow reactions, the size of compartment is of little significance on overall conversion and is therefore not examined. As can

TABLE A-5 LOGIC DIAGRAM FOR COMPUTER SIMULATION

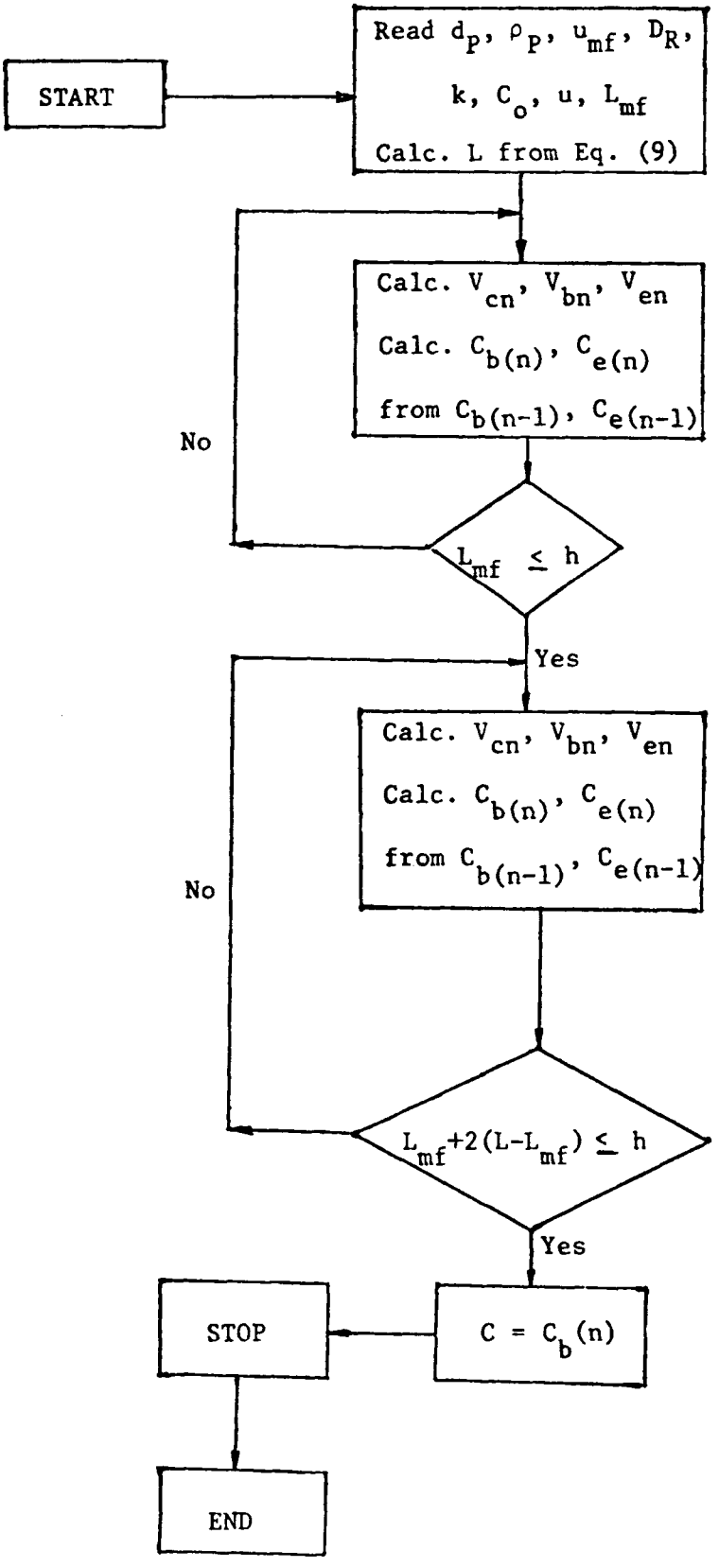

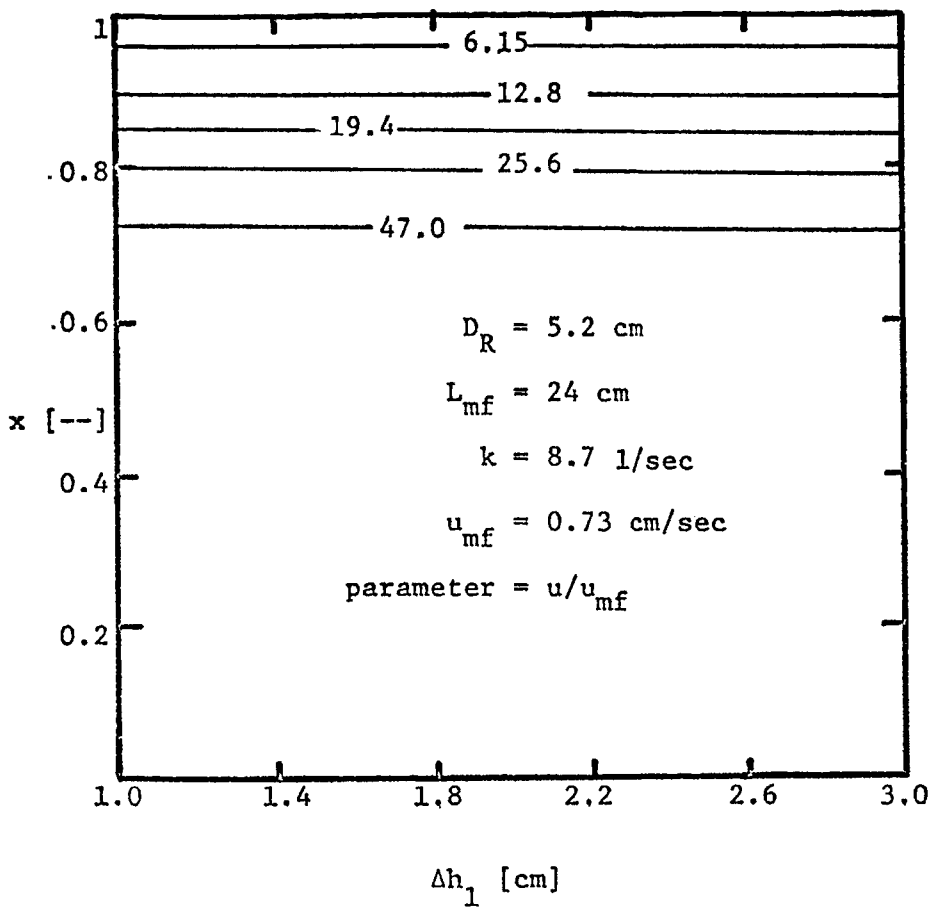

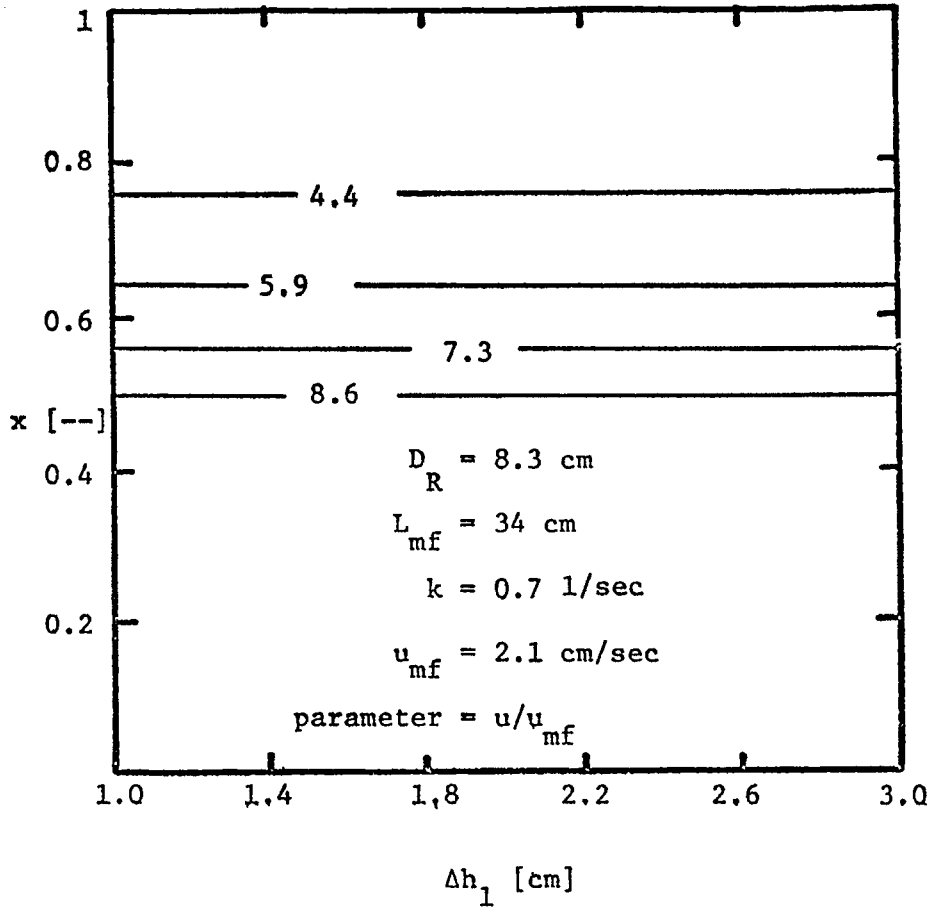

FIGURE A-3 EFFECT OF Δh_1 ON THE CONVERSION

be seen from the figure, the initial height of the compartment, Δh_1, does not affect greatly on overall conversion even for fast reactions. In actual calculation therefore, Δh_1 = 1.0 cm. is used.

For a large fluidized bed reactor which has a perforated plate distributor, Equation (15) together with information on the number and the size of holes must be used to calculate the height of initial compartment.

In order to demonstrate the validity of the proposed model, conversions in fluidized beds based on the kinetic information given in Table 2 are calculated. The results of calculation are then compared with actual experimental conversions. In Figs.A-4,5,and 6 the extent of conversion along the bed height are shown for three sets of data; those of Lewis, et al.[26] for comparatively large reactions rates, those of Kobayashi and Arai [20] for intermediate reaction rates and those of Massimilla and Johnstone[29] for small reaction rates, respectively.

As can be seen from these figures, when the rate of reaction is small, the concentration of gas in the emulsion phase is not too much different from that in the bubble phase. However, when the rate of reaction is large, the difference in concentrations between the two phases become very significant. For a fast reaction, a great deal of gaseous reactant in the emulsion phase is seen to be converted in the immediate vicinity of the distributor. These observations imply that for fast reactions the gas interchange between the two phases is of primary importance whereas for slow reactions the gas interchange between the two phases does not affect significantly on the conversion.

To examine the gas velocity effect, a comparison of the conversion predicted by the model and that from actual experiments is shown in Figure A-7. In Figure A-8 the calculated conversion is compared with the experimental

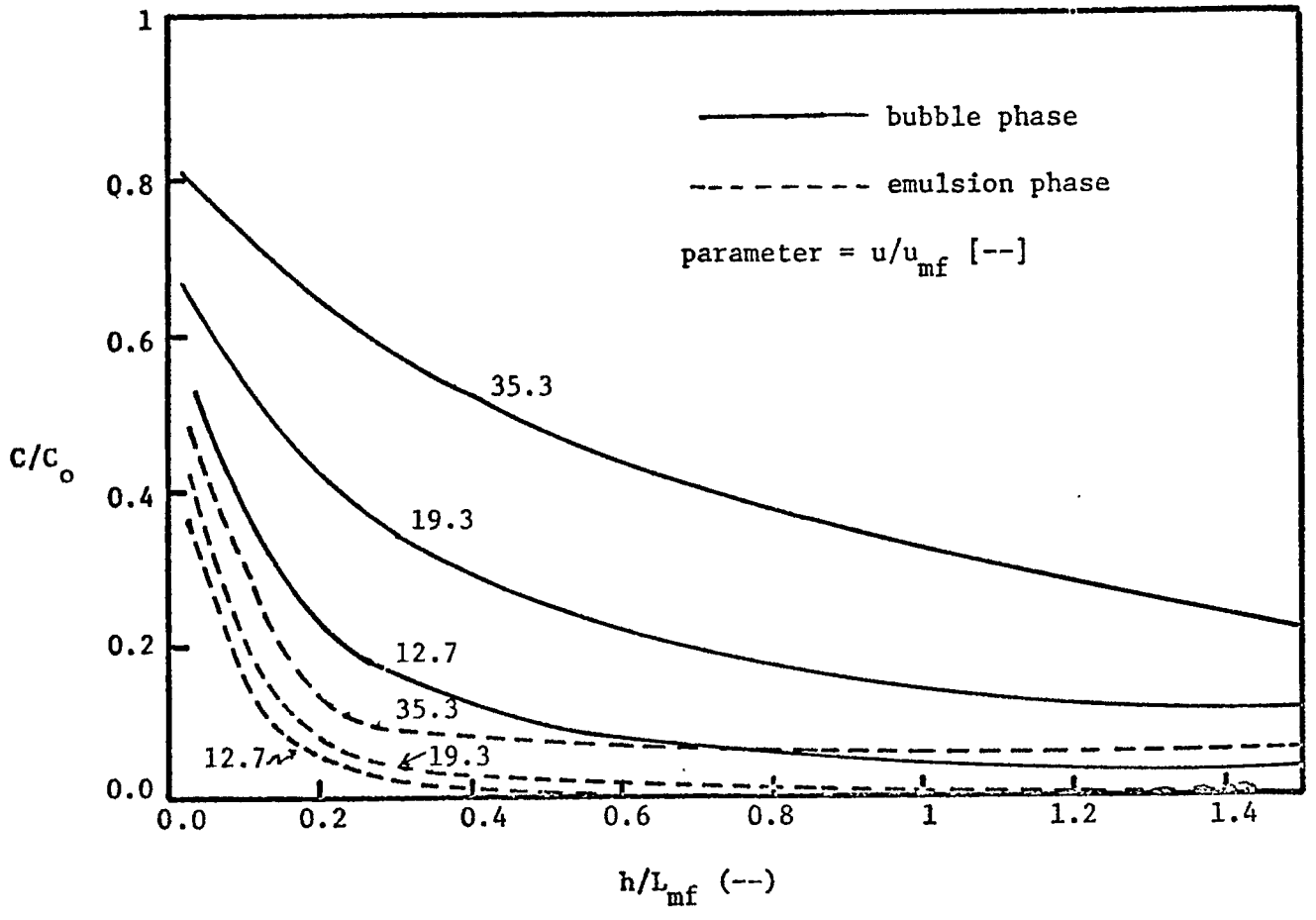

FIGURE A-4 RELATION BETWEEN THE CONCENTRATION PROFILE AND BED HEIGHT WHEN THE REACTION RATE CONSTANT IS LARGE

Lewis, et al.[26] (D_R = 5.2 cm, L_{mf} = 24.2 cm, k = 8.7 sec^{-1})

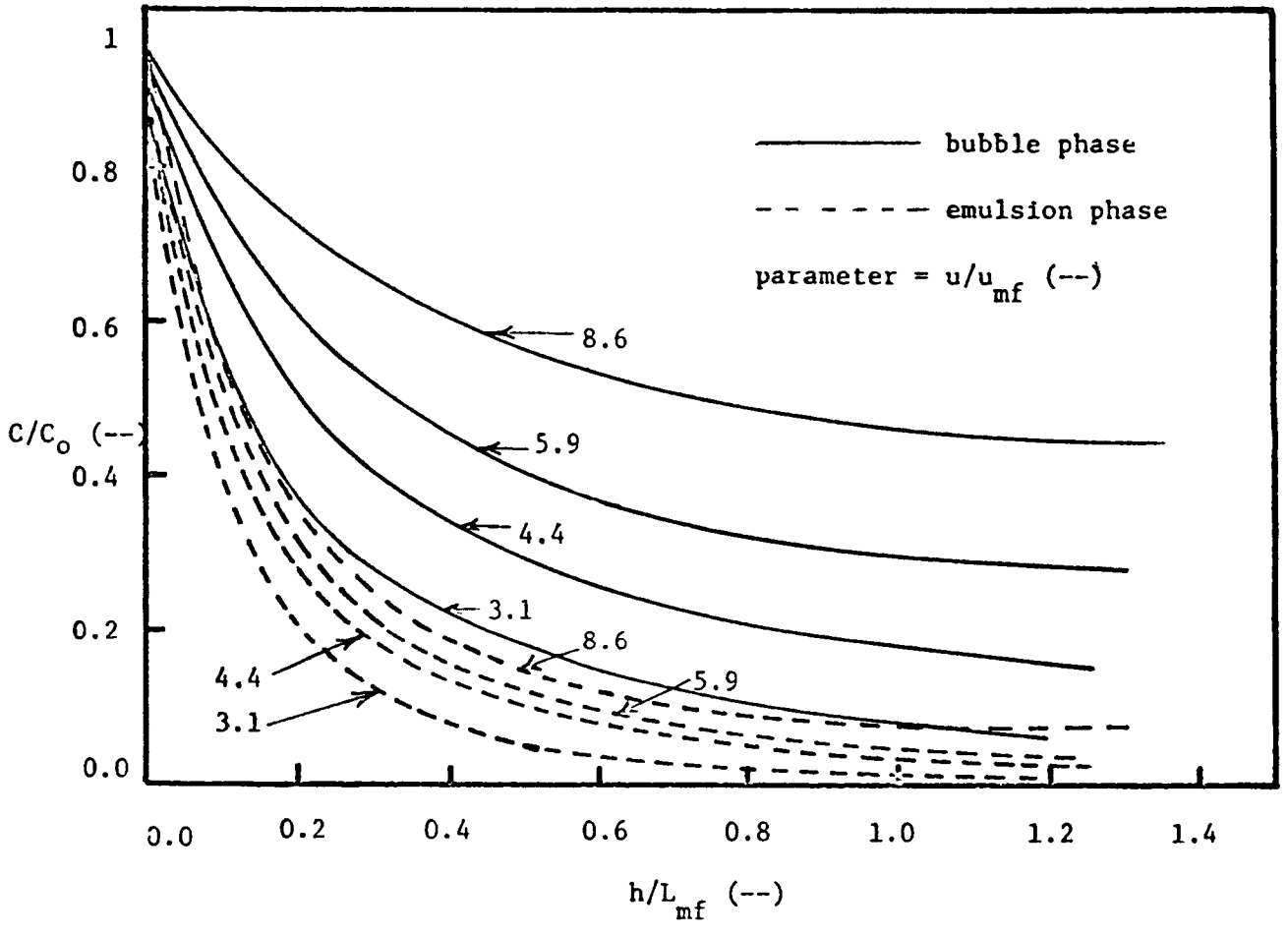

FIGURE A-5 RELATION BETWEEN THE CONCENTRATION PROFILE AND BED HEIGHT FOR AN INTERMEDIATE RATE CONSTANT

Kobayashi, et al.[21] (D_R = 20 cm, L_{mf} = 67 cm, k = 0.7 sec^{-1})

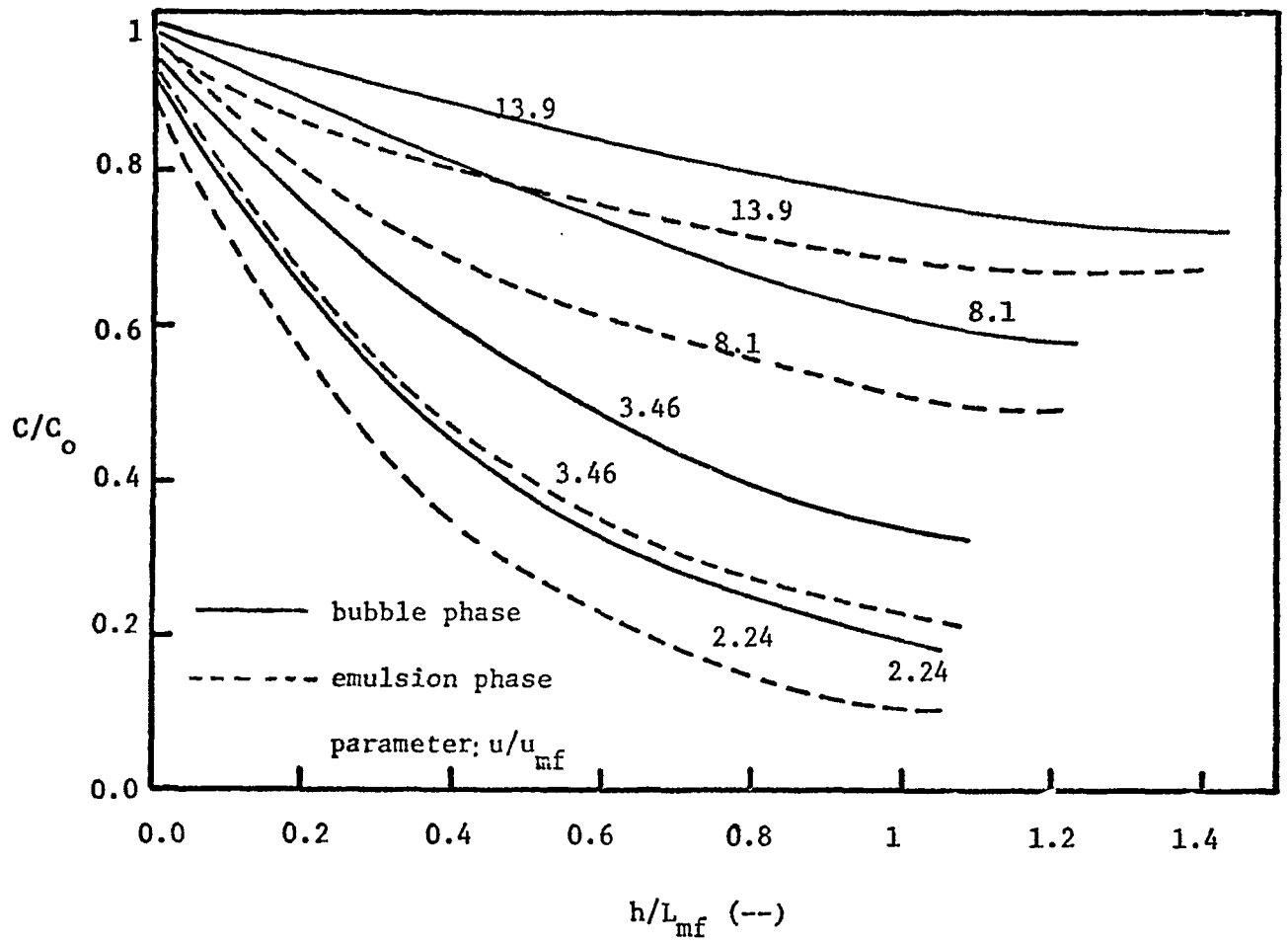

FIGURE A-6 RELATION BETWEEN THE CONCENTRATION PROFILE AND BED HEIGHT WHEN THE REACTION RATE CONSTANT IS SMALL

Massimilla, et al.[29] (D_R = 11.4 cm, L_{mf} = 54.3 cm, k = 0.0707 1/sec)

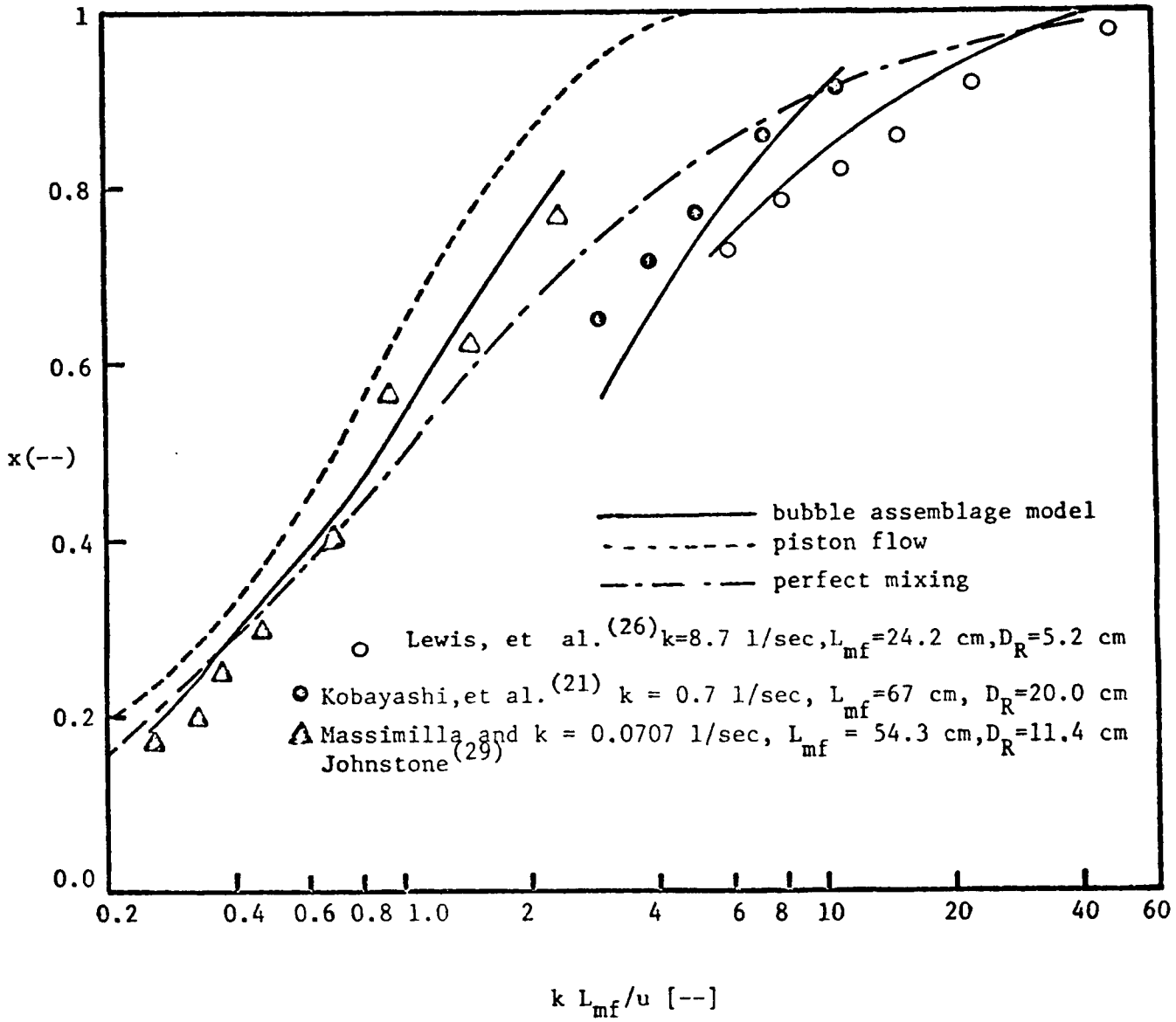

FIGURE A-7 COMPARISON OF EXPERIMENTAL CONVERSION WITH CALCULATED RESULTS

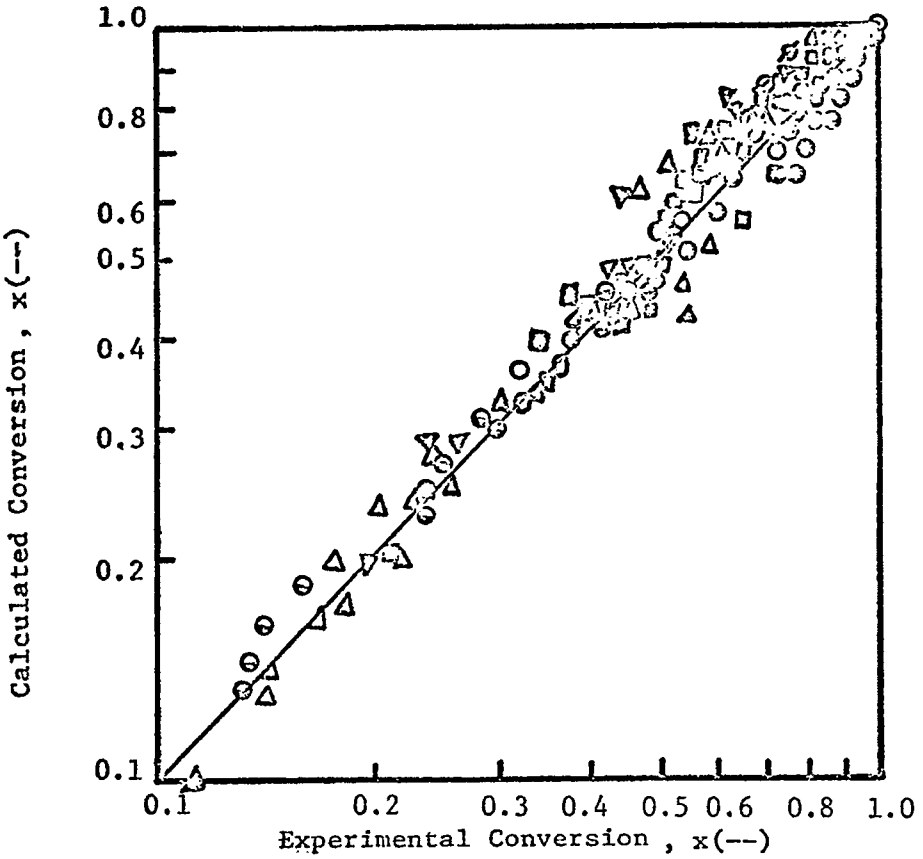

FIGURE A-8 COMPARISON OF EXPERIMENTAL CONVERSION WITH CALCULATED CONVERSION

KEY TO FIGURE A-8

		d_p(cm)	ρ_p(g/cc)	D_R(cm)	L_{mf}(cm)	k(1/sec)
o	Lewis, et al.[26]	0.0122	0.93	5.2	24 ~ 46	1.4 ~ 8.7
●	Kobayashi,et al.[20]	0.0194	1.25	8.3	19 ~ 100	0.8 ~ 0.2
△	Massimilla and Johnstone[29]	0.0105	2.06	11.4	18.1 ~ 54	0.0707
⊖	Shen and Johnstone[37]	0.00806	1.91	11.4	27 ~ 54	0.022~0.0068
□	Kobayashi,et al.[21]	0.0194	1.25	20.0	34 ~ 67	0.2 ~ 1.4
▼	Orcutt,et al.[34]	0.0038~0.0042	1.14	15.25~10.15	61~29.4	0.2 ~ 3.0
▲	Mathis and Watson [30]	0.0103	1.2	8.07	10 ~ 50	0.65
⌀	Echigoya,et al.[7]	0.0122	1.15	5.3	5 ~ 17	4.0 ~ 8
■	Gomezplata and Shuster[10]	0.0105	0.98	7.6	4 ~ 20	0.775
▽	Ishii and Osberg (13)	0.0088	1.65	15.2	4.5 ~ 26	0.31 ~ 1.5

conversion based on nearly all the data presented in the studies listed in Table 2. Considering the difficulties in obtaining accurate kinetic information from fixed bed experimentation and the possible variation of catalyst activities during the fluidized bed operation, the agreement must be regarded to be quite remarkable.

1.6 Discussion

The computation using the "Bubble Assemblage Model" indicates that for most of the experimental conditions tested, the number of compartments are usually greater than 10. This means, in terms of the flow pattern, the gas passing through the bubble phase is close to plug flow. This is probably a reasonable conclusion. The flow pattern of gas in the emulsion phase may be also regarded to be close to plug flow although in the actual computation, because $u_e = 0$ is used, it turns out to be a dead space interchanging gas with the bubble phase. This may invite an argument since some investigators regard the flow in this phase to be close to complete mixing. However, as Lewis, et al.[26] and Muchi[32] pointed out that under normal operations, the calculation of conversion in a fluidized bed reactor based on the two phase model is not affected significantly by the flow parterns in the emulsion phase; whether it is assumed to be plug flow or completely mixed. The important aspect of a flow model for a fluidized bed is to correctly account for the bubbling phenomena and associating gas interchange between the two phases. Using probes, Tanaka[38], recently measured the concentration profile along axial direction in a 20 cm. diameter column for the decomposition of ozone. Since the concentration obtained by the probe is an average between the emulsion phase and the bubble phase, it may be compared with the concentrations predicted by the model using the following relation.

$$\bar{C} = \frac{L - L_{mf}}{L_{mf}} C_b + \frac{L_{mf}}{L} C_e, \text{ for } h \leq L_{mf} \qquad (24)$$

Figure A-9 shows this comparison. The agreement again seems to be remarkable. Notice that the reaction progresses very rapidly just above the distributor. The profile calculated from a model characterized by a single effective bubble size is unlikely to exhibit such a trend.

The foundation of the proposed "Bubble Assemblage Model" lies on the knowledge of variation in bubble diameters along the bed axis. Hence more accurate measurement of bubble growth is necessary to ascertain the bubble diameter correlation presented here. In addition the knowledge of gas interchange between the two phases is also a very important factor particularly for fast reactions and therefore should be further investigated. The characteristics of the proposed model is its versatility and adaptability for varying situations. This is believed to be due to the fact that the model is developed based on an assemblage of multiple bubbles which grow as they rise through the bed. The scale-up consideration is now possible with fair amount of confidence in the accuracy of the results. The model is also convenient for computer simulation and can handle rather easily even cases involving complex reaction rate expressions. One of the weaknesses of this model as in any other model is the uncertainty of knowledge of gas velocity in the emulsion phase, u_e. It can be shown that the conversion calculated based on this model is rather insensitive to the value of u_e, nevertheless, further investigation on this subject is needed. The model can be extended to include solid particle mixing pattern which may be used to develop a fluidized bed reactor model for a non-catalytic solid-gas reacting system. This will be presented in another paper.

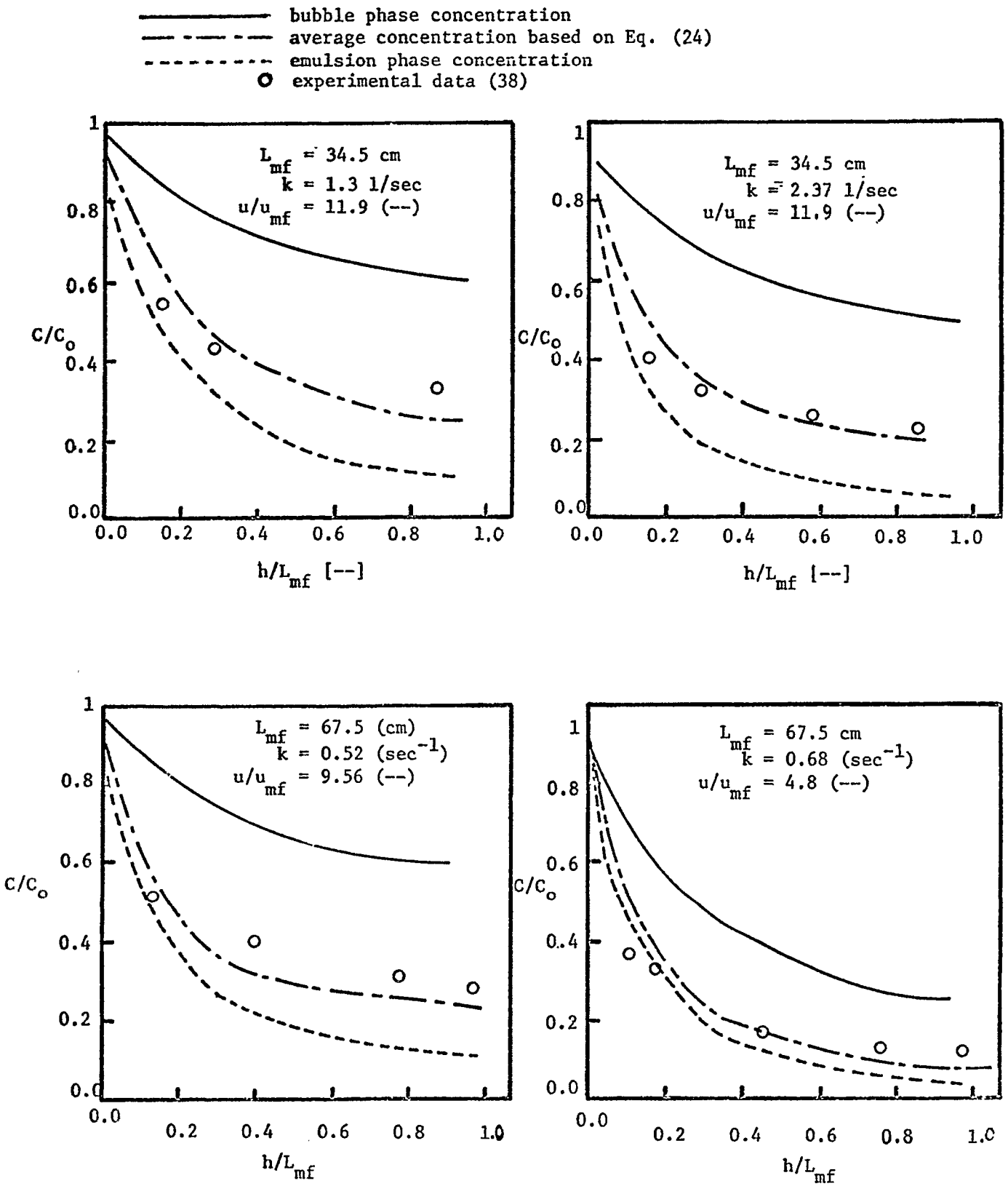

FIGURE A-9 COMPARISON OF EXPERIMENTAL CONCENTRATION PROFILE WITH CALCULATED VALUES

1.7 Conclusion

The catalytic conversion measured by experiments of others can be predicted by the "Bubble Assemblage Model" in terms of the reported kinetic constants and the operating conditions. The model needs no adjustable parameters and is useful for design and scale-up of the fluidized bed reactor. The correct grasp of the bubbling phenomena together with the knowledge of bed expansion, voidage distribution, gas interchange between bubbles and the emulsion pahse, are the key to the success of the development of this model. It is hoped that models developed will promote further investigations so that a more accurate and versatile model can be developed.

Notation

a	fraction of fluidized particles in bubble phase	(--)
c	concentration of reactant	(g-mol/cc)
c_b	concentration of reactant in bubble phase	(g-mol/cc)
c_e	concentration of reactant in emulsion phase	(g-mol/cc)
c_{bn}	concentration of reactant in bubble phase at n-th compartment	(g-mol/cc)
c_{en}	concentration of reactant in emulsion phase at n-th compartment	(g-mol/cc)
$\bar{C}$	average concentration of reactant defined in Eq. (23)	(g-mol/cc)
D	diffusivity of reactant gas	(cm^2/sec)
D_o	bubble diameter at surface of distributor	(cm)
D_b	axial dispersion coefficient of reactant in bubble phase	(cm^2/sec)
D_e	axial dispersion coefficient of reactant in emulsion phase	(cm^2/sec)
D_B	effective bubble diameter	(cm)
D_P	packing diameter in packed fluidized bed	(cm)
D_S	axial solid dispersion coeffficient in emulsion phase	(cm^2/sec)
D_T	maximum stable bubble diameter	(cm)
d_p	fluidized particle diameter	(cm)
E_z	axial gas dispersion coefficient in the bed	(cm^2/sec)
F	volumetric fraction of gas in the bubble phase	(--)
F_d	overall gas interchange coefficient per unit volume of gas bubble	(1/sec)
F_o	gas interchange coefficient per unit volume of gas bubble	(1/sec)
F_{on}	gas interchange coefficinet at the n-th compartment	(1/sec)
F_s	volumetric fraction of solid in bubble phase	(1/sec)
f	volumetric fraction of gas in emulsion phase	(1/sec)
f_s	volumetric fraction of solids in emulsion phase	(1/sec)
g	gravitational acceleration	(cm/sec^2)

h	distance from the distributor	(cm)
Δh	length of the n-th compartment	(cm)
h_n	distance between the distributor and n-th compartment	(cm)
K'	adsorption equilibrium constant	(--)
k	reaction rate constant	(1/sec)
L	bed height	(cm)
L_{mf}	bed height at minimum fluidized velocity	(cm)
L_{cal}	bed height calculated from Equation (9)	(cm)
L_{ob}	observed bed height in the fluidized bed	(cm)
M	solid interchange coefficient between the bubble phase and the emulsion phase per unit volume of bubble	(1/sec)
N	number of bubbles in n-th compartment	(--)
N_{Rep}	particle Reynolds number	(--)
n_o	number of holes per unit surface area of distributor	($1/cm^2$)
R_c	radius of cloud	(cm)
R_b	radius of bubble	(cm)
r	reaction rate per unit volume of catalyst	(gmole/sec.cc)
r_b	reaction rate in bubble phase per unit volume of cloud	(gmole/sec.cc)
r_e	reaction rate in emulsion phase per unit volume of cloud	(gmole/sec.cc)
S	cross sectional area of the bed	(cm^2)
t	time	(sec)
u	superficial gas velocity	(cm/sec)
u_b	bubble rising velocity	(cm/sec)
u_b'	bubble rising velocity based on fixed axis	(cm/sec)
u_{mf}	superficial gas velocity at minimum fluidization velocity	(cm/sec)
u_e	superficial gas velocity in the emulsion phase	(cm/sec)
u_T	terminal velocity of fluidized particles	(cm/sec)
V_{bn}	volume of the bubble phase at the n-th compartment	(cc)
V_{cn}	volume of the cloud at the n-th compartment	(cc)
V_{en}	volume of the emulsion phase at the n-th compartment	(cc)

x	conversion of the reactant gas	(--)
α	ratio of the volume of wake to volume of bubble	(--)
ε	void fraction	(--)
ε_p	void fraction of fixed packing	(--)
ε_{mf}	void fraction at u_{mf}	(--)
ν	kinematic viscosity	(cm^2/sec)
ρ_p	particle density	

Literature

1. Bakker, P. J., Chem. Eng. Sci., 12, 260 (1960).

2. Baugarten, P. K., Pigford, R. L., A. I. Ch. E. Journal 6, 1, 115 (1960).

3. Cooke, M. J., Harris, W., Highley, J., and Williams, D. F., paper to be presented at Tripartite, Montreal, Canada, September, 1968.

4. Davidson, J. F., Trans. Inst. Chem. Engrs., 39, 230 (1961).

5. Davidson, J. F. and Harrison, D., FLUIDIZED PARTICLES, Cambridge University Press (1963).

6. De Groot, J. H., "Proceedings of the International Symposium on Fluidization" 348-361 (1967).

7. Echigoya, E., Iwasaki, M., Kanetomo, T. and Niyama, H., Chem. Eng. Japan, 32, 571 (1968).

8. Fan, L. T., Lee, C. Y. and Bailie, R. C., A. I. Ch.E. Journal, 8, 2, 239 (1962).

9. Gilliland, E. R. and Mason, E. A., Ind. Eng. Chem., 41, 6, 1191 (1949).

10. Gomezplata, A. and Shuster, W. W., A. I. Ch. E. Journal 6, 454 (1960).

11. Harrison, D., Davidson, J. F. and Kock, J. W., Trans. Instn. Chem. Engrs., 39, 202 (1961).

12. Hiraki, I., Yoshida, K. and Kunii, D., Chem. Eng. Japan, 29, 11, 846 (1965).

13. Ishii, T. and Osberg, G. L., A. I. Ch. E. Journal, 11, 279 (1965).

14. Iwasaki, M., Furuoya, I., Sueyoshi, H.,Shirasaki, T. and Echigoya, E., Chem. Eng. Japan, 29, 892 (1965).

15. Kato, K., Imafuku, K. and Kubota, H., Chem. Eng. Japan, 31, 10, 967 (1967).

16. Kato, K., Ph. D. Thesis, Tokyo Institute of Technology (1967).

17. Kobayashi, H. and Arai, F., Chem. Eng. Japan, 29, 885 (1965).

18. Kobayashi, H., Arai, F. and Shiba, T., Chem. Eng. Japan, 29. 858 (1965).

19. Kobayashi, H., Arai, F. and Sunagawa, T., Chem. Eng. Japan, 31, 239 (1967).

20. Kobayashi, H., Arai, F., Isawa, S., Sunagawa, T. and Miya, K., Chem. Eng. Japan, 30, 656 (1966).

21. Kobayashi, H., Arai, F., Tanaka, T., Sakaguchi, Y., Sagawa, N., Sunagawa, T., Shiba, T. and Takahashi, K., "The 6th Reaction Engineering Symposium (Japan)", 13 (1966).

22. Kunii, D. and Levenspiel, O., Ind. Eng. Chem. Fund., 7, 3, 446 (1968).

23. Kunii, D. and Levenspiel, O., FLUIDIZATION ENGINEERING, John Wiley & Sons, Inc., to be published.

24. Latham, R., Hamilton, C. and Potter, O. E., Brit. Chem. Eng., 13, 666 (1968).

25. Leva, M., Weintraub, M., Grummer, M., Pollchik, M. and Storch, H. H., Bulletin 504, Bureau of Mines (1949).

26. Lewis, W. K., Gilliland, E. R. and Glass, W., A.I.Ch.E. Journal, 5, 419 (1959).

27. Lewis, W. K., Gilliland, E. K. and Bauer, W. C., Ind.Eng.Chem., 41, 1104 (1949).

28. Mamuro, T. and Muchi, I., J.of Ind. Chem.(Japan), 68, 126 (1965).

29. Massimilla, L. and Johnstone, H. F., Chem.Eng.Sci., 16, 105 (1961).

30. Mathis, J. F. and Watson, C. C., A.I.Ch.E. Journal, 2, 518 (1956).

31. May, W. G., Chem.Eng.Progr., 55, 49 (1959).

32. Muchi, I., "Memoirs of the Faculty of Engineering," Nagoya University, Japan, 17, No. 1, May (1965).

33. Muchi, I., Mamuro, T. and Sasaki, K., Chem.Eng.Japan, 25, 747 (1961).

34. Orcutt, J. C., Davidson, J. E. and Pigford, R. L., Chem.Eng.Prog. Symp. Series, 58, 38, 1 (1962).

35. Romero, J. B., A.I.Ch.E. Journal, 11, 595 (1965).

36. Rowe, P. N. and Partridge, B. A., Trans.Instn.Chem.Engrs., 43, T157 (1965).

37. Shen, C. Y. and Johnstone, H. F., A.I.Ch.E. Journal, 1, 349 (1955).

38. Tanaka, T., M. S. Thesis, Hokkaido University, Japan, 1967.

39. Toei, R., Matsuno, R., Kojima, H., Nagai, Y. and Nakagawa, K., Chem. Eng. Japan, 29, 851 (1965).

40. Toei, R., Matsuno, R., Miyakawa, H., Nishiya, K. and Komagawa, Y., Chem.Eng. Japan, 32, 565 (1968).

41. Van Deemter, J. J., Chem. Eng. Sci., 13, 143 (1961).

42. Van Deemter, J. J., "Proceedings of the International Symposium on Fluidization," 322, Eindhoven (1967).

43. Wen, C. Y. and Chang, T. M., "Proceedings of the International Symposium on Fluidization," 492, Eindhoven (1967).

44. Winter, D. H., "Symposium on Fundamental and Applied Fluidization I," A.I.Ch.E. 51st National Meeting.

45. Yasui, G., Johanson, L. N., A. I. Ch. E. Journal, 4, 445 (1958)

46. Zenz, F. A., Othmer, O. F., Fluidization And Fluid-Particle Systems, Reinhold Publishing Corporation, New York (1960).

2. Mass Transfer in Fixed and Fluidized Beds

2.1 Introduction

Masstransfer between particle and fluid in fixed and fluidized beds has been the subject of study by many investigators because it is fundamentally associated with many chemical engineering processes such as catalytic reaction, gasification of fossil fuel, iron exchange operation, drying, adsorption, etc. In gas-solid systems, mass transfer coefficients have been evaluated usually by evaporation of water from porous particles and by sublimation of naphthalene particles in a gas stream. In liquid-solid systems, dissolution of organic particles such as benzoic acid in water and electrolytic reactions are usually employed to obtain mass transfer coefficients. The mass transfer coefficients thus obtained are usually correlated via J_d factor plot in terms of Reynold's number and Sherwood's number. A summary of mass transfer data obtained by previous investigators is shown in Figures A-10 and A-11 for fixed beds and fluidized beds respectively. Shirai[27] presented an empirical equation for both fixed beds and fluidized beds for Reynold's number above 100:

$$(N_{sh})\,\varepsilon = 2.0 + 0.75\,(N_{Rep})^{1/2} \cdot (N_{sc})^{1/3} \qquad (1)$$

McConnachie and Thodos[18] also presented a correlation based on mass transfer data in fixed bed of many investigators as follows:

$$J_d = \frac{1.127}{(N_{Rep})^{0.41} - 1.52} \qquad (2)$$

where $$N_{Rep} = \frac{dU\rho}{\mu(1-\varepsilon)}$$

Neither equation (1) nor equation (2) represents satisfactorily for solid-gas mass transfer in fixed beds at low Reynold's number. As shown in Fig. A-11

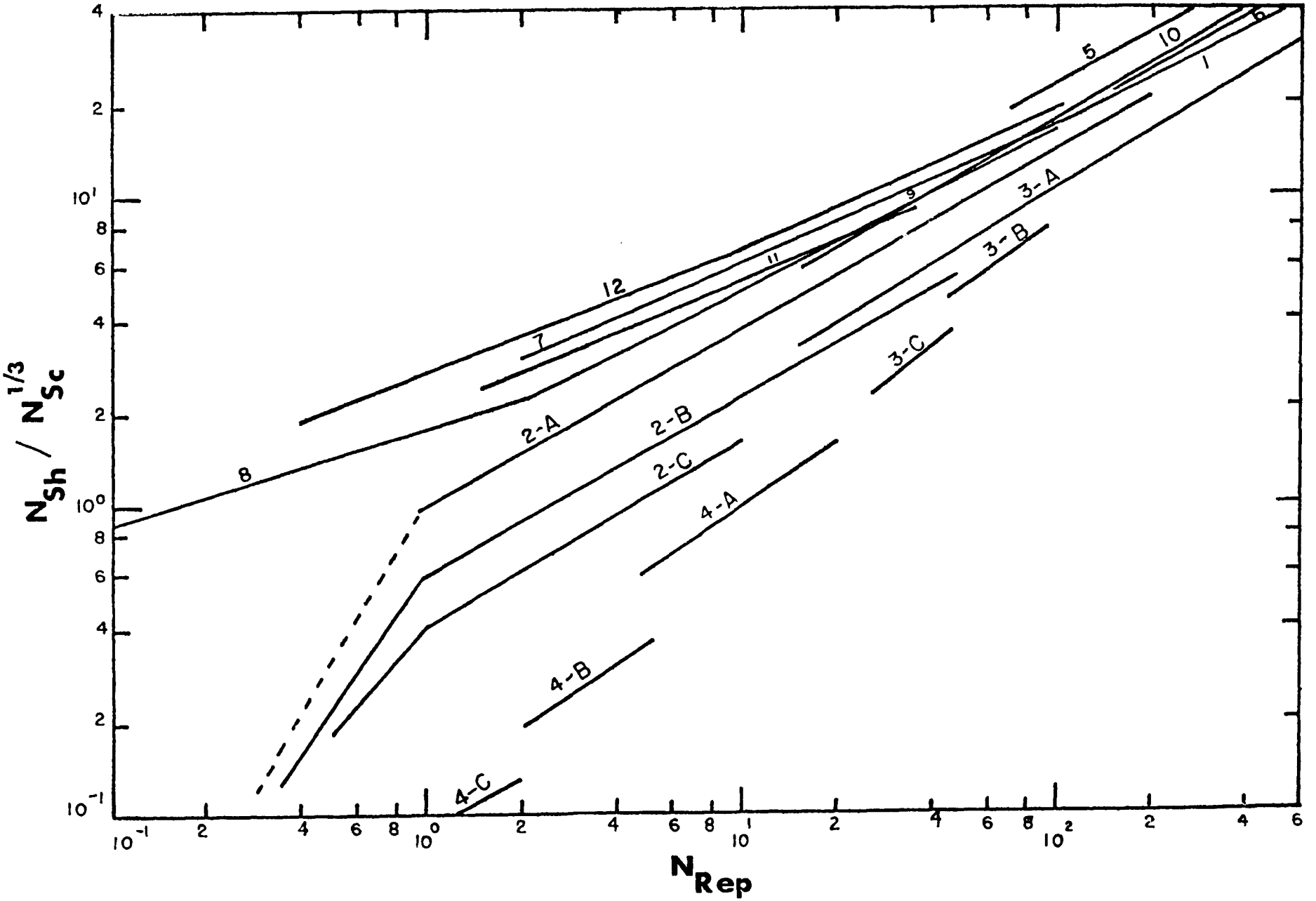

Figure A-10 Previous Investigations on Mass Transfer in Fixed Bed

Key to Fig. A-10

Author		d,(cm)
1. Hobson and Thodos		
2. Bar Ilan and Resnick		
	2-A	0.8~0.4
	2-B	0.048
	2-C	0.037
3. Hurt		
	3-A	0.96~0.4
	3-B	0.28
	3-C	0.203
4. Resnick and White		
	4-A	0.099
	4-B	0.07
	4-C	0.0497
5. Bradshaw and Bennett		
6. Gamson and Thodos		
7. White and Hougen		
8. Dryden et al		
9. Ishino et al		
10. McCune and Wilhelm		
11. Gaffney and Drew		
12. Akehata and Sato		

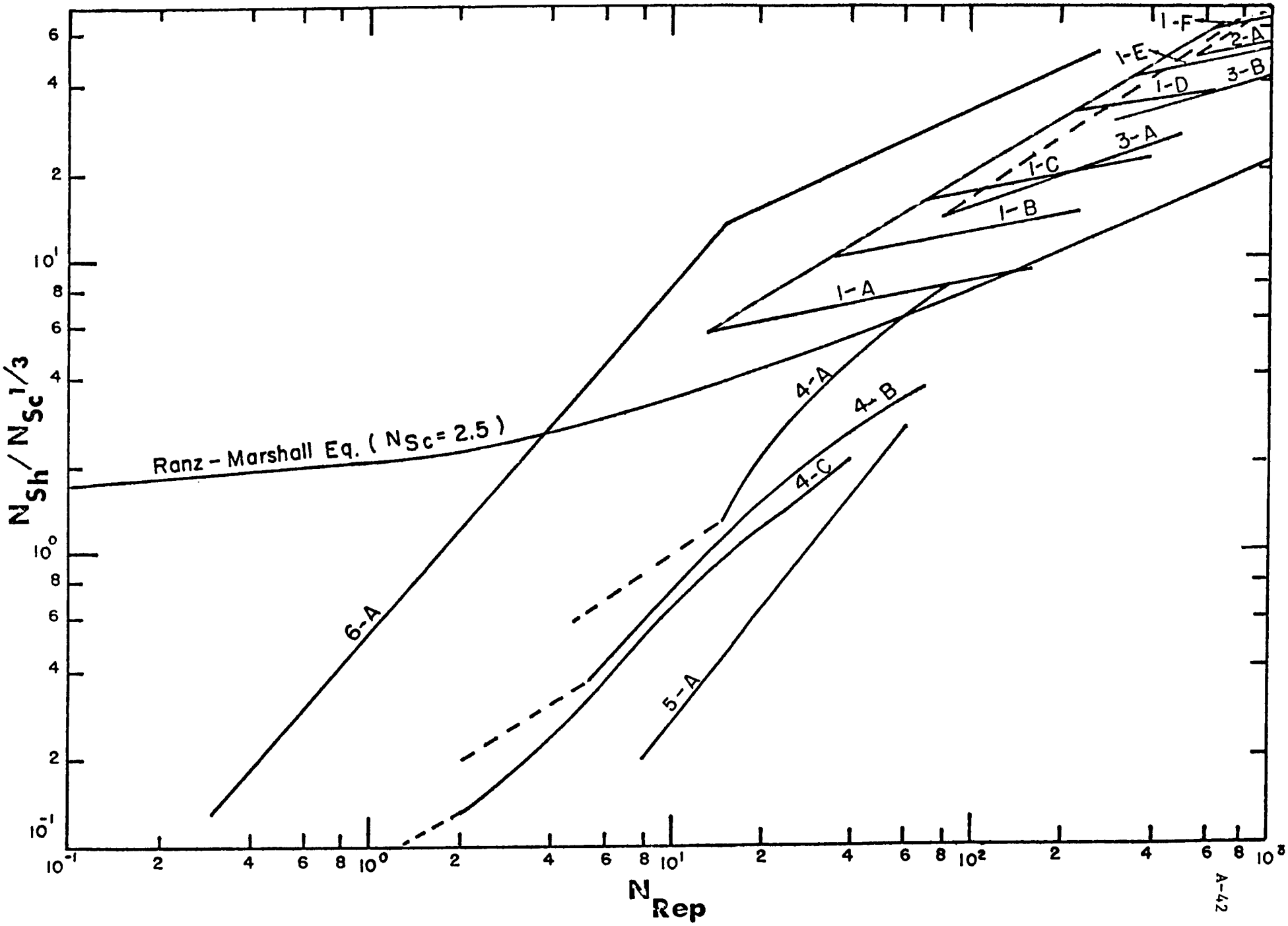
$N_{Sh} / N_{Sc}^{1/3}$
N_{Rep}
Ranz - Marshall Eq. ($N_{Sc} = 2.5$)
1-F
1-E
2-A
1-D
3-B
1-C
3-A
1-B
1-A
4-A
4-B
4-C
5-A
6-A

Key to Fig. A-11

Author		d,(cm)
(a) Chu et al		
	1-A	0.0762
	1-B	0.0736
	1-C	0.195
	1-D	0.546
	1-E	0.874
(b) Bradshaw and Myers		
(c) Riccetti and Thodos		
	3-A	0.09~0.195
	3-B	0.296
(d) Resnick and White		
	4-A	0.0986
	4-B	0.070
	4-C	0.0495
(e) Kettenring et al		
(f) Richardson and Szekey		

when Reynold's number is less than 10, the mass transfer coefficient in solid-gas fixed beds becomes considerably smaller then the theoretical coefficient for a single particle in a stagnant gas medium ($N_{sh} = 2.0$). In addition it is also evident that for low Reynold's number, Sherwood's number for the solid-gas systems is considerably lower than that of the solid-liquid systems. The deviation among the various investigators also becomes substantial indicating questionable reliability of the data in this range. In this paper experimental data were obtained for the sublimation of small naphthalene particles ($d = 0.4 \sim 0.016$ cm) in fixed bed. These data together with experimental data by the previous investigators are correlated to obtain a generalized relation for solid-gas mass transfer coefficient in fixed bed systems. Furthermore, this correlation is used to show how mass transfer coeficient for fluidized beds can be predicted from the "Bubble Assemblage Model" previously proposed [14]. The calculated coefficients are then compared with the experimental values reported by various investigators.

2.2 Experimental Equipment and Procedure

The experimental equipment used is shown in Fig. C-12. Air from compressor (A) is dried in dehydration tower (C) packed with slica gel and is freed from CO_2 and moisture in decarbonation tower (D) packed with soda-lime (CaO NaOH). It then enters the rotameter (G_1), for metering the flow rate and passes through a constant temperature bath (H) in which it is heated to 29.5°C before being introduced to the fixed bed, (I). Naphthalene is sublimed in the fixed bed and is carried into converter (J) where it is completely burned to CO_2 and H_2O. The gas chromotgraph (K) is used for

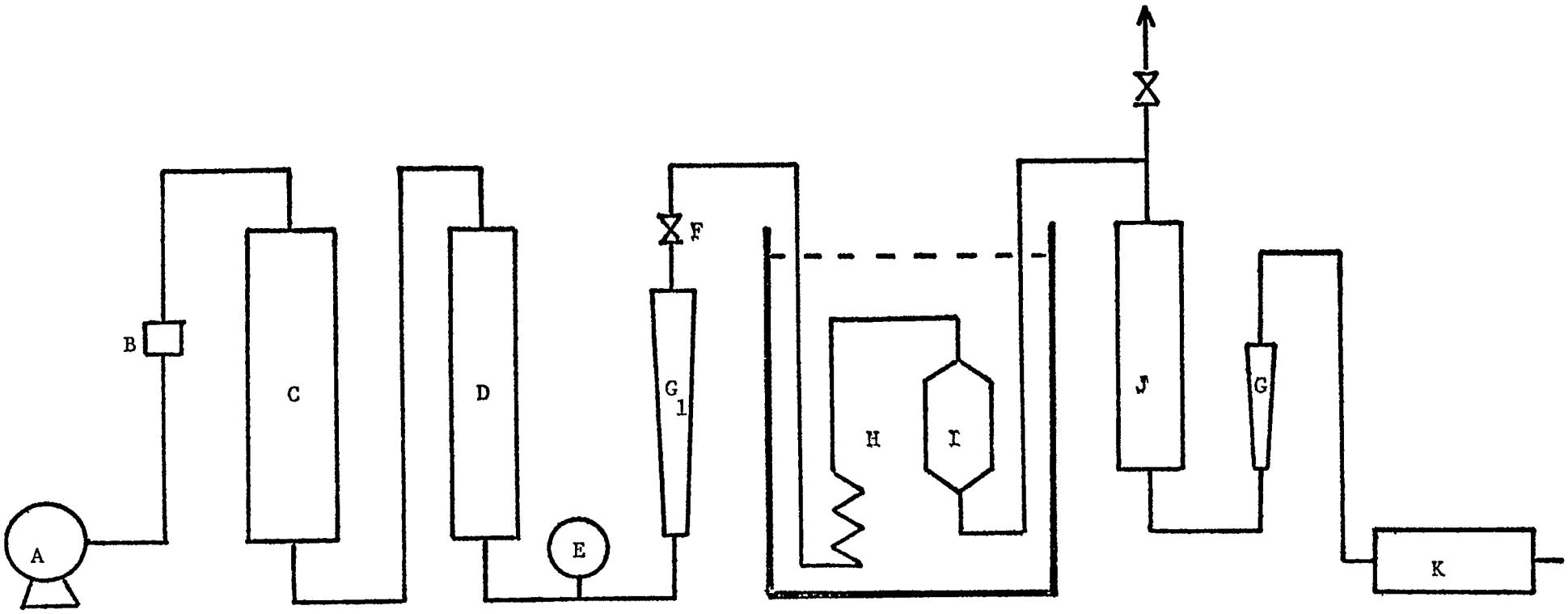

A. Compressor

B. Pressure regulator

C. Dehydration tower

D. Decarbonate tower

E. Pressure gauge

F. Valve

H. Constant Temperature Bath

I. Packed Bed

J. Naphthalene convertor

K. Gas chromatograph

G_1, G_2 Rotameters

Figure A-12. Schematic Diagram of Experimental Apparatus

analysis of CO_2 from which the concentration of naphthalene in air stream is calculated. The converter (J) is packed with oxidized copper screen and is heated to 600°C. The gas chromatograph detects no trace of other oxides in the gas stream. To prevent condensation of naphthalene vapor between the exit point of the constant temperature bath (H) and the entrance point of the converter (J), the tube is heated to 50°C. Since in this experiment relatively small particles are used, the specific surface area of particles is quite large indicating considerably large mass transfer rate. This implies that the amount of naphthalene particles in the fixed bed can not be too great and that the length of time of experiment can not be too long so that no substantial change in particle diameter may take place. (Reduction in diameter of particle less than 10% in all cases.)

The reasons why naphthalene is converted to CO_2 for the gas analysis are:

(a) A higher temperature must be maintained in the gas chromatograph if naphthalene is to be analyzed directly.

(b) A longer retention time is required for naphthalene analysis.

(c) The vapor pressure of naphthalene (0.129 mm H_g) is small resulting a considerably lower peak than that of CO_2 which occupies 10 times the volume of naphthalene.

The gas chromatograph column is packed with 35-42 mesh activated carbon and is kept at 55°C, while the carrier gas used is hydrogen.

The fixed bed used for experimentation is shown in Fig. A-13 It is a cylinder with 2.5 cm I.D. and 4 cm tall packed first with inert particles (acryl beads or glass beads) having the same particle size (0.5 ~ 1.0 cm) as that of naphthalene particles. Approximately 5 to 10 times more naphthalene particles are then placed on the top of the inert particles. Additional

1. Gas inlet
2. Thermocouple
3. Pressure Jap
4. Inert Particles
5. Wire screen (100 mesh)
6. Sample particles
7. Gas distributor
8. Gas outlet

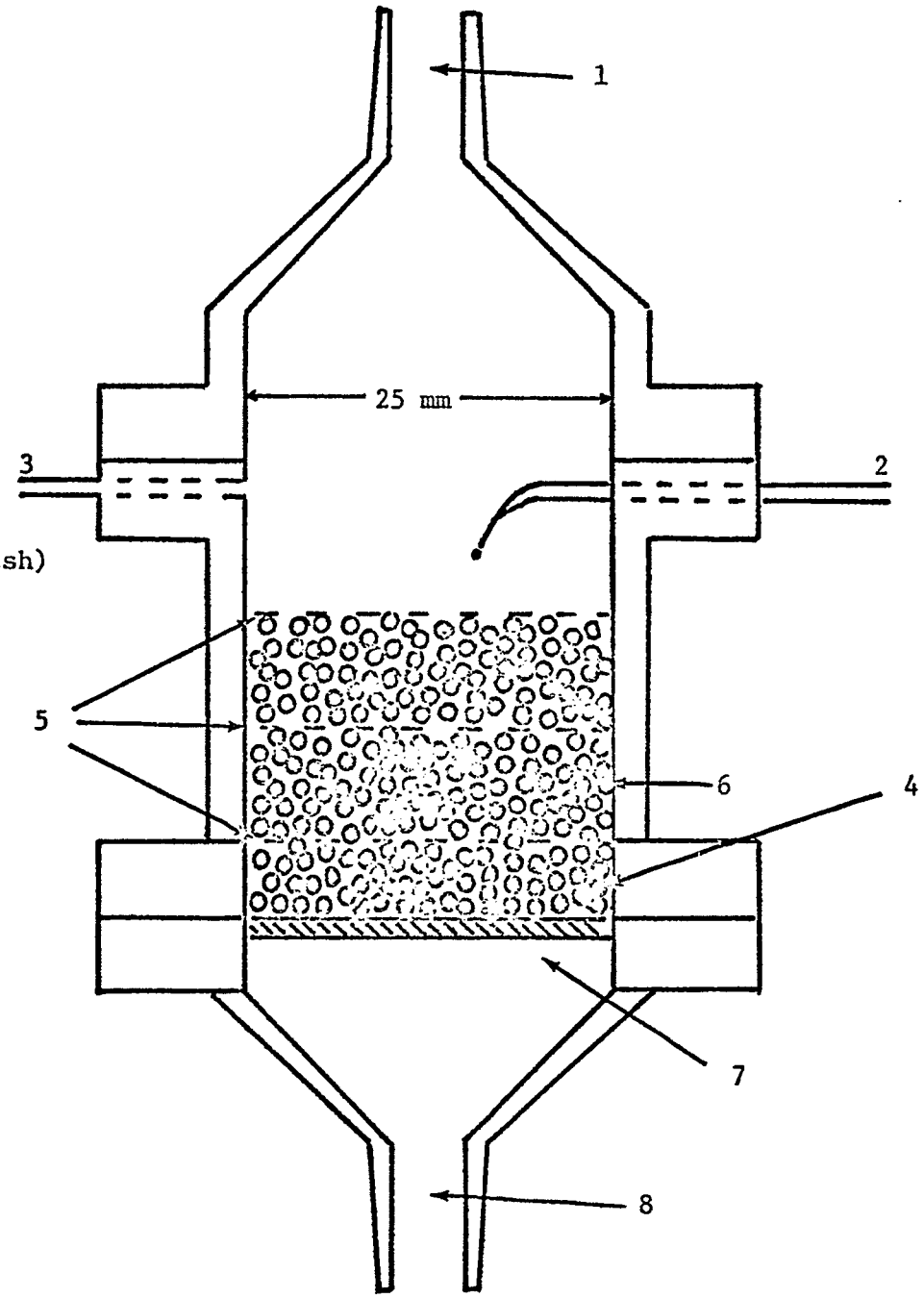

Figure A-13 Packed Bed

inert particles are placed on the top of the naphthalene particles. The top and the bottom of the bed are supported by 100~200 mesh wire gauze. The inert particles placed above and below the naphthalene particles are to reduce the end effects as well as to smooth out the radial velocity profile of the gas in the bed. The temperature of the bed is maintained at 29.6°C by means of a constant temperature bath. The pressure is measured by a manometer and is found to be exactly 1 atm.

Naphthalene particles used in mass transfer study are prepared as follows. The upper portion of a cylindrical vessel containing water is heated to boiling. Pure naphthalene powder is introduced gradually into the boiling water. Since the melting point of naphthalene is 81°C, the powder quickly melts in the boiling zone and slowly becomes tiny liquid droplets. As these droplets slowly sink to the bottom of the vessel because of the small density difference, they become spherical naphthalene particles. These small particles are then dried and screened. Examination under microscope shows that particles thus obtained are almost perfect spheres.

The molecular diffisivity of naphthalene in air at 29.6°C and 1 atm is 0.0619 cm^2/sec [24] and the corresponding Schmidt number is calculated to be 2.57.

2.3 Analysis of Experimental Data and Results

If the flow of gas through fixed beds can be approximated by a plug flow, a material balance on naphthalene in the bed can be written as

$$U \frac{dC}{dz} = k_f \, a \, (C_s - C) \tag{3}$$

With the boundary conditions at $z = 0$, $C = 0$, we have

$$k_f = \frac{U}{aL} \ln \frac{C_s}{C_s - C} = \frac{q}{A_s} \ln \frac{C_s}{C_s - C} \tag{4}$$

Where $a = \frac{6(1-\varepsilon)}{d}$ and $A_s = \frac{6W}{d\rho_p}$

Mass transfer coefficient, k_f, can be calculated from equation (4) if weight of naphthalene used, the gas flow rate and the concentration of naphthalene at the exit of the fixed bed (calculated from CO_2 concentration measurement) are known.

Preliminary tests indicate that the mass transfer coefficient is not affected by the weight ratio of naphthalene particles and the inert particles in the bed. The experimental data are plotted in Fig. A-14 in terms of Sherwood number and Reynolds number. It can be seen from the figure, Sherwood number is not only affected by the Reynolds number but also affected by the particle diameter and the effective bed height (the height of naphthalene particles bed alone). In Fig. A-15 Sherwoods number is plotted against the ratio of particle diameter to bed height, $(d/_L)$, at a given particle Reynolds number. It is clear from the figure that at a constant Reynolds number, the Sherwood number is approximately proportional to $(d/_L)^{0.6}$. Thus the mass transfer data for solid-gas fixed bed obtained in this experiment and those of the previous investigators are plotted in Fig. A-16 in terms of $N_{sh}/(N_{sc})^{\frac{1}{3}}$ and $N_{Rep}(\frac{d}{L})^{0.6}$. Comparing Fig. A-10, in which $N_{sh}/(N_{sc})^{\frac{1}{3}}$ is plotted against N_{Rep}, the data of Bar-Ilan and Resnick,[3] that of Resnick and White[21] and those of Hurt [12] which were not satisfactorily correlated in Fig. A-10 is now well correlated into one line in Fig. A-16 The following empirical equations are obtained from Fig. A7 for solid-gas mass transfer in fixed beds.

$$N_{sh}/(N_{sc})^{\frac{1}{3}} = 0.72\,[N_{Rep}\cdot(d/_L)^{0.6}]^{0.95} \qquad (5)$$

$$\text{for } 0.1 \leq N_{Rep}(d/_L)^{0.6} \leq 5.$$

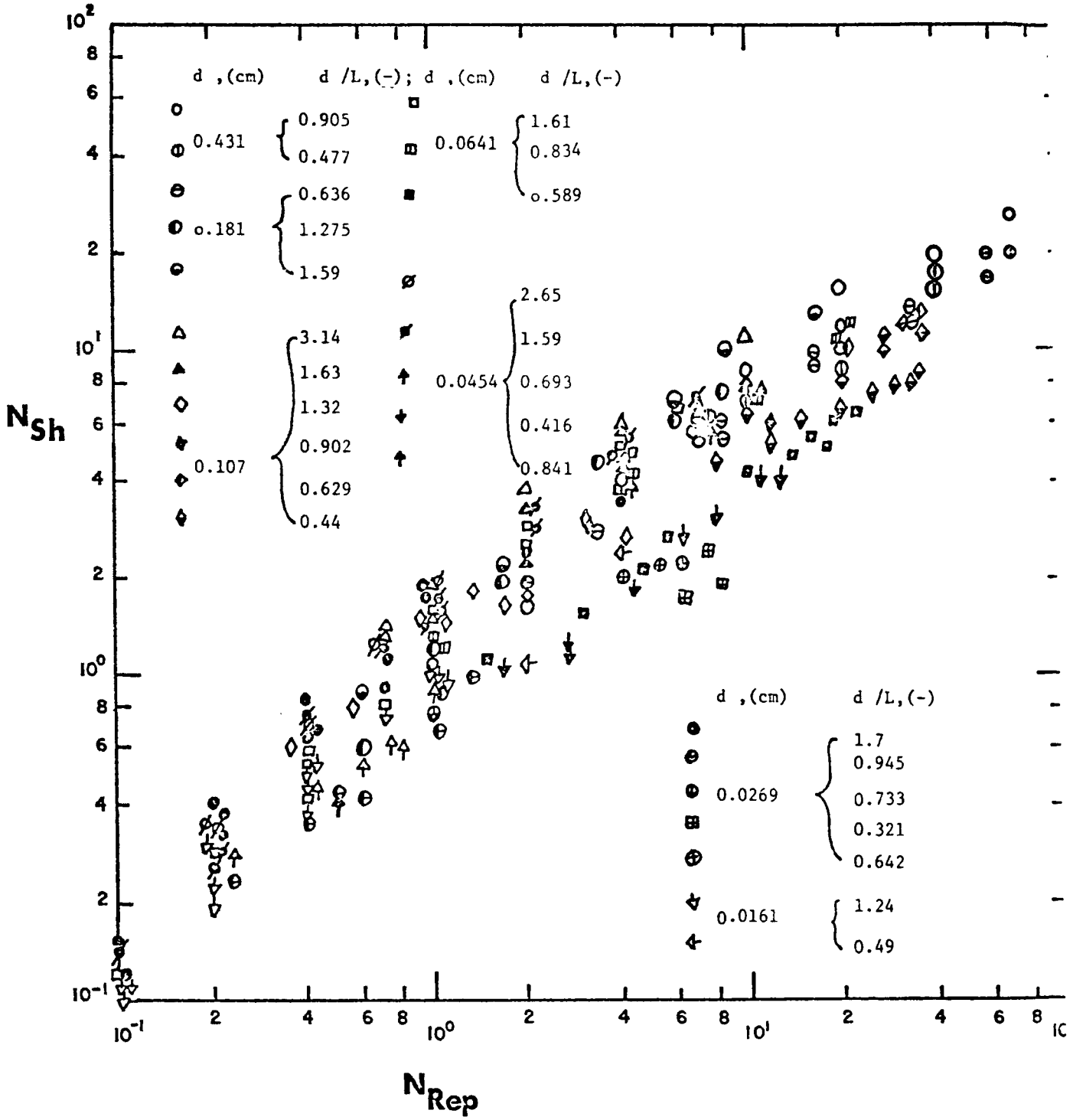

Figure A-14 Experimental Data for Sublimation of Naphthalene in Fixed Bed Indicating Relation Between N_{Sh} vs N_{Rep}

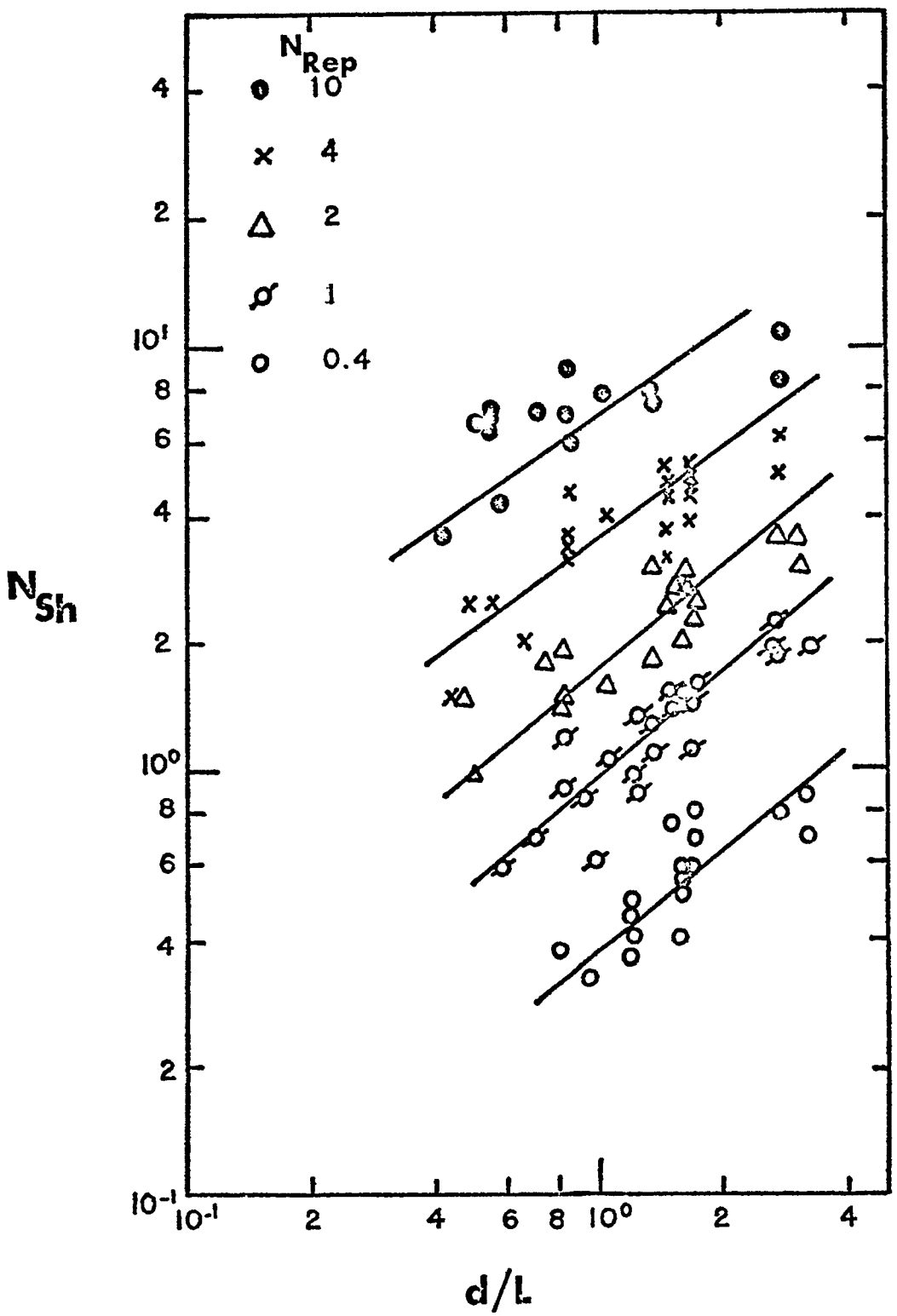

Figure A-15 Relation Between N_{Sh} and d/L

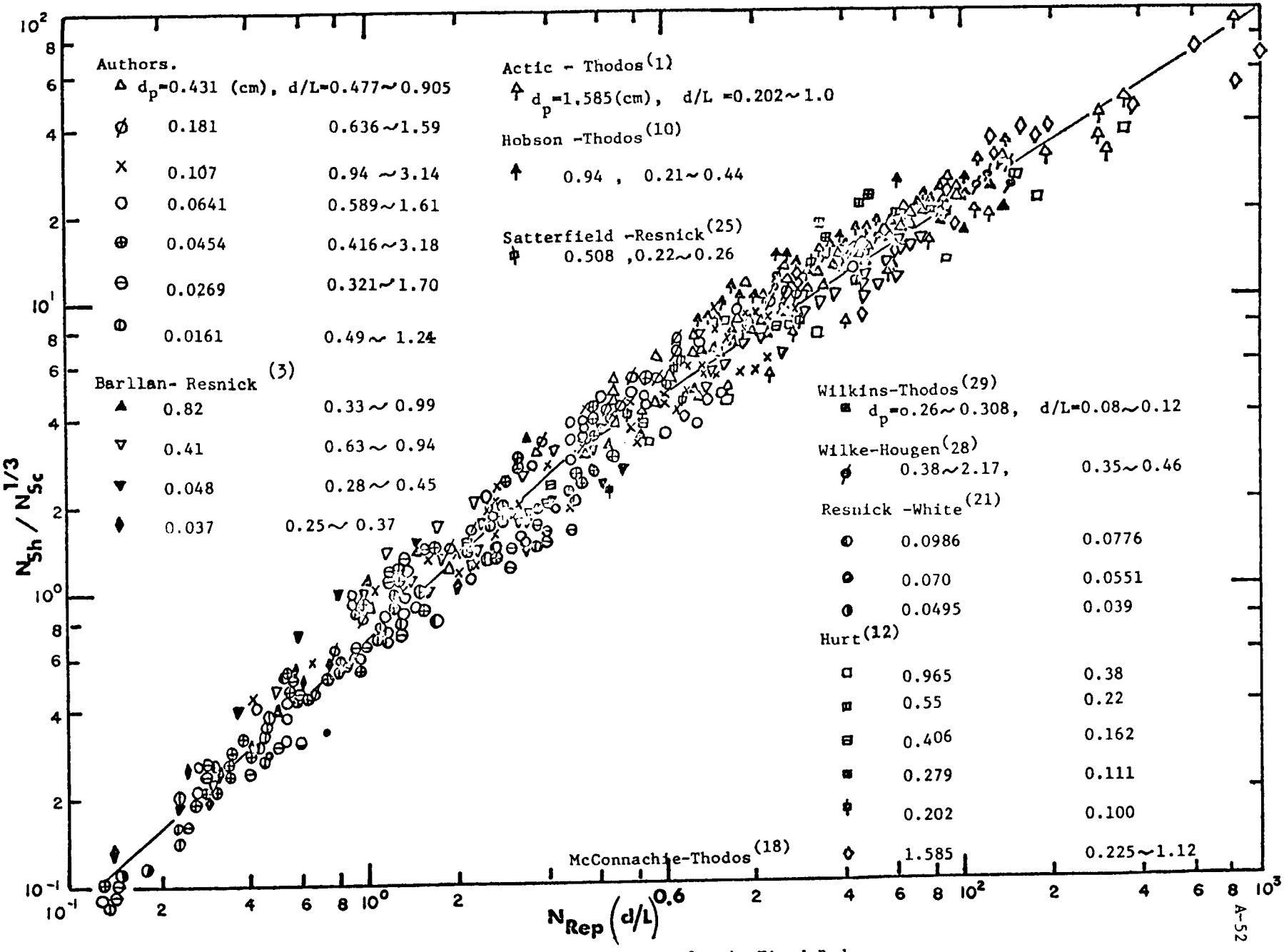

Figure A-16 Gas-Particle Mass Transfer in Fixed Bed

$$N_{sh}/(N_{sc})^{1/3} = 1.25\,[N_{Rep}\cdot(d/L)^{0.6}]^{0.63} \qquad (6)$$

$$\text{for } 10^3 \geq N_{Rep}\,(d/L)^{0.6} \geq 5$$

2.4 Application of "Bubble Assemblage" Model for Solid-Gas Mass Transfer in Fluidized Bed Operations

Recently a new model for fluidized bed operation called "Bubble Assemblage" model [4] was proposed for catalytic reactors. In this section, the proposed mass transfer correlation in fixed beds is applied to the "Bubble Assemblage" model to calculate the particle -gas mass transfer coefficients in fluidized beds.

As has been discussed elsewhere[4], the "Bubble Assemblage" model for fluidized bed mass transfer operations is based on the following assumptions:

Assumptions

(a) Mass transfer coefficient in the bubble phase may be approximated by the fixed bed solid-gas mass transfer coefficient at the gas velocity equivalent to U_b, the bubble velocity.

(b) Mass transfer coefficient in the emulsion phase may be approximated by that in fixed beds at the gas velocity equivalent to U_{mf}.

(c) Solid-gas mass transfer coefficient is usually an order of magnitude faster than catalytic chemical reaction rate. Consequently, experimental measurement of concentration profile for mass transfer study must be carried out in a very shallow bed. (If measurements are obtained in a tall bed, exit concentration would approach too close to the saturation concentration and accurate determination becomes difficult.)

Therefore, the size of the first compartment in the fluidized

bed becomes an important factor in this model.

As $(U_b - U_{mf}/\varepsilon_{mf})$ approaches zero, the cloud around the bubble can no longer exit. In this region, since the bubble diameter is small and bubble velocity is nearly the same as velocity of gas in the emulsion phase, the two phases concept no longer applies. It is more reasonable to assume one phase with bubble velocity represented by

$$U_b = 1.1\, U_{mf}/\varepsilon_{mf}$$

$$\text{and} \quad U_b = 0.711\sqrt{g\, D_b}$$

$$\text{where} \quad D_b = 1.4\, \rho_p\, d\, \left(\frac{U}{U_{mf}}\right)\, (\Delta h_1)$$

$$\text{and thus} \quad \Delta h_1 = \frac{(1.1 U_{mf}/\varepsilon_{mf})^2}{0.708\, \rho_p\, d\, (U/U_{mf})\, g}$$

(d) Since bubbles are very small in the first compartment, the gas interchange between the bubble phase and the emulsion phase can be regarded to be extremely fast and therefore the flow pattern in this compartment may be approximated by a plug flow.

(e) The maximum bed expansion is assumed to reach when the gas bubbles occupy roughly fifty per cent of the bed volume. (The loosely arranged spheres can occupy approximately 50% of the bed volume).

The concentration of gaseous component participating mass transfer at the exit of the first compartment $C_{(1)}$ can be represented by

$$C_{(1)}/C_s = 1 - \exp\left(-\frac{k_f a\, \Delta h_1}{U}\right) \qquad (8)$$

Where k_f can be calculated based on equations (5) and (6) in which N_{Rep} is evaluated at the superficial gas velocity U, and $a = 6(1-\varepsilon)./d$. The

concentration of gas at the exit of the first compartment, $C_{(1)}$ is then taken to be that entering the bubble phase as well as the emulsion phase of the second compartment.

$$\Delta h_n = \frac{2m\Delta h_1}{(2-m)} \left(\frac{2+m}{2-m}\right)^{n-2} \tag{9}$$

Where $m = 1.4 \rho_p d (U/U_{mf})$

Hence the number of the bubbles in the n-th compartment becomes

$$N = \frac{6S (L - L_{mf})}{\pi L (\Delta h_n)^2} \tag{10}$$

And the volume of the cloud, the bubble phase and the emulsion phase in the n-th compartment becomes, respectively,

$$V_{cn} = N \left(\frac{3 U_{mf}/\varepsilon_{mf}}{U_b - U_{mf}/\varepsilon_{mf}}\right) \frac{\pi(\Delta h_n)^3}{6} \tag{11}$$

$$V_{bn} = N \left(\frac{U_b + 2 U_{mf}/\varepsilon_{mf}}{U_b - U_{mf}/\varepsilon_{mf}}\right) \frac{\pi(\Delta h_n)^3}{6} \tag{12}$$

$$V_{en} = S\Delta h_n - V_{bn} \tag{13}$$

The material balance for the component participating mass transfer in the bubble phase can be written as

$$S (U - U_e) C_{bn} = S (U - U_{mf}) (C_b)_{n-1} + F_{on}' V_{bn} (C_{en} - C_{bn})$$

$$+ k_{fn} a_{mf} V_{cn} (C_s - C_{bn}) \tag{14}$$

and that for the emulsion phase is

$$SU_e C_{en} = SU_e (C_e)_{n-1} + a_{mf} k_{fmf} V_{en} (C_s - C_{bn})$$

$$- F'_{on} V_{bn} (C_{en} - C_{bn}) \qquad (15)$$

F'_{on} in equation (14) and (15) is the gas interchange coefficient between the bubble phase and the emulsion phase and can be estimated by the following equation proposed by Kobayashi et al.[16]

$$F_{on} = 11/D_{bn} \quad \text{and} \quad F'_{on} = F_{on} \frac{U_b - U_{mf}/\varepsilon_{mf}}{U_b + 2U_{mf}/\varepsilon_{mf}}$$

The gas velocity in the emulsion phase, U_e can be calculated by

$$U_e = U_{mf} \left[1 - \frac{\varepsilon_{mf}\, \alpha \left(\frac{L - L_{mf}}{L}\right) \bar{U}_b}{U_{mf} \left\{ 1 - \left(\frac{L - L_{mf}}{L}\right) - \alpha \left(\frac{L - L_{mf}}{L}\right) \right\}} \right]$$

Where $\bar{U}_b$ is the average bubble velocity in the bed. k_{fn} and k_{fmf} in equations (14) and (15) are the mass transfer coefficients in the bubble phase and the emulsion phase respectively and can be obtained from equation (6) by substituting U_{bn} and U_{mf} for the Reynolds number term, respectively. a_{mf} is the specific surface area of particles corresponding to the gas velocity at U_{mf} or $a_{mf} = \frac{6(1 - \varepsilon_{mf})}{d}$. The boundary condition is

$$C_{e1} = C_{b1} = C_{(1)} \qquad (16)$$

Consequently the overall mass transfer coefficient for the entire bed is

$$k_{overall} = \frac{U}{a_{mf} L_{mf}} \ln \frac{1}{1 - \bar{C}_N / C_s} \qquad (17)$$

$\bar{C}_H$ is the concentration of gas compound participating mass transfer at the exit of the last compartment. When operating conditions such as particle size, d, particle density, ρ_p, gas density and viscosity, ρ_f and μ_f, characteristics of the gas distributor, column diameter, D_R, bed height at incipient fluidization, L_{mf}, the diffusivity of transfering component, D_v, minimum fluidization velocity, U_{mf}, gas velocity, U, and the saturation concentration, C_s, are known, the computational procedure is as follows: Based on the procedure previously described (14), the expanded bed height, L, can be calculated. The first compartment is then computed using equation (7) and the concentration of gas at the exit of the first compartment is obtained by equation (8). The size of the n-th compartment is calculated by equation (9) and the volumes of the cloud, the bubble phase, and the emulsion phase for the n-th compartment are calculated by equations (11), (12) and (13) respectively. C_{bn} and C_{en} are calculated from $(C_b)_{n-1}$ and $(C_e)_{n-1}$ by equations (14) and (15). This procedure is continued until the bed height reaches L_{mf}. For bed height above L_{mf}, as indicated in the previous paper[14]

V_{cn}, V_{bn}, and V_{en} are calculated for the corresponding bed voidages. Equations (14) and (15) are then used to calculate the concentration at exit of the each compartment based on the entrance concentration of that compartment. This calculation is continued to the height equivalent to $L_{mf} + 2(L - L_{mf})$. The overall mass transfer coefficients can then be calculated from equation (18) and are compared with experimental data. The computational procedure for computer is shown in Table A-6. In Fig. A-17, solid-gas mass transfer coefficients in fluidized beds reported by the previous investigators are plotted in terms of $N_{sh}/(N_{sc})^{1/3}$ vs $N_{Rep}(d/L_f)^{0.6}$ following the correlation of the fixed bed mass transfer. (Here the data of Kettenring et. al.[15] can not be considered to have been obtained from the bed where height

Table A-6 Logic Diagram for Computer Simulation of Fluidized Bed Mass Transfer Operation

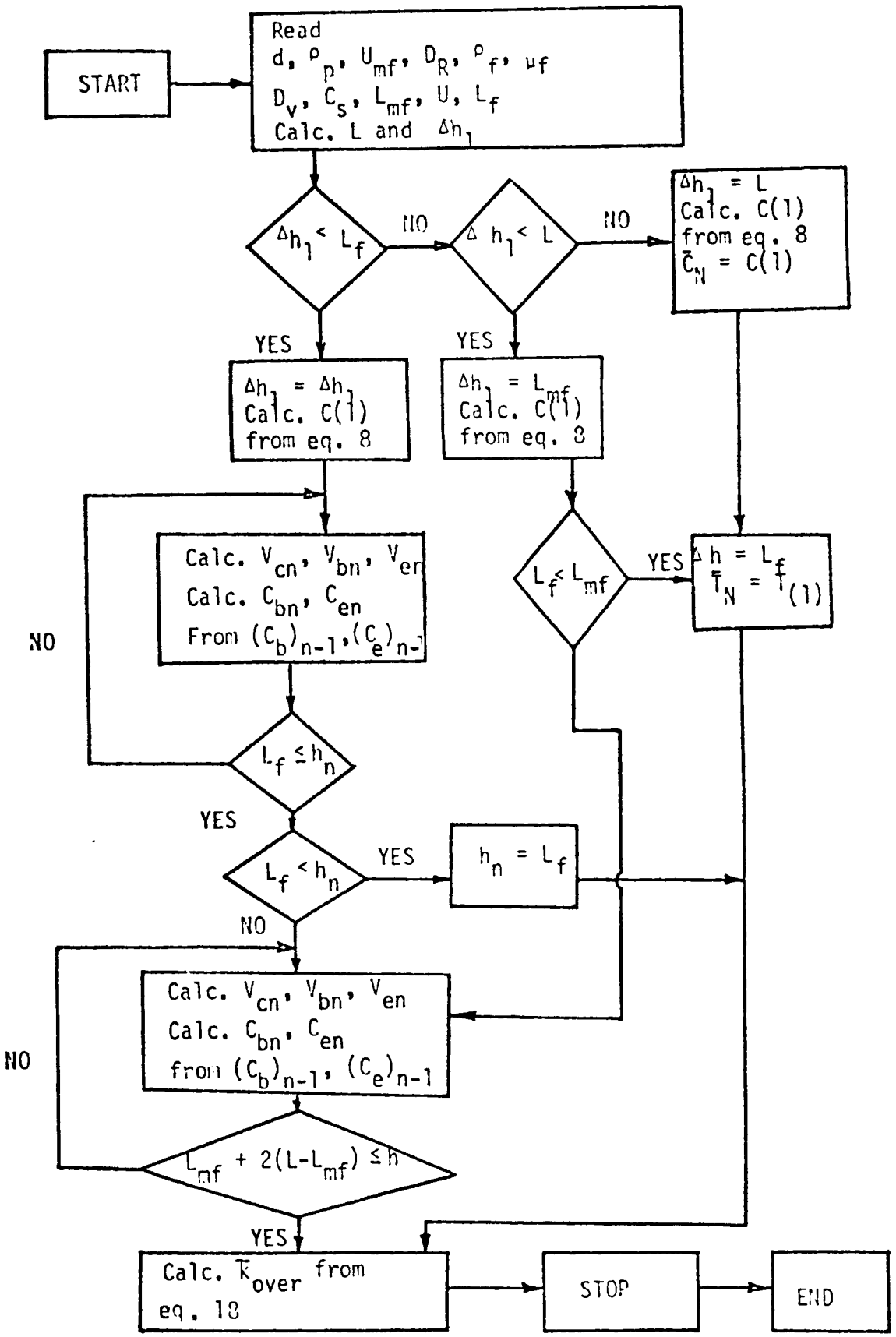

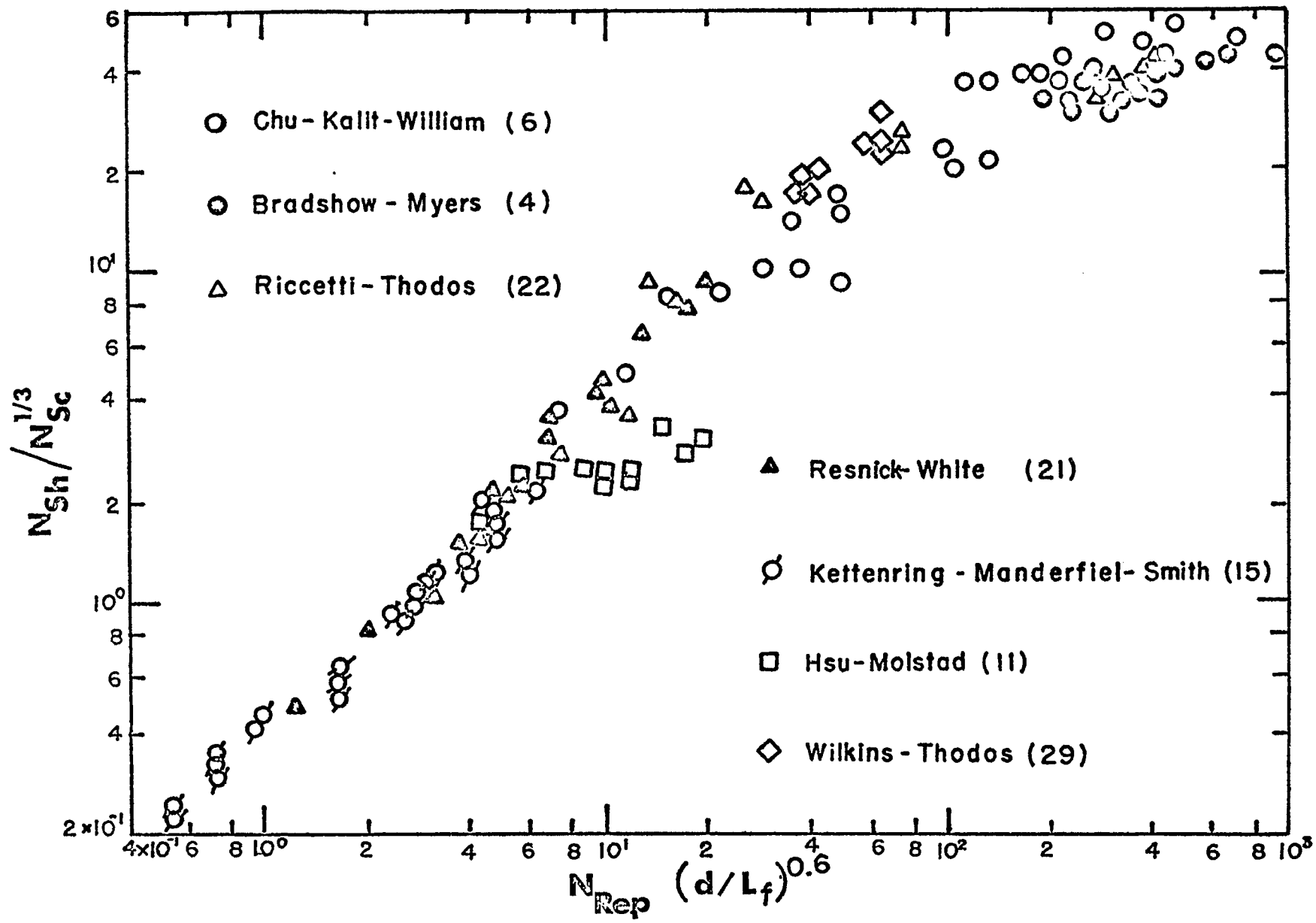

Figure A-17 Gas-Particle mass transfer in fluidized bed

First Compartment — Plug Flow

- Hsu - Molstad[11)]
- Bradshaw - Myers[4)]
- Resnick- White[21)]
- Kettenring - Manderfield - Smith[(15)]
- Riccetti- Thodos[22)]
- Chu - Kalil - Wetteroth[6)]

Both

Bubble and Emulsion Phase

$N_{Sh}/N_{Sc}^{1/3} = 0.72\ (N_{Rep}(d/L)^{0.6})^{0.95}$; $N_{Rep}(d/L)^{0.6} \leq 5$

$N_{Sh}/N_{Sc}^{1/3} = 1.25\ (N_{Rep}(d/L)^{0.6})^{0.63}$; $N_{Rep}(d/L)^{0.6} > 5$

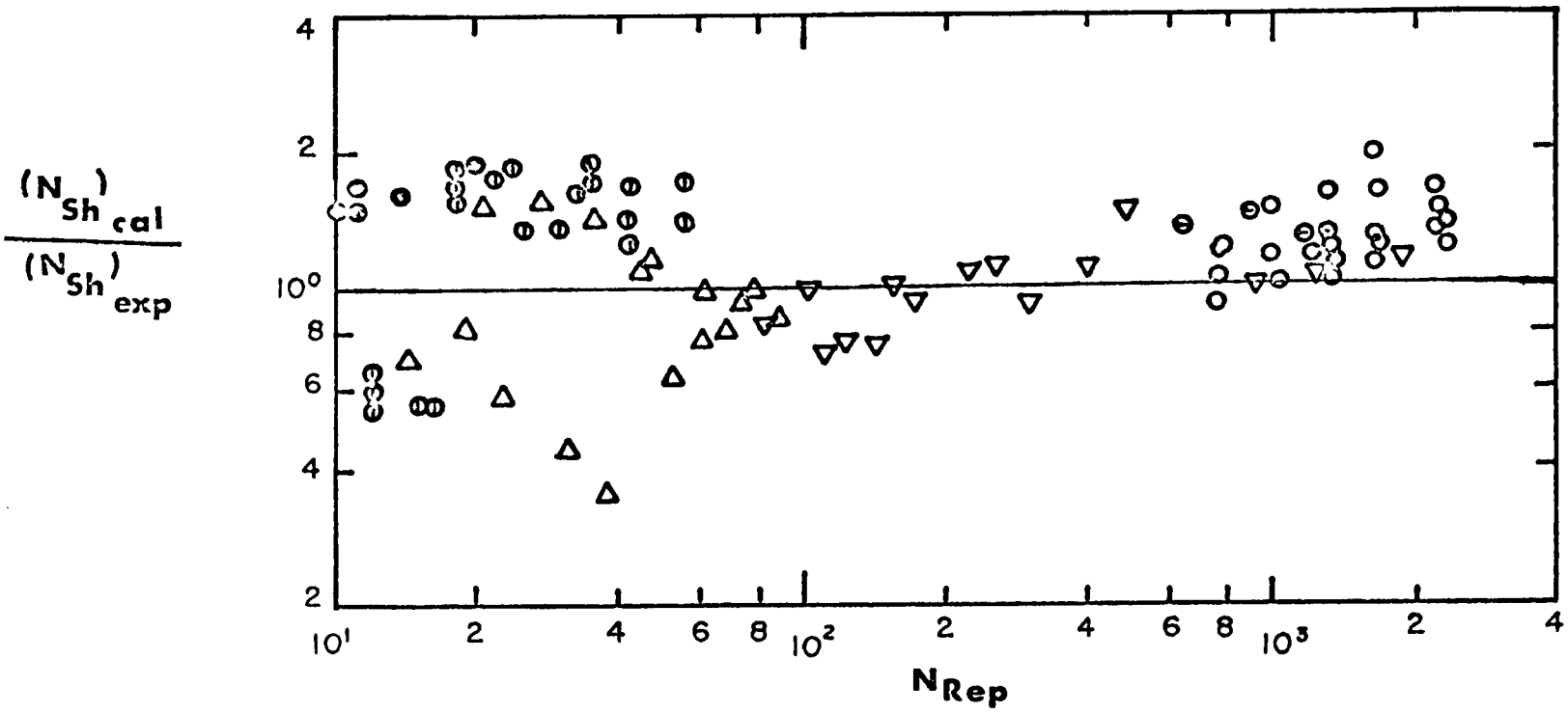

Figure A-18 Comparison of Experimental Sherwood Number with Calculated Sherwood Number

is totally effective to the mass transfer. From the concentration profile data reported,[15] an effective bed height of 3.8 cm is used for the calculation.)

In Fig. A-18 particle-gas mass transfer coefficients in fluidized beds calculated based on the "Bubble Assemblage" model are compared with the experimental values indicating satisfactory agreement.

2.5 Discussion

i. Particle-gas masstransfer in Fixed Bed

As indicated by equations (5) and (6), the Sherwood number in fixed beds operation is not only affected by the Reynolds number and the Schmidt number, but also affected by $(d/_L)$. This implies that for a given gas flow rate, the mass transfer coefficient, k_f, becomes smaller as the bed height becomes higher. This phenomenon may be explained as follows: According to the boundary layer theory[26], the thickness of fluid film is proportional to some power of Reynolds number and that the ratio of the mass boundary layer thickness to the momentum boundary layer thickness, δ_M/δ, is inversely proportional to some power of Schmidt number. Consequently with solid-gas systems for very low Reynolds number region the Schmidt number is also rather small (under normal operating conditions N_{sc} is less than 5), causing overlapping of the boundary layers and reducing the effective mass transfer surface area as shown in Fig. A-19. As the result, the surface area of the particles used to define mass transfer coefficient given in equation (3) is much larger than the actual effective surface area. This phenomenan becomes more accentuated as the bed height becomes taller and the bulk concentration of gas becomes higher or $(d/_L)$ becomes smaller. This fact can be seen from equations (5) and (6) more clearly as the effect of $(d/_L)$. At low Reynolds number the Sherwood number is seen to be proportional to 0.57 power while at higher Reynolds number, it is proportional to 0.378 power.

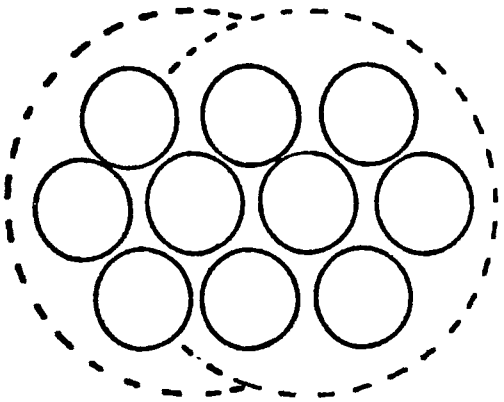

Gas-Solid System

Figure A-19a

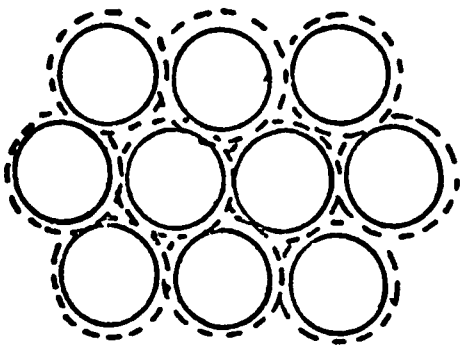

Liquid-Solid System

Figure A-19b

Figure A-19 Schematic Diagram Showing Relative Magnitude of the Mass Boundary Layer Thickness in Gas-Solid System and Liquid-Solid System

On the other hand, for liquid-solid systems, because the Schmidt numbers are usually very much larger than that of gas-solid systems, the mass boundary layer thickness is very thin even when the momentum boundary layer may be considerably thick. Therefore, for liquid-solid systems distinguishable individual films around the particles can exist without serious overlapping. The Sherwood number for liquid-solid systems converges close to the theoretical value of 2 as the Reynolds number becomes small.[30]

The above argument may be elaborated based on the boundary layer theory[26] as follows. The thickness of fluid boundary later on a flat plate can be approximated from Blasius' solution as

$$\frac{\delta}{\ell} = \frac{5}{\sqrt{N_{Re}}} \tag{18}$$

where $$N_{Re} = \frac{\ell \rho_f U}{\mu_f}$$

If the length of the flat plate, ℓ, is replaced by the particle diameter, d, by assuming that the fixed bed cosists of flat plates of length d, equation (18) becomes,

$$\frac{\delta}{d} = \frac{5}{\sqrt{N_{Rep}}} \tag{19}$$

Since the ratio of the mass boundary layer thickness and the momentum boundary layer thickness is given by

$$\delta_M/\delta = 1/(N_{Sc})^{\frac{1}{3}} \tag{20}$$

δ_M can be estimated from equations (19) and (20).

Table A-7 compares the mass boundary layer thickness for the liquid-solid system and the gas-solid system. As evident from the table, the mass boundary layer thickness for gas-solid systems is considerably

Table A-7

Comparison of the order of magnitude of mass boundary layer thickness in the liquid-solid system with that in the gas-solid system.

N_{Rep}	δ/d	Liquid (N_{sc} = 150) δ_M/d	Gas (N_{sc} = 2.5) δ_M/d
0.1	15.8	1.36	12.0
1	5	0.44	3.8
10	1.58	0.137	1.2
100	0.5	0.044	0.38

larger than that of liquid-solid systems and therefore when the Reynolds number is small, the effect on mass transfer becomes particularly important. Although the flow characteristics in a fixed bed must be greatly different from that approximated by equation (19), the general trend nevertheless must be considered to exist. It is noted that in equations (5) and (6), the Sherwood number can be related to 1/3 power of Schmidt number, even for the gas-solid system for which the Schmidt number range is rather low (N_{Sc} = 0.6~3.0).

Equations (5) and (6) can be applied to those mass transfer operation such as drying, adsorption, sublimation, etc. for which the exit concentration can be calculated. However, for catalytic reaction systems involving mass transfer, equations (5) and (6) must be applied with great caution. If the catalyst bed height in the reactor is used as L in equation (5) and (6), the mass transfer coefficient calculated can often become extremely small. This is because equations (5) and (6) are based on the experimental data which are obtained based on concentrations below the saturation concentration. In addition, since the effect of($^{d}/_{L}$) on the Sherwood number is due to the effective surface area for mass transfer as the bed approaches the saturation concentration, the bed height can not be directly used as L in equations (5) and (6).

ii Mass Transfer Between Gas and Particles in Fluidized Beds

In most of the fluid bed operations, very fine particles are employed resulting extremely large specific surface area of the particles. Since the gas diffusivity is also large, if a tall bed is employed in experimentation, the exit gas concentration would approach too close to the saturation concentration making accurate measurements of concentration very difficult. Consequently, many investigators measured mass transfer rate in a very shallow bed (L_{mf} = 1 to 3 cm). Under such conditions,

the bubbles are small and the gas flow patterns are similar to those in fixed beds. This may be seen in Fig.C-20 which shows the concentration profiles of the plug flow and that based on the "Bubble Assemblage" model for fluidized bed. The figure indicates the importance of the size of Δh_1 for the first compartment relative to the bed height. Therefore, the analysis based on the data obtained from a shallow fluidized bed can not be used to assess the applicability of the "Bubble Assemblage" model. It is nevertheless interesting to observe that the "Bubble Assemblage" model has the flexibility for adaptation to such a special case. Since the experimental data and correlations obtained by these previous investigators on mass transfer between gas and particles are not only restricted to shallow beds but also contain inheriting problems such as the distributor design and contacting efficiency, and the small diameter cloumn etc., it is dangerous to directly apply the equations for the design of a large commercial unit for which large bubbles above the distributor are possible, and a deep bed operation are often employed. Recently Kunii and Levenspiel[17] used the so-called "Bubbling Bed" model to analyze particle-gas mass transfer in fluidized beds. They employed Ranz-Marshall [20] equation for a single particle to estimate mass transfer coefficient in the bubble phase and the emulsion phase. For the bubble phase the particle terminal velocity is used as the relative velocity between the gas and the particles that exist in the bubble. For the emulsion phase U_{mf} is used to calculate the mass transfer coefficients. However, as discussed previously, under the experimental conditions of the reported investigations, it is not likely that the bubbles are large enough to reach the terminal velocity and that the mass transfer coefficient for emulsion phase particularly for very fine particles can be approximated by the expression of Ranz and Marshall

developed for a single particle. (The deviation of single particle behavior at low Reynolds numbers from fixed bed has already been demonstrated). In addition an average bubble diameter must be assumed which may introduce subjectiveness in the use of the bubbling bed model.

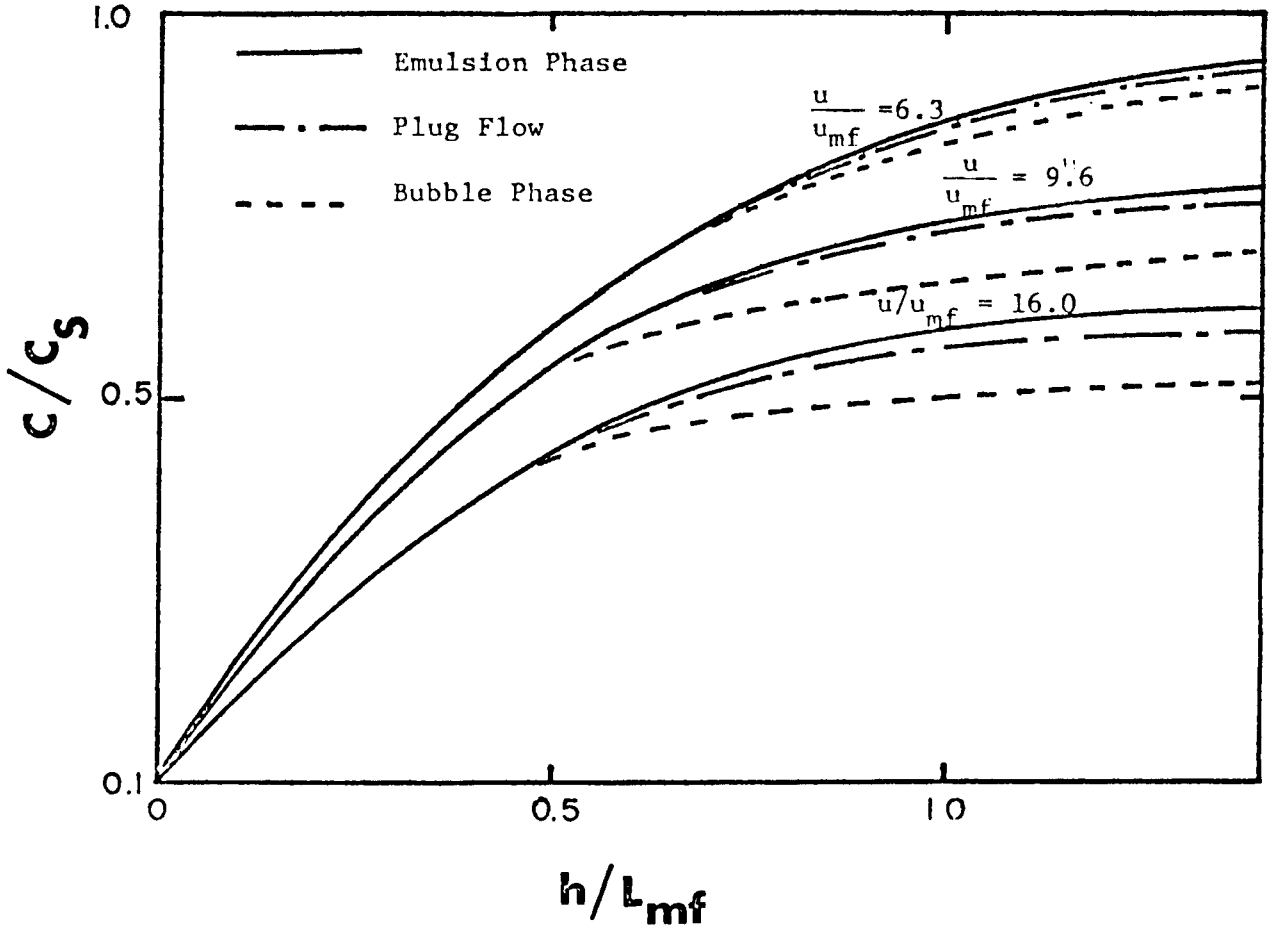

Figure A-20 Relation Between the Concentration Profile and the Bed Height

2.6 Conclusion

Experimental observation of sublimation of naphthalene from fixed beds together with the previously reported data of mass transfer in fixed bed indicate that the Sherwood number is affected not only by the Reynolds number and the Schmidt number but also by the $(^{d}/L)$ ratio particularly for low Reynolds number regions. The empirical correlations for fixed bed mass transfer are obtained and are given by equations (5) and (6). The mass transfer in fluidized bed is analyzed based on the "Bubble Assemblage" model and the limited value of the previous experimental data and correlations for use in design of large fluidized bed unit is demonstrated.

Notation

a = specific surface area of the particle [$^{1}/_{cm}$]

a_{mf} = specific surface area of the particle per unit volume of bed at minimum fluidization [$^{1}/_{cm}$]

A_s = total surface area of naphthalene particles [cm^2]

C = concentration of the transferring species in the bed [$^{g\ mole}/_{cc}$]

C_{bn} = concentration of the transferring species in bubble phase at n-th [$^{g\ mole}/_{cc}$]

C_{en} = concentration of the transferring specied in emulsion phase at n-th compartment [$^{g\ mole}/_{cc}$]

C_N = concentration of the transferring species at the outlet of the fluidized bed compartment [$^{g\ mole}/_{cc}$]

C_s = concentration of the transferring species at saturation [$^{g\ mole}/_{cc}$]

$C_{(1)}$ = concentration first compartment of the transferring at the outlet of the [$^{g\ mole}/_{cc}$]

d = particle diameter [cm]

D_b = bubble diameter [cm]

D_{bn} = bubble diameter at the n-th compartment [cm]

D_R = diameter of column [cm]

D_v = diffusivity of the transferring species [cm^2/sec]

F_{on} = gas interchange coefficient between bubble phase and emulsion phase at the n-th compartment [$^{1}/_{sec}$]

g = gravitational acceleration [$^{cm}/_{sec^2}$]

h = distance from the distributor [cm]

Δh_n = length of the n-th compartment [cm]

J_d = mass transfer factor [-]

k_f = fluid-particle mass transfer coefficient [$^{cm}/_{sec}$]

k_{fmf} = fluid-particle mass transfer coefficient at minimum fluidized velocity [$^{cm}/_{sec}$]

k_{fn} = fluid-particle mass transfer coefficient in bubble phase at n-th compartment [cm/sec]

$\bar{k}_{overall}$ = over-all mass transfer coefficient in the fluidized bed [cm/sec]

ℓ = length of flat plate parallel to the direction of flow [cm]

L = bed height [cm]

L_f = effective bed height [cm]

L_{mf} = bed height at minimum fluidization velocity [cm]

N = number of bubbles in n-th compartment [-]

q = total flow rate in the bed [cm^3/sec]

N_{Rep} = particle Reynolds Number = $\frac{d\rho_f U}{\mu_f}$ [-]

$N_{R\ell}$ = Reynolds Number of flat palte = $\frac{\ell U \rho}{\mu}$

N'_{Rep} = Modified particle Reynold Number $\frac{d\rho_f U}{\mu_f(1-\varepsilon)}$ [-]

N_{Sh} = Sherwood Number [-]

N_{Sc} = Schmidt Number [-]

S = cross sectional area in the bed

U = superficial gas velocity [cm/sec]

U_b = bubble rising velocity [cm/sec]

$\bar{U}_b$ = average bubble velocity in the bed [cm/sec]

U_{mf} = superficial gas velocity at minimum fluidization [cm/sec]

U_e = superficial gas velocity in the emulsion phase [cm/sec]

V_{bn} = volume of the bubble phase at the n-th compartment [cc]

V_{cn} = the cloud at the n-th compartment [cc]

V_{en} = the emulsion phase at the n-th compartment [cc]

W = weight of the naphthalene particles [g]

z = distance from the gas inlet [cm]

α = ratio of the volume of wake to volume of bubble [-]

γ_b = volume fraction of the particles in the bubble [-]

δ = momentum boundary layer thickness [cm]

δ_M = mass boundary layer thickness [cm]

ρ_p = particle density [g/cm^3]

ρ_f = fluid density [g/cm^3]

μ_f = fluid viscosity [g/cm sec]

ε = void fraction [-]

ε_{mf} = void fraction at Umf [-]

Literature

1. Acetis J. D. and Thodos, G., Ind.Eng.Chem. 52, 1003 (1960).

2. Akehata, T., Ph.D. Thesis, Tokyo Institute of Technology (1957).

3. Bar-Ilan, M. and Resnick W.,Ind.Eng.Chem. 49, 313 (1957).

4. Bradshaw, R. D. and Myers, J. E., A.I.Ch.E. Journal 9, No. 5, 590 (1963).

5. Bradshaw, R. D. and Bennett, C. O , A.I.Ch.E. Journal 7, No. 1, 48 (1961).

6. Chu, J. C., Kalil, J. and Wetteroth, W. A., Chem.Eng.Progr. 49-, No. 3 141 (1953).

7. Dryden, C. E., Strang, D. A. and Withrow, A.E., Chem.Eng.Progr 49, No. 4 191 (1953).

8. Gaffney, B. J. and Drew, T. B., Ind.Eng.Chem. 42, 1120 (1950).

9. Gamson, B. W., Thodos, G. and Hougen, O. A., Trans.A.I.Ch.E. 39, 1 (1943).

10. Hobson, M. and Thodos, G., Chem.Eng.Progr. 47, No. 7, 370 (1951).

11. Hsu, C. T. and Molstad, M. C., Ind.Eng.Chem. 47, No. 8, 1550 (1955).

12. Hurt, D. M., Ind.Eng.Chem. 35, No. 5, 522 (1943).

13. Ishino, T. and Otake, T., Kagaku Kogaku 15, 255 (1951).

14. Kato, K. and Wen, C. Y.,to be published in Chem.Eng.Sci.

15. Kettenring K. N., Manderfield, E. L. and Smith, J. M., Chem.Eng.Progr. 46, No. 3, 139 (1950).

16. Kobayashi, H., Arai, F. and Sunagawa, T., Chem.Eng.Japan 31, 239 (1967).

17. Kunii, D. and Levenspiel, O., Ind.Eng.Chem.Process Design and Develop 7, No. 4, 481 (1968).

18. McConnachie, J. T. L. and Thodos, G., A.I.Ch.E. Journal 9, No. 1, 60 (1963).

19. McCune, L. K. and Wilhelm, R. H., Ind.Eng.Chem. 41, 1124 (1949).

20. Ranz, W. E. and Marshall, W. R., Chem.Eng.Progr. 48, 173 (1952).

21. Resnick, W. and White, R. R., Chem.Eng.Progr. 45, No. 6, 377 (1949).

22. Riccetti, R. E. and Thodos, G., A.I.Ch.E. Journal 7, No. 3, 442 (1961).

23. Richardson, J.F ,. and Szekely, J., Trans.Instn.Chem.Engrs. 39, 212 (1961).

24. Sata, K., BUSEITEISU SUISAN HO, Maruzen Book Company, Tokyo, Japan (1955).

25. Satterfield, C. N. and Resnick, H., Chem.Eng.Progr. 50, No. 10, 505 (1954).

26. Schlichting, H., "BOUNDARY LAYER THEORY",McGraw-Hill Book Company, New York (1955).

27. Shirai, T., Ph.D. Thesis, Tokyo Institute of Technology.

28. Wilke, C. R. and Hougen, O. A., Trans.A.I.Ch.E. 41, 445 (1945).

29. Wilkins, G. S. and Thodos, G., A.I.Ch.E. Journal 15, No. 1, 47 (1969).

30. Wen, C.Y., Miller, E. and Fan, L.T. 140 ACS Meeting, Chicago, Illinois, Sept. 3-8, 1961.

3. Gas-Particle Heat Transfer in Fixed and Fluidized Bed

3.1 Introduction

Heat transfer between particles and gas in fixed beds and in fluidized beds is an important problem associated with many gas-solids operations such as coal gasification processes, heating and cooling of solid particles, catalytic reations etc. Many experimental investigations have been conducted to evaluate heat transfer coefficient in fixed beds; some used heat generating particles as packings, some employed evaporation of material from porous particles and others used the technique of dynamic response of thermal conductivities to measure the heat transfer coefficient. The data thus obtained are usually correlated in terms of J_H factor or Nusselt number and Reynolds number plot. Although a few correlations have been proposed, agreement is far from satisfactorly when the particle Reynolds number is very small. At low Reynolds numbers, the heat transfer coefficient becomes considerably lower than the value calculated from single particle heat transfer in stagnant fluid ($N_{Nu} = 2.0$). In the previous paper[9] the following correlations were proposed for particle-gas mass transfer in fixed beds.

$$N_{sh}/(N_{sc})^{1/3} = 0.72 \left[N_{Rep} \cdot (d/L)^{0.6} \right]^{0.95} \qquad (1)$$

$$\text{for } 0.1 \leq N_{Rep}\,(d/L)^{0.6} \leqq 5.0$$

$$N_{sh}/(N_{sc})^{1/3} = 1.25\left[N_{Rep}\cdot(d/L)^{0.6}\right]^{0.63} \qquad (2)$$

$$\text{for } 5 < N_{Rep}\,(d/L)^{0.6} < 10^3$$

As indicated by equations (1) and (2), the mass transfer between particle and gas in fixed bed when expressed in terms of Sherwood number is found to be not only the function of the Reynolds number and Schmidt number but also affected by (d/L) ratio.

In this paper an attempt is made to correlate the published data on heat transfer in gas-solid fixed beds based on the similar point of view as presented in the mass transfer study and to extend this analysis into fluidized bed heat transfer operation based on the "Bubble Assemblage" model. The results are then compared with the available experimental data.

3.2 Gas-Particle Heat Transfer in Fixed Beds

Experimental investigations of heat transfer between gas and particles in fixed beds are summarized in Table C-8.

Based on an analogy between heat and mass transfer in fixed bed operations, the experimental data for heat transfer are correlated in terms of $N_{Nu}/(N_{Pr})^{1/3}$ and $N_{Rep}(d/L)^{0.6}$ as shown in Fig.A-21 . Empirical equations obtained based on Fig. A-21 are

$$N_{Nu} = 0.72\,(N_{Pr})^{1/3}\left[N_{Rep}\,(d/L)^{0.6}\right]^{1.1} \qquad (3)$$

$$\text{for } 0.01 \leq N_{Rep}\,(d/L)^{0.6} \leq 5$$

$$N_{Nu} = 1.5\,(N_{Pr})^{1/3}\left[N_{Rep}\,(d/L)^{0.6}\right]^{0.63} \qquad (4)$$

$$\text{for } 5 < N_{Rep}\,(d/L)^{0.6} < 10^3$$

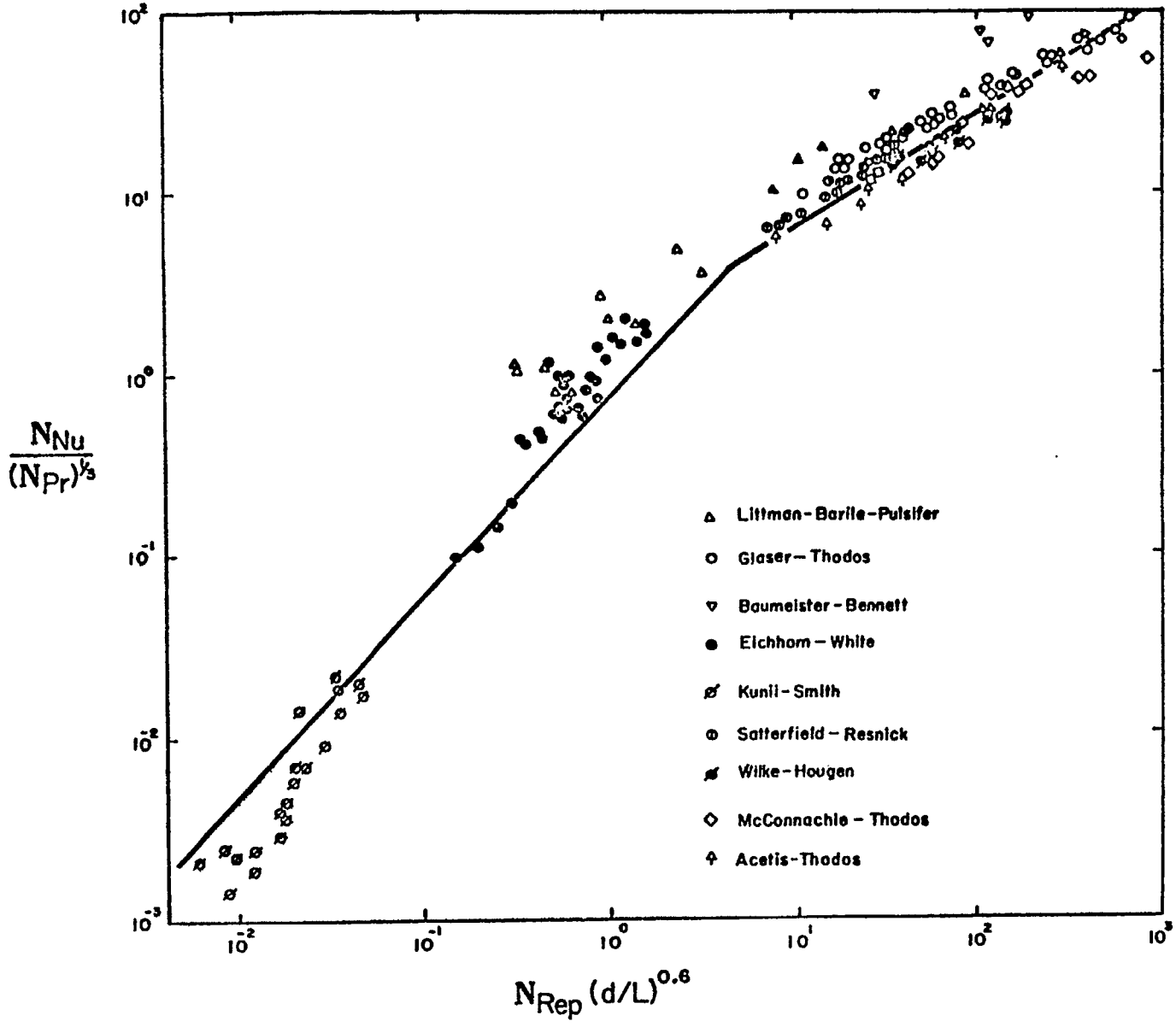

Figure A-21. Fluid-Particle Heat Transfer in Fixed Bed

3.3 Application of the "Bubble Assemblage" Model for Heat Transfer Between Gas and Particles in Fluidized Beds

The "Bubble Assemblage" model has been proposed to represent flows in fluidized beds for catalytic reactions[8] and for mass transfer operations [9]. Here this model is applied to particle-gas heat transfer in fluidized beds for prediction of heat transfer coefficients which are then compared with the experimental data.

Since the detail of the "Bubble Assemblage" model has been presented,[8] a brief summary of assumptions and computational procedures necessary for heat transfer operations in fluidized beds are presented below.

i. The heat transfer coefficient in the bubble phase between the particles and gas is assumed to be the same as that for fixed beds at a velocity equivalent to U_b, the bubble velocity.

ii. The particle-gas heat transfer in the emulsion phase is assumed to be the same as that in the fixed bed at a velocity equivalent to U_{mf}.

iii. Since the rate of heat transfer between the gas and the particles is usually much faster than the rate of catalytic chemical reactions, in order to maintain a substantial temperature difference between the gas and the particle, a shallow bed of only a few cm. is usually employed in the experimentation. Consequently, as in the previous paper[9], the first compartment for the "Bubble Assemblage" model must be determined with caution. As in the previous paper the following condition is selected.

$$U_b - U_{mf}/\varepsilon_{mf} = 0.1\, U_{mf}/\varepsilon_{mf}$$

Based on the following relations for the bubble velocity and bubble diameter,

Table A-8 Summary of Previous Investigations on Gas-Particle Heat Transfer in Fixed Beds

Authors	Fluid Material	N_{Pr}(-)	Particle Material	Particle Diameter [cm]	d/L(-)	Range of Reynolds Number $\left(\frac{d\rho_f U}{\mu_f}\right)$	Experimental Method
Satterfield[16] -Resnik	air	0.708	Catalyst	0.508	0.216 ~ 0.267	22~150	Evaporation of H_2O_2 from the particle
Wilke[19] -Hougen	air	0.705	Celit Pellets	0.385 ~ 2.17	0.35 ~ 0.46	45~200	Evaporation of water from wet particles
McConnachie[14] -Thodos	air	0.75	Silica Sphere	1.585	0.225 ~ 1.12	55~1050	Evaporation of water from the wet particles
Actic[1] -Thodes	air	0.708	Celit Sphere	1.585	0.20 ~ 1.00	16~1000	Evaporation of water from the wet particles
Littman[13] Barile Pulsifer	air	0.708	Copper, Glass, Lead	0.0503 ~ 0.203	0.012 ~ 0.102	2 ~ 100	Dynamic thermal conductivities of the fixed bed

Table A-8 Summary of Previous Investigations on Gas-Particle Heat Transfer in Fixed Beds (Cont.)

Authors	Fluid Material	N_{Pr} (-)	Particle Material	Particle Diameter [cm]	d/L(-)	Range of Reynolds Number $(\frac{d \rho_f U}{\mu_f})$	Experimental Method
Glaser[5] -Thodos	air H_2 CO_2	0.71 0.716 0.665	Brass, Steel	0.476 ~ 0.794	0.094 ~ 0.156	44 ~ 1600	Heating the particles by passing the electric current through the particles
Baumeister[2] -Bennett	air	0.71	Steels	0.395 ~ 0.95	0.0389 ~ 0.0927	200 ~ 5000	Heating the particle by a high-frequency induction coil
Eichhorn[4] -White	air CO_2	0.71 0.665	Dowe X-50	0.0278 ~ 0.0658	0.008 ~ 0.02	2 ~ 19	Dielectric heating of particles
Kunii[11] -Smith	air	0.71	Sand, Glass Beads	0.024 ~ 0.102	0.00144 ~0.01335	0.02 ~ 0.9	Axial temperature profile in fixed bed at steady state

$$U_b = 0.71 \sqrt{gD_B} \qquad D_B = 1.4\ \rho_P\ d\ \left(\frac{U}{U_{mf}}\right)\ h$$

the height of the first compartment becomes

$$\Delta h_1 = \frac{(1.1\ U_{mf}/\varepsilon_{mf})^2}{0.707\, g\, \rho_P\ d\ U/U_{mf}} \tag{5}$$

iv. Since in the first compartment, the sizes of bubbles are small and the interchange of gas between the bubble phase and the emulsion phase is believed to be great, the flow pattern can be approximated by a plug flow.

v. The maximum bed expansion is assumed to be attained when bubble volume reaches 50% of the bed volume.

vi. Due to the vigorous movement of the particle in the bed, the temperature of the particles in the bed is assumed to be uniform.

vii. The interchange of particles between the two phases is so rapid that the temperature of particles in the bubble phase can be assumed to be the same as that in the emulsion phase.

Under the above assumptions, let us compute the heat transfer coefficients based on this model. Although there are a number of ways by which the heat transfer coefficients may be evaluated, here we consider the steady state heating of the particles by the gas.

The temperature of the gas at the exit of the first compartment is

$$T_{(1)} = T_s - (T_s - T_o)\ \exp\left[-\frac{h_f\ A\Delta h_1}{U\ C_{pf}\ \rho_f}\right] \tag{6}$$

where $A = 6(1 - \varepsilon)/d$

The heat transfer coefficient h_f in equation (6) can be calculated from equations (3) and (4) for fixed bed at a Reynolds number N_{Rep} corresponding to the superficial velocity U.

The temperature $T_{(1)}$ is then taken as that of the gas in the bubble phase and the emulsion phase entering the second compartment. The sizes of the n-th compartment, of the cloud of the bubble and of the emulsion phase are calculated as indicated in the previous paper[8]. Also, the gas interchange coefficient between the two phases is estimated as shown in the previous paper[8].

The heat balance of the gas in the bubble phase across the n-th compartment can be obtained from,

$$S\,(U - U_e)\,C_{Pf}\,\rho_f\,T_{bn} = C_{Pf}\,\rho_f\,V_{bn}\,F'_{on}\,(T_{en} - T_{bn})$$
$$+ A_{mf}\,h_{bn}\,V_{en}\,(T_s - T_{bn}) + S\,C_{Pf}\,\rho_f\,(U - U_e)\,T_{b(n-1)} \qquad (7)$$

The heat balance of the gas in emulsion phase across the n-th compartment can be written as

$$SU_e\,C_{Pf}\,\rho_f\,T_{en} = A_{mf}\,h_{en}\,V_{en}\,(T_s - T_{en}) + SU_e\,C_{Pf}\,\rho_f\,T_{e(n-1)}$$
$$- C_{Pf}\,\rho_f\,V_{en}\,F'_{on}\,(T_{en} - T_{bn}) \qquad (8)$$

h_{bn} and h_{en} in equations (7) and (8) are obtained from equations (3) and (4) by substituting U_{bn} and U_{mf} into the velocity term in N_{Rep}, respectively. Also A_{mf} is the specific surface area of the particle at the gas velocity U_{mf} or $A_{mf} = \frac{6\,(1-\varepsilon_{mf})}{d}$. Consequently, T_{bn} and T_{en} can be calculated from $T_{b(n-1)}$, $T_{e(n-1)}$ from equations (7) and (8) respectively. The following boundary conditions is used:

$$T_{e1} = T_{b1} = T_{(1)}$$

The overall heat transfer coefficient for the entire bed becomes,

$$(h_f)_{over} = \frac{U\, C_{Pf}\, \rho_f}{A_{mf}\, L_{mf}} \cdot \ln \frac{T_s - T_o}{T_s - \bar{T}_n} \qquad (9)$$

$\bar{T}_n$ is the average gas temperature at the exit of the last compartment.

The computational procedure is as follows. Knowing the particle diameter, d, particle density ρ_p gas properties, C_{Pf}, ρ_f, μ_f k_g, the minimum fluidization velocity U_{mf}, gas velocity, U, the bed diameter D_r, incipient bed height L_{mf}, characteristics of gas distributor, the inlet gas temperature, T_o, and the particle temperature, the following quantities can be calculated; the bed expansion, L, as shown in the previous paper[8], the exit gas temperature from the first compartment from equation (6), $T_{b(n-1)}$, $T_{e(n-1)}$, T_{bn} and T_{en} calculated by repeated use of equations (7) and (8). The overall heat transfer coefficient can be calculated finally from equation (9).

A complete logic diagram describing the computational procedure, in determining heat transfer coefficients in a fluidized bed is presented in Table A-9.

In Fig. A-22 most of the published experimental data on particle-gas heat transfer in fluidized beds are plotted in terms of $N_{Nu}/(N_{Pr})^{1/3}$ and N_{Rep}. As is seen from the figure, the data of Wamsley and Johanson[18] are about an order of magnitude smaller than the most of other investigators. Among the various possible reasons attributed to the deviations of their data, their assumption of the complete mixing of the gas for the calculation of heat transfer coefficient is probably most significant. Thus the data of

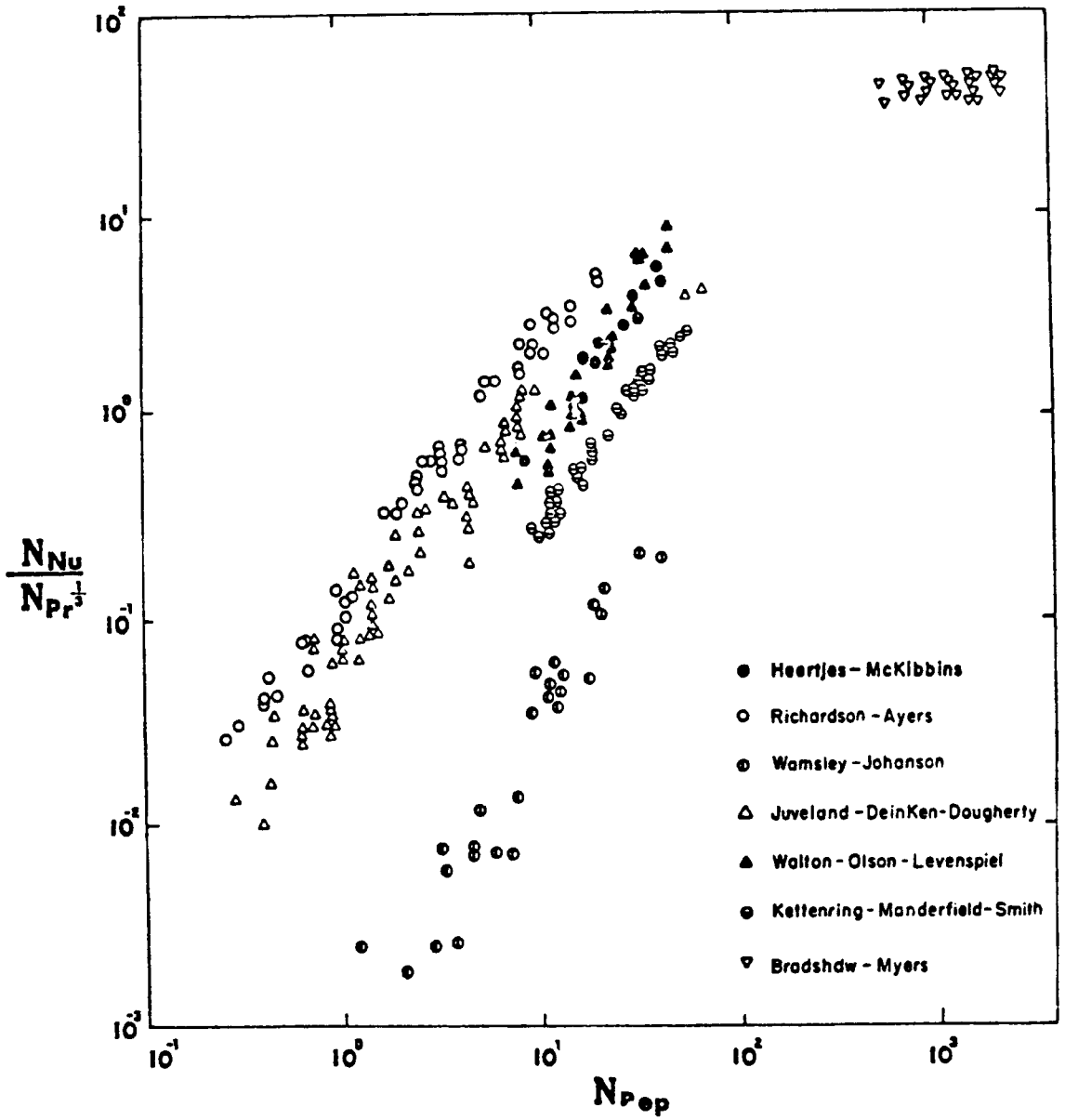

Figure A-22 Gas-Particle Heat Transfer in Fluidized Bed

Wamsley and Johanson will be eliminated from consideration for the time being. In Fig A-23 the experimental data on fluidized gas-solid heat transfer coefficient are plotted in terms of $N_{Nu}/(N_{Pr})^{\frac{1}{3}}$ v.s. $N_{Rep}\ (d/L_f)^{0.6}$. The effective bed heights L_f appearing in Fig.A-23 for the data of Kettenring et.al.[10], and Herrtjes and McKibbins[6] are approximated from their experimental values as 3.8cm and 1.2cm respectively. L_f for the data of Walton et.al.[17] is based on their experimental values of 0.572cm and 0.826cm. The rest of the experimental investigations is based on the value of L_{mf} reported.

Comparison of Fig. A-22&23 indicated that Fig. A-23 is a much better correlation than Fig.A-22. In Fig.A-24, the gas particle heat transfer coefficients in fluidized beds estimated based on the "Bubble Assemblage" model are compared with the experimental data. The agreement between the estimated values and the experimental data is generally good except those of Javeland et.al[7].

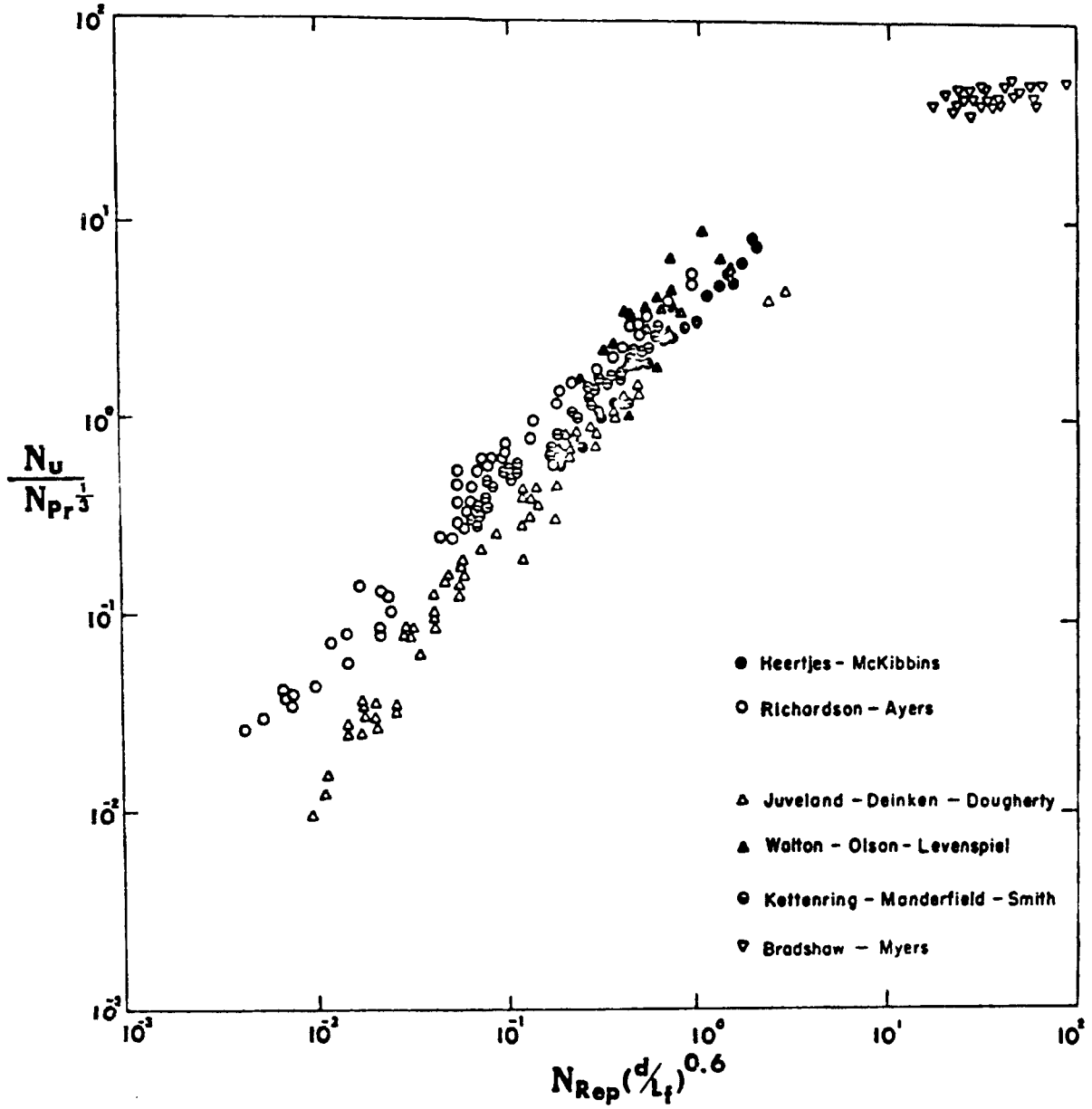

Figure A-23 Gas-Particle Heat Transfer in Fluidized Bed Correlated with d/L_f

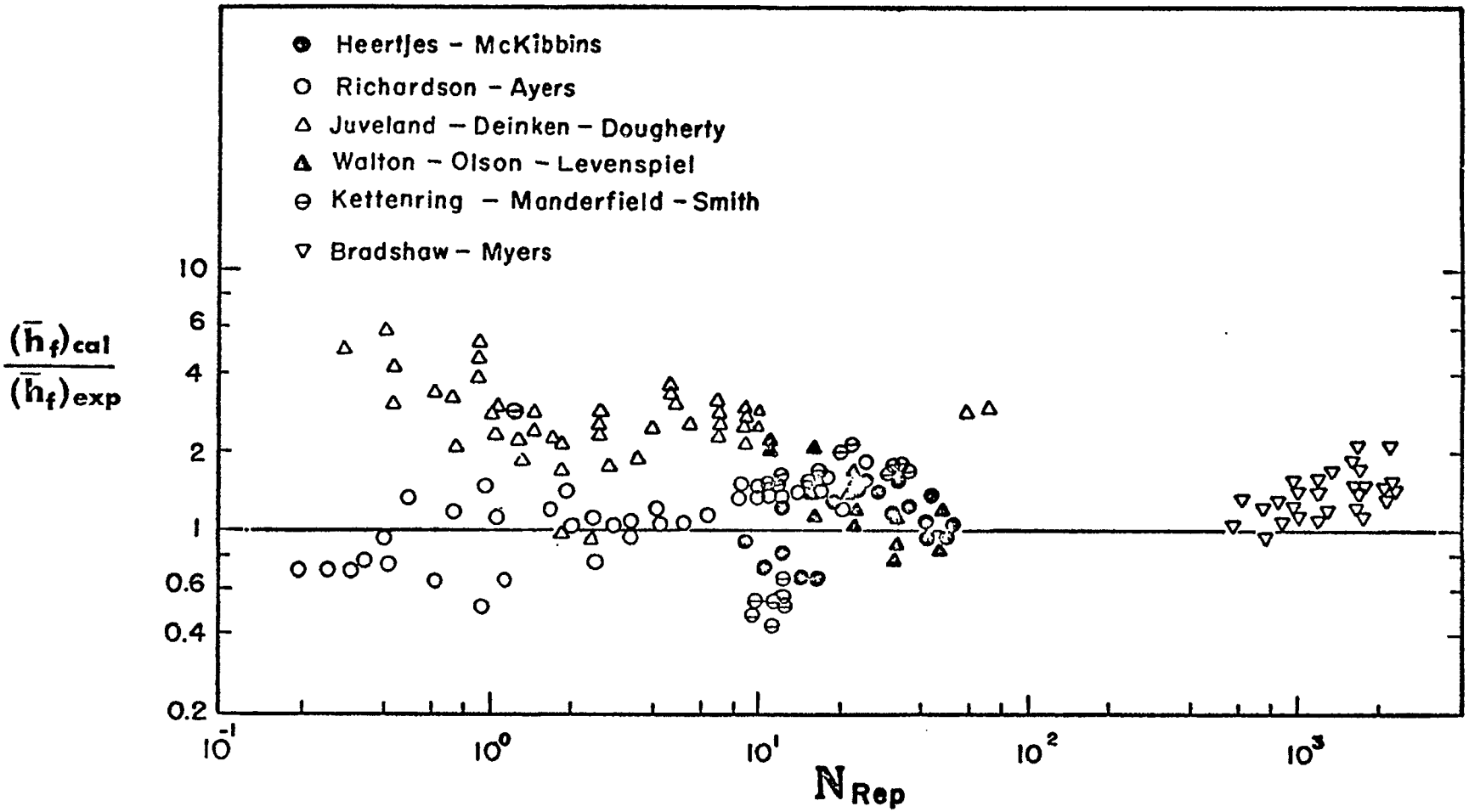

Figure A-24 Comparison of Experimental Heat Transfer Coefficient with Calculated Values

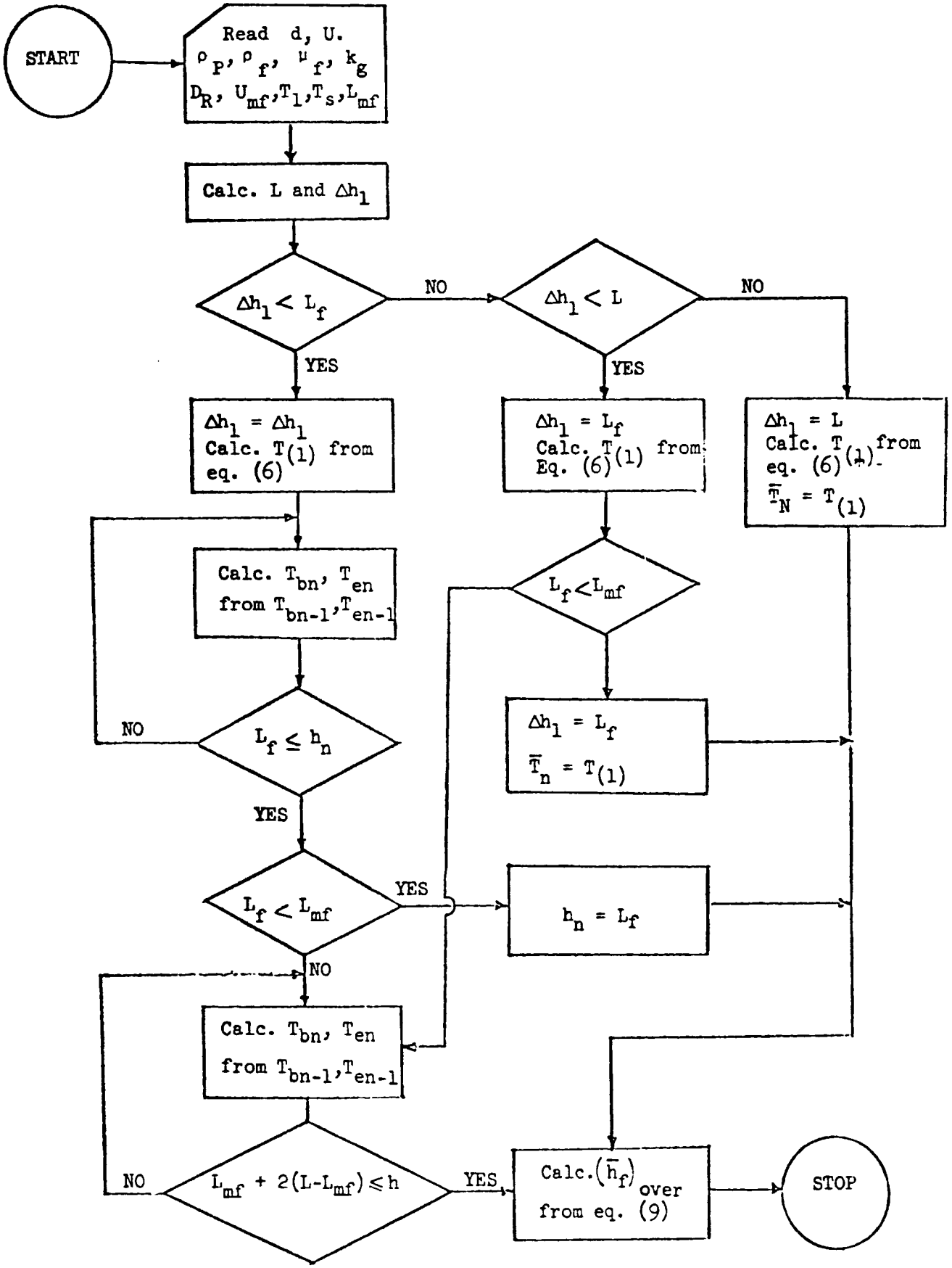
START
Read d, U. ρ_p, ρ_f, μ_f, k_g D_R, U_{mf}, T_1, T_s, L_{mf}
Calc. L and Δh_1
$\Delta h_1 < L_f$
NO
$\Delta h_1 < L$
NO
YES
YES
$\Delta h_1 = \Delta h_1$ Calc. $T_{(1)}$ from eq. (6)
$\Delta h_1 = L_f$ Calc. $T_{(1)}$ from Eq. (6)
$\Delta h_1 = L$ Calc. $T_{(1)}$ from eq. (6) $\bar{T}_N = T_{(1)}$
Calc. T_{bn}, T_{en} from T_{bn-1}, T_{en-1}
$L_f < L_{mf}$
NO
$L_f \leq h_n$
YES
$\Delta h_1 = L_f$ $\bar{T}_n = T_{(1)}$
$L_f < L_{mf}$
YES
$h_n = L_f$
NO
Calc. T_{bn}, T_{en} from T_{bn-1}, T_{en-1}
NO
$L_{mf} + 2(L-L_{mf}) \leq h$
YES
Calc. $(\bar{h}_f)_{over}$ from eq. (9)
STOP

3.4 Discussion

The Nusselt number for heat transfer between gas and particles in fixed bed has been shown as in equations (3) and (4) to depend not only on the particle Reynolds number and the Prandtl number but also on the ratio of the particle diameter to the bed height, $^{d}/_{L}$. Assuming an analogy between heat and mass transfer in fixed bed operations to hold, as discussed in the previous paper on gas-solid mass transfer in fixed beds[9], the individual thermal boundary layer for heat transfer does not exist particularly for low Reynolds number and small Prandtl number regions. This is because the thermal boundary layer thickness is much larger than the diameter of the particle causing overlapping of the thermal boundary layers in a multiparticle system thereby reducing effective surface area for heat transfer. Consequently the calculation based on heat transfer surface area: $6(1-\varepsilon)\,{}^{SL}/_{d}$, gives a much greater surface than the actual effective heat transfer area. As shown in Fig. A-22 the Nusselt number thus becomes considerably smaller than the theoretical value of 2 for a single particle in a stagnant gas when Reynolds number becomes very small.

The serious problem associated with the experiment in obtaining heat transfer coefficients between gas and particles in a fluidized bed is the accuracy of temperature measurement. The thermocouples inserted along the bed axis probably neither indicates the gas temperature nor the solid particle temperature. The assumption normally employed concerning the uniformity of particle temperature may not be valid in many instances. The location of thermocouples near the distributor and close to the flange causes the heat loss which is difficult to accurately estimate. These are some of the reasons which make the disagreement of the experimental data among the investigators. Under normal fluidized bed operation, the particle diameter

is quite small resulting a large specific surface area. Thus, to avoid experiments too close to the thermal equilibrium, bed temperatures are usually measured at very shallow positions of the bed.

The analysis of such data based on the "Bubble Assemblage" model some times results in the effective bed height, L_f, smaller than the height of the first compartment, Δh_1. For example, the bed height of Walton et.al. (L_f = 0.57 - 0.83cm), those of Juveland (L_f = 0.35 - 1.3cm), and those of Richardson and Ayers (L_f = 0.18 - 0.22cm) are all smaller than Δh_1. This implies that the estimation of heat transfer coefficient based on the "Bubble Assemblage" model is identical with that based on a simple plug flow model. Even for other cases in which the effective bed height, L_f, is larger than Δh_1, the first compartment occupied a large fraction of the total bed height.

In other words, most of the experimental data previously reported are limitted to the special type of operations in which the bubbles are rather small and distinct clouds associating with the bubbles either do not exist or exist only near the top of the bed. Hence, the application of a correlation based on such data directly to industrial size unit in which large size bubbles could exist immediately above the gas distributor may cause disastrous plant operation. Since the distinct cloud boundary around the bubble will isolate the bubble phase from the emulsion phase, a sharp temperature difference could exist between the two phases. For an exothermic reaction, this could cause high solid particle temperature and the high gas temperature in the emulsion phase, but relatively low temperature of the gas in the bubble rising through the bed.

Therefore analysis of such a reactor must be performed with caution.

The poor agreement between the values of heat transfer coefficients predicted from the model and the experimental data of Juveland et.al.[7] is probably due to the channeling of gas through the center of the bed evidenced by the low pressure drop of the gas distributor. In addition, because of the relatively high temperature employed in the experiment, heat loss could have been considerable and therefore the temperature uniformity of the particles assumed by them is doubtful.

Recently Kunii and Levenspiel[12] used their bubbling fluidized bed model to illustrate the phenomena of heat transfer in fluidized beds. Their model is useful in understanding many aspects of fluidized bed heat transfer operations.

Notation

A = specific surface area of the particle per unit volume of bed $(^{1}/_{cm})$

A_{mf} = specific surface area of the particle per unit volume of bed at minimum fluidization $(^{1}/_{cm})$

C_{pf} = heat capacity of particles $(cal/g°c)$

D_B = bubble diameter (cm)

D_r = bed diameter (cm)

d = particle diameter (cm)

F_{on} = gas interchange coefficient at the n-th compartment $(^{1}/_{sec})$

g = gravitational acceleration $(^{cm}/_{sec^2})$

h = distance from the distributor (cm)

h_{bn} = heat transfer coefficient in the bubble phase at n-th compartment $(^{cal}/_{cm^2\ sec°c})$

h_{en} = heat transfer coefficient in the emulsion phase at n-th compartment $(^{cal}/_{cm^2\ sec°c})$

h_f = heat transfer coefficient in the first compartment $(^{cal}/_{cm^2\ sec°c}$

$(h_f)_{over}$ = calculated over-all heat transfer coefficient in the fluidized bed $(^{cal}/_{cm^2\ sec°c}$

$(h_f)_{exp}$ = experimental over-all heat transfer coefficient in the fluidized bed $(^{cal}/_{cm^2\ sec°c}$

Δh_1 = length of the first compartment (cm)

k_g = thermal conductivity of the gas $(^{cal}/_{cm\ sec°c}$

L = bed height (cm)

L_f = effective bed height for heat transfer (cm)

Notation (Cont.)

L_{mf}	=	bed height at minimum fluidized velocity	(cm)
N_{Nu}	=	Nusselt Number $(h_f\, d/k_g)$	(-)
N_{Pr}	=	Prandtl Number $(C_{Pf}\, \mu_f/k_g)$	(-)
N_{Rep}	=	Reynolds Number $\dfrac{(d\, U\, \rho_f)}{\mu_f}$	(-)
N_{Sc}	=	Schmidt Number $\dfrac{(\mu_f)}{\rho_f\, D_v}$	(-)
S	=	cross sectional area in the bed	(cm^2)
T_{bn}	=	gas temperature in the bubble phase at n-th compartment	(°c)
T_{en}	=	gas temperature in the emulsion phase at n-th compartment	(°c)
$\overline{T}_n$	=	gas temperature of the outlet of the bed	(°c)
T_s	=	temperature of the particle	(°c)
$T_{(1)}$	=	gas temperature at the outlet of the first compartment	(°c)
T_o	=	inlet gas temperature	(°c)
U	=	superficial gas velocity	(cm/sec)
U_b	=	bubble rising velocity	(cm/sec)
U_e	=	superficial gas velocity in the emulsion phase	(cm/sec)
U_{mf}	=	superficial gas velocity at incipient fluidization	(cm/sec)
V_{bn}	=	volume of the bubble phase at the n-th compartment	(cc)
V_{cn}	=	volume of the cloud at the n-th compartment	(cc)
V_{en}	=	volume of the emulsion phase at n-th compartment	(cc)
ρ_f	=	fluid density	(g/cm^3)
μ_f	=	fluid viscosity	(g/cm sec)
ε	=	void fraction	(-)
ε_{mf}	=	void fraction at minimum fluidization	(-)

Literature

1. DeAcetis, J. D. and Thodos, G.
Ind. Eng. Chem. 52 1003 (1960)

2. Baumeister, E. B. and Bennett, C. O.
A.I.Ch.E. Journal 4 No. 1 69 (1958)

3. Bradshaw, R. D. and Myers, J. E.
A.I.Ch.E. Journal 9 No. 5 590 (1963)

4. Eichhorn, J. and White, R. R.
Chem. Eng. Prog. Simp. Series 48 No. 4, 11 (1952)

5. Glaser, M. B. and Thodos, G.
A.I.Ch.E. Journal 4 No. 1 63 (1958)

6. Heertjes, P. M. and McKibbins, S. W.
Chem. Eng. Sci. 5 161 (1956)

7. Juveland, A. C. , Deinken, H. P. and Dougherty, J. E.
I.E.C. Fundamentals 3 No. 4 329 (1964)

8. Kato, K. and Wen, C. Y.
to be published in Chem. Eng. Sci.

9. Kato, K. , Wen, C. Y. , Kubota, H.
to be published

10. Kettenring, K. N. , Manderfield, E. L. and Smith, J. M.
Chem. Eng. Prog. 46 No. 3 139 (1950)

11. Kunii, D. and Smith, J. M.
A.I.Ch.E. Journal 7 No. 1 29 (1961)

12. Kunii, D. and Levenspiel, O.
Ind. Eng. Chem. Process Design and Development 7 No 4 481 (1968)

13. Littman, H. , Barile, R. G. and Pulsifer, A. H.
I.E.C. Fundamentals 7 554 (1968)

14. McConnachie, J. T. L. and Thodos, G.
A.I.Ch.E. Journal 9 No. 1 60 (1963)

15. Richardson, J. F. and Ayers, P.
Tran. Inst. Chem. Eng. 37 314 (1959)

16. Satterfield, C. N. and Resnick, H.
Chem. Eng. Prog. 50 505 (1954)

17. Walton, J. S. , Olson, R. L. and Levenspiel, O.
Ind. Eng. Chem. 44 No. 6 1475 (1952)

18. Wamsley, W. W. and Johanson, L. N.
Chem. Eng. Prog. 50 No. 7 347 (1954)

Literature (Cont.)

19. Wilke, C. R. and Hougen, O. A.
Trans. Am. Inst. of Chem. Eng. 41 445 (1945)

20. Chang, T. M. and Wen, C. Y.
CEP Symposium Series, No. 67 Vol. 62, p 11 (1966)

4. Noncatalytic Solid-Gas Reaction in a Fluidized Bed Reactor

4.1 Introduction

Since the fluidized bed has been commercially applied to the gasification of coal, this technique has been used for a number of other chemical processes. However, owing to the complex gas and solid flow patterns within the fluidized beds, design procedure has not been well established.

Researches in recent years have provided a good understanding of the phenomena associated with bubbles in fluidized beds. Kunii and Levenspiel[6] proposed the bubbling bed model in order to analyze the various phenomena within the bed based on one parameter-the effective size of bubbles. Although this model is very useful for elucidating the performance of a fluidized bed reactor, one difficult problem still remains, i.e. the problem of how to predict the effective bubble diameter, since the bubble vary in its size during the rise through the bed.

Kato and Wen[3] proposed the bubble assemblage model for the catalytic reactions and showed the possibilities of removing this difficulties by taking into account the bubble growth and coalescence.

With a continuous feed of solids into a fluidized reactor, the outgoing stream of solids consist of particles of different ages and degrees of conversion. The average conversion of this stream is thus dependent on two factors, namely the rate of reaction of individual particles in the reactor environment and the flow characteristics of solids in the reactor. The conversion level of solids is dependent on the gas-phase environment and therefore must be determined simultaneously. Kunii and Levenspiel showed in their book[6] a procedure to predict the conversion of both gas and solids leaving the bed, using roasting of ZnS as an example. They assumed that the solids mixing is complete in the bed. However, this assumption may

not be realistic particularly when the aspect ratios and solids throughput are high.

Based on the relation derived from the above two models, an attempt is made to simulate the fluidized-bed reactors in which a non-catalytic gas-solid reaction is taking place.

4.2 Model for the Conversion of Solids

In the following we exclusively consider the case in which solid particles react with fluidizing gas while maintaining its original size because of the formation of inert solid product. The gasification of coal, the roasting of sulphide ores and the reduction of iron ores are a few of the examples. The following stoichiometric equation can be used to represent these reactions.

$$aA(gas) + S(solid) \longrightarrow \text{gaseous or/and solid products} \qquad (1)$$

The proposed calculation method assumes that solids follow the shrinking core model and the overall conversion rate is controlled by chemical reaction step[9]; in the unreacted-core shrinking model the reaction is confirmed at the surface of the core which recedes from the outer surface towards the interior of the particle. As this mechanism is employed to present a working model, when diffusion through the product layer becomes rate controlling, or when other single particle reaction models are used, the conversion versus time expressions must be changed accordingly.

The reaction of a gaseous component by a first order irreversible reaction can be given as

$$-\frac{1}{4\pi r_c^2 a} \cdot \frac{dN_A}{dt} = -\frac{1}{4\pi r_c^2} \cdot \frac{dN_s}{dt} = k_c C_A \qquad (2)$$

where r_c is the radius of unreacted core and k_c is the rate constant for the reaction.

When the reaction is carried out in the bulk phase reactant gas concentration, C_A, the extent of conversion, X_S, of a particle having radius R is given by

$$\frac{t}{\tau} = 1 - \frac{r_c}{R} = 1 - (1 - X_s)^{1/3} \tag{3}$$

where time for complete conversion, τ, is

$$\tau = \frac{\rho_p \, d_p}{2 a \, k_c \, C_{Ao}} \tag{4}$$

When the resistance of chemical reaction step and that of diffusion through the ash layer are comparable, the rate constant, k_c, is replaced by $\bar{k}$ defined by

$$\frac{1}{\bar{k}} = \frac{1}{k_c} + \frac{d_p}{12 \, D_{eA}} \tag{5}$$

Next, let us consider a reactor with a constant feed rate of both solids and gas, the solids being of uniform size and complete mixing. Since the conversion of an individual particle of solids depends on its length of stay in the reactor the mean conversion $\bar{X}_S$, of the exit stream of solids is given by

$$1 - \bar{X}_s = \int_{t=0}^{\tau} (1 - X_s) \, E(t) \, dt \tag{6}$$

where the exit age distribution function for a reactor of complete mixing is

$$E(t) = \frac{1}{\bar{t}} \, e^{-t/\bar{t}} \tag{7}$$

When chemical reaction is the rate controlling step in a shrirking core particle, substitution eqs. (3) and (7) into eq. (6) and subsequent integration yields,

$$1 - \bar{X}_s = 1 - 3\left(\frac{\bar{t}}{\bar{\tau}}\right) + 6\left(\frac{\bar{t}}{\bar{\tau}}\right)^2 - 6\left(\frac{\bar{t}}{\bar{\tau}}\right)^3 \left[1 - \exp\left(-\bar{\tau}/\bar{t}\right)\right] \qquad (8)$$

4.3 Gas and Solid Flows in a Fluidized Bed

A fluidized bed is assumed to be approximately represented by "N" numbers of compartment in series. The height of each compartment is considered to be equal to the size of each bubble at the corresponding bed height[3]. Each compartment is considered to consist of bubble phase and emulsion phase.

Gas flow: Based on the above assumption, the bubble assemblage model for the flow of gas through a fluidized bed has been proposed [3]. Since this model is employed in this paper to describe the gas flow, we first summarize the essentials of this model.

The bubble phase is assumed to consist of spherical clouds. The diameter of bubble and that of cloud are given [1] by

$$\left(\frac{d_c}{d_b}\right)^3 = \frac{u_{br} + 2\,u_{mf}/\varepsilon_{mf}}{u_{br} - u_{mf}/\varepsilon_{mf}} \qquad (9)$$

where $u_{br} = 0.711\,(g \cdot d_b)^{1/2}$.

In the vicinity of the distributor, bubbles are small and rise slower than the gas percolating through the emulsion phase; i.e. $u_{br} < u_{mf}/\varepsilon_{mf}$, in this zone the gas shortcuts only through the rising bubble. On the otherhand, as the velocity of bubble increases, i.e. $u_{br} \geq 5u_{mf}/\varepsilon_{mf}$, the thickness of cloud becomes negligibly small. The maximum stable bubble diameter d_{bt} can be found from [2],

$$d_{bt} = \left(\frac{u_t}{0.71}\right)^2 \cdot \frac{1}{g} \qquad (10)$$

The change of the bubble diameter along the bed height can be approximated [4] by

$$d_b = 1.4\rho_p\, d_p \left(\frac{u_o}{u_{mf}}\right) h + d_o \qquad \text{(c.g.s. unit)} \tag{11}$$

where

d_o = bubble diameter just above the perforated plate distributor

$$= \left[\frac{6\,(u_o - u_{mf})}{\pi\, N_o}\right]^{0.4} g^{0.2}$$

The rising verocity of bubbles is given by

$$u_b = u_o - u_{mf} + [0.711\,(g\, d_b)^{1/2}] \tag{12}$$

The bed expansion ratio is expressed as

$$(L_f - L_{mf})/\, L_{mf} = (u_o - u_{mf})/\left[0.711\,(g\,\bar{d}_b)^{1/2}\right] \tag{13}$$

where $\bar{d}_b$ is an average bubble diameter at level $L_{mf}/2$.

From an arithmetic average of the bubble sizes, the height of i-th compartment can be expressed as

$$\Delta h_i = 2\, d_o\, \frac{(2 + m)^{i-1}}{(2 - m)^{i}} \tag{14}$$

where $m = 1.4\rho_p\, d_p(u_o/u_{mf})$.

The voidage distribution is assumed that up to the bed height corresponding to L_{mf}, ε can be considered uniform while above L_{mf}, ε increases linealy along the bed height, as shown in Fig. A-25.

$$1 - \varepsilon = \frac{L_{mf}}{L_f}\,(1 - \varepsilon_{mf}) \qquad \text{for } h \leq L_{mf} \tag{15a}$$

and

$$1 - \varepsilon = \frac{L_{mf}}{L_f}\,(1 - \varepsilon_{mf}) - \frac{L_{mf}\,(1 - \varepsilon_{mf})\,(h - L_{mf})}{2\, L_f\,(L_f - L_{mf})} \tag{15b}$$

$$\text{for } L_{mf} \leq h \leq L_{mf} + 2\,(L_f - L_{mf})$$

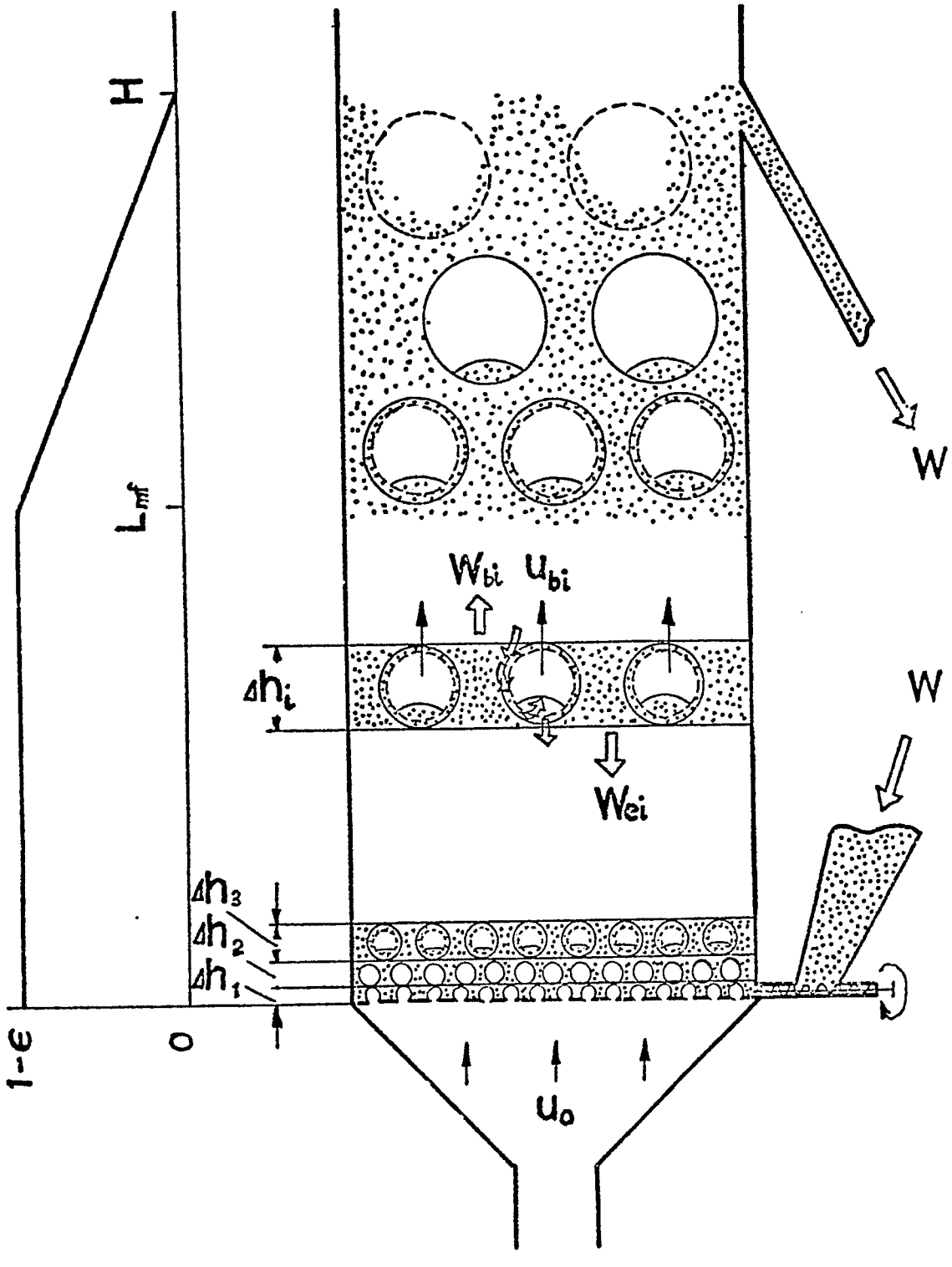

Figure A-25 Main features of solid movement and gas flow as visualized

Therefore, the number of bubbles, n, in the i-th compartment is given by

$$n = \frac{6\ S_t}{\pi\ (\Delta h_i)^2}\ \frac{\varepsilon - \varepsilon_{mf}}{1 - \varepsilon_{mf}} \tag{16}$$

The volume of bubbles, clouds and emulsion in the i-th compartment can be computed, respectively as

$$V_{bi} = n \cdot \frac{\pi}{6}\ (\Delta h_i)^3 \tag{17}$$

$$V_{ci} = n \cdot \frac{\pi}{6}\ (\Delta h_i)^3 \left(\frac{3\ u_{mf}/\varepsilon_{mf}}{u_{bri} - u_{mf}/\varepsilon_{mf}} \right) \tag{18}$$

$$V_{ei} = S_t\ \Delta h_i - V_{bi} - V_{ci} \tag{19}$$

The overall interchange coefficient of the gas between the bubble and the emulsion phase based on a unit volume of gas bubbles, may be approximated by the following experimental relation[5].

$$(K_{be})_b = 11/d_b \tag{20}$$

The velocity of gas in the emulsion phase is assumed to be negligibly small for large values of u_o/u_{mf}.

Solid movement: First, let us define the distribution of solids between the two regions of the bed by

$$\gamma_c = \frac{\text{volume of solids dispersed in clouds and wake}}{\text{volume of bubbles}}$$

$$\gamma_e = \frac{\text{volume of solids in emulsion}}{\text{volume of bubbles}} \tag{21}$$

Values of γ_c are estimated from eq. (18) as,

$$\gamma_c = (1 - \varepsilon_{mf}) \left(\frac{3\, u_{mf}/\varepsilon_{mf}}{u_{br} - u_{mf}/\varepsilon_{mf}} + \alpha \right) \tag{22}$$

where α = volume of wake/ volume of bubble, may be estimated from experimental results; such as those of Rowe and Partridge[8]

As solids are carried upward as a part of wake of the rising bubbles from the i-th compartment to the (i+1)-th compartment, this sets up a circulation in the bed with downward movement of solids in the emulsion phase from the (i+1)-th compartment to the i-th compartment. We first consider the case in which the solids are fed to the bottom of the bed at a constant volumetric flow rate, W, (cocurrent feed), as shown in Fig.A-25 Hence the solids move upward at a net average flow rate W. Thus, the total upward flow rate W_b from the i-th compartment to the (i+1)-th compartment is given by

$$W_{bi} = \left(\frac{W}{S_t} + \frac{\alpha\, u_{bi} S_{bi}}{S_{bi}} \right) S_{bi} \tag{23}$$

where $S_{bi} = n \cdot \frac{\pi}{4} (\Delta h_i)^2$.

The total downward flow rate W_e from the (i+1)-th compartment to the i-th compartment is given by

$$W_{e(i+1)} = \left(\frac{\alpha\, u_{bi} \cdot S_{bi}}{S_t - S_{bi}} - \frac{W}{S_t} \right) (S_t - S_{bi}) \tag{24}$$

For the case in which the solids are fed at the top of the bed and withdrawn from the bottom (countercurrent feed), W must be replaced by -W in the above equations. Since in fluidized-bed reactors, solids are usually fed slowly to assure near complete conversion, the value of W is relatively small. Even for the cocurrent flow, the downward flow of solids must be considered as given in eq. (24). The interchange coefficient of solids between bubble phase and emulsion phase is given[11] by

$$(K_{be})_{bs} = 3 \frac{(1 - \varepsilon_{mf})\, u_{mf}\, u_b}{\varepsilon_{mf} \cdot u_{br} \cdot d_b} \qquad (25)$$

Figure A-26 shows a schematic diagram of the i-th compartment.

4.4 Noncatalytic Gas-Solid Reactions in Fluidized Beds

Let us define the rate of first-order irreversible reaction, based on unit volume of particles, as

$$- \frac{1}{a\, V_s} \cdot \frac{dN_A}{dt} = K_r\, C_A \qquad (26)$$

where $K_r = 4\, r_c k_c/(\pi/6)d_p$. K_r is not a constant at a given temperature but is dependent on the conversion level of solids.

Hence, the material balance for gaseous reactant around the i-th compartment becomes

$$U\, C_{gb(i-1)} - U\, C_{gbi} = (K_r)_{bi}\, V_{bi}\, C_{gbi} \qquad (27a)$$

$$= (K_{be})_{bi}\, V_{bi}\, (C_{gbi} - C_{gei}) + \gamma_{ci}\, V_{bi}\, K_{ri}\, C_{gbi} \qquad (27b)$$

$$(K_{be})_{bi}\, V_{bi}\, (C_{gbi} - C_{gei}) = \gamma_{ei}\, V_{bi}\, K_{ri}\, C_{gei} \qquad (27c)$$

Therefore

$$U\, C_{gb(i-1)} = (U + (K_r)_{bi}\, V_{bi})\, C_{gbi} \qquad (28)$$

where

$$(K_r)_{bi} = (K_{be})_{bi} + \gamma_{ci}\, K_{ri} - \frac{(K_{be})^2_{bi}}{(K_{be})_{bi} + \gamma_{ei}\, K_{ri}} \qquad (29)$$

and

$$C_{gei} = \frac{(K_{be})_{bi}}{(K_{be})_{bi} + \gamma_{ei}\, K_{ri}}\, C_{gbi} \qquad (30)$$

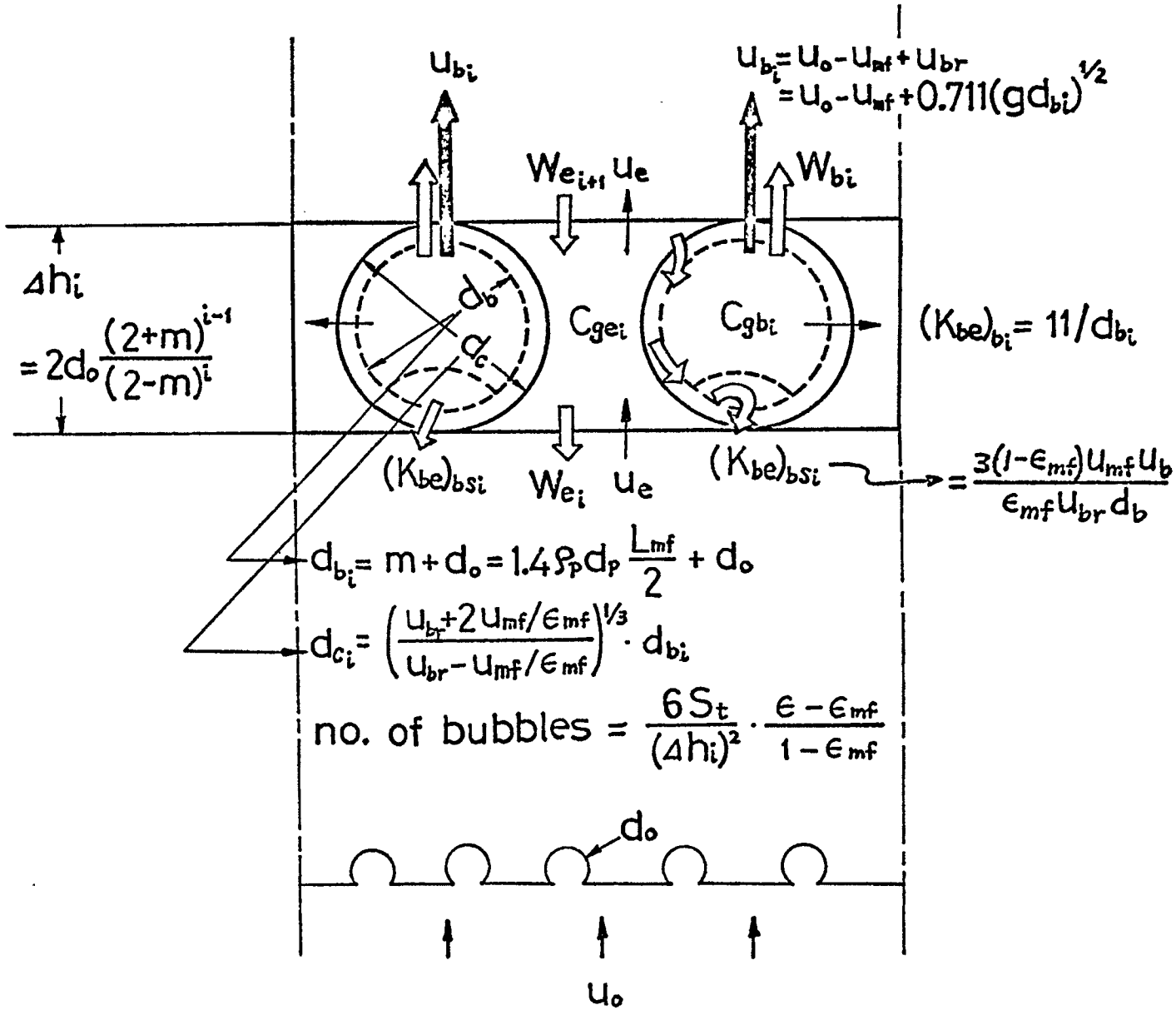

Figure A-26 Schematic diagram of i-th compartment in the bubble assemblage model for fluidized bed

In the fluidized bed, solids react in the bubble phase with the gas of concentration, C_{gbi}, and react in the emulsion phaseswith that of C_{gei}. These solids also undergo interchange between both phase according to eq. (25). Therefore equations similar to eq. (27) can be written for the conversion of solids. If a simplifying assumption that the solids mixing is complete in each compartment is made, the time average concentration of gas in the i-th compartment becomes

$$\bar{C}_{gi} = \frac{\gamma_{ci}}{\gamma_{ci} + \gamma_{ei}} C_{gbi} + \frac{\gamma_{ei}}{\gamma_{ci} + \gamma_{ei}} C_{gei} \qquad (31)$$

$\bar{C}_{gi}$ from eq. (31) is used to calculate the time required for complete conversion of solid reactant, τ in each compartment.

The mean residense time of particles in the i-th compartment is

$$\bar{t}_i = (\alpha V_{bi} + V_{ci} + V_{ei})(1 - \epsilon_{mf})/W \qquad (32)$$

By using eqs. (4), (31) and (32) the mean conversion, $\bar{X}_s$, of the exit stream of solids in the i-th compartment is calculated from eq. (8).

Finally, in each compartment a material balance for both the solids and gas streams must be satisfied.

4.5 Calculation Procedure

First let us consider the case for cocurrent feed of solids. The following operating conditions are given: superficial gas velocity, particle density, terminal velocity of particle, incipient bed height, cross sectional area of bed, inlet gas and solid concentration, feed rate of solid and reaction rate constant.

Calculation is accomplished by following the steps listed below;

(a) Calculate the values of bed characteristics, L_f, Δh, V_b, V_c, V_e, $(K_{be})_b$, γ_c, γ_e, W_b and W_e, as indicated in the previous section.

(b) Assume the concentration of the final exit gas stream, C_{gbN}.

Calculation of the (N)-th compartment:

(c) Select values of K_r.

(d) For each value of K_r, calculate C_{geN} by eq. (30) and then $\bar{C}_{gN}$ by eq. (31).

(e) Calculate $\bar{\tau}$ and $\bar{t}$ by eq. (4) and eq. (32), respectively and obtain $\bar{X}_{sN}$ by eq. (8).

(f) From the overall material balance over the (N-1)-th compartment to the first compartment, as shown in Fig. A-27 calculate the value of $C_{s(N-1)}$.

$$\frac{1}{a} U (C_{go} - C_{gb(N-1)}) = W C_{so} + W_{eN} C_{sN} - W_{b(N-1)} C_{s(N-1)}$$

(g) The material balance for both streams in the N-th compartment is

$$\frac{1}{a} U C_{gb(N-1)} \cdot X_{gN} = U C_{gb(N-1)} \cdot \frac{C_{gb(N-1)} - C_{gbN}}{a C_{gb(N-1)}} = W_{b(N-1)} \cdot C_{s(N-1)} \bar{X}_{sN} \quad (33)$$

(h) Find the correct value of K_r by repeating the calculation until eq. (33) is satisfied. The value of K_r thus obtained is the desired value from which $C_{gb(N-1)}$, C_{sN} and $C_{s(N-1)}$ can be found based on the initially assumed value of C_{gbN}.

Calculation of the (N-1)-th compartment:

(i) Select values of K_r.

(j) For each value of K_r repeat the same procedures as in steps (c) to (e) by using the values of $C_{gb(N-1)}$, C_{sN} and $C_{s(N-1)}$ obtained in step (h).

(k) By making the overall material balance over the compartments from (N-2)-th

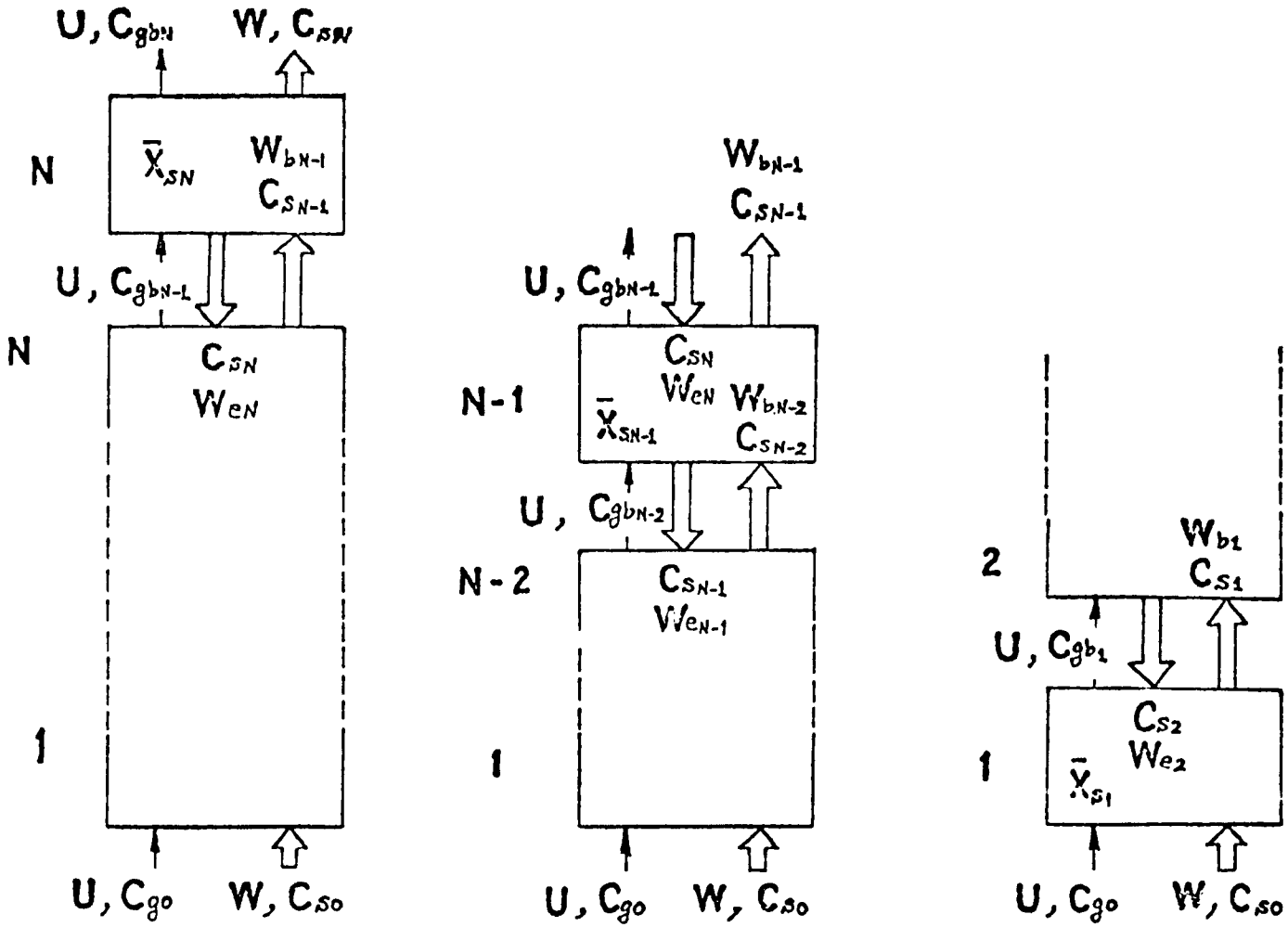

(a) cocurrent feed of solid

Figure A-27 Illustrative computational procedures

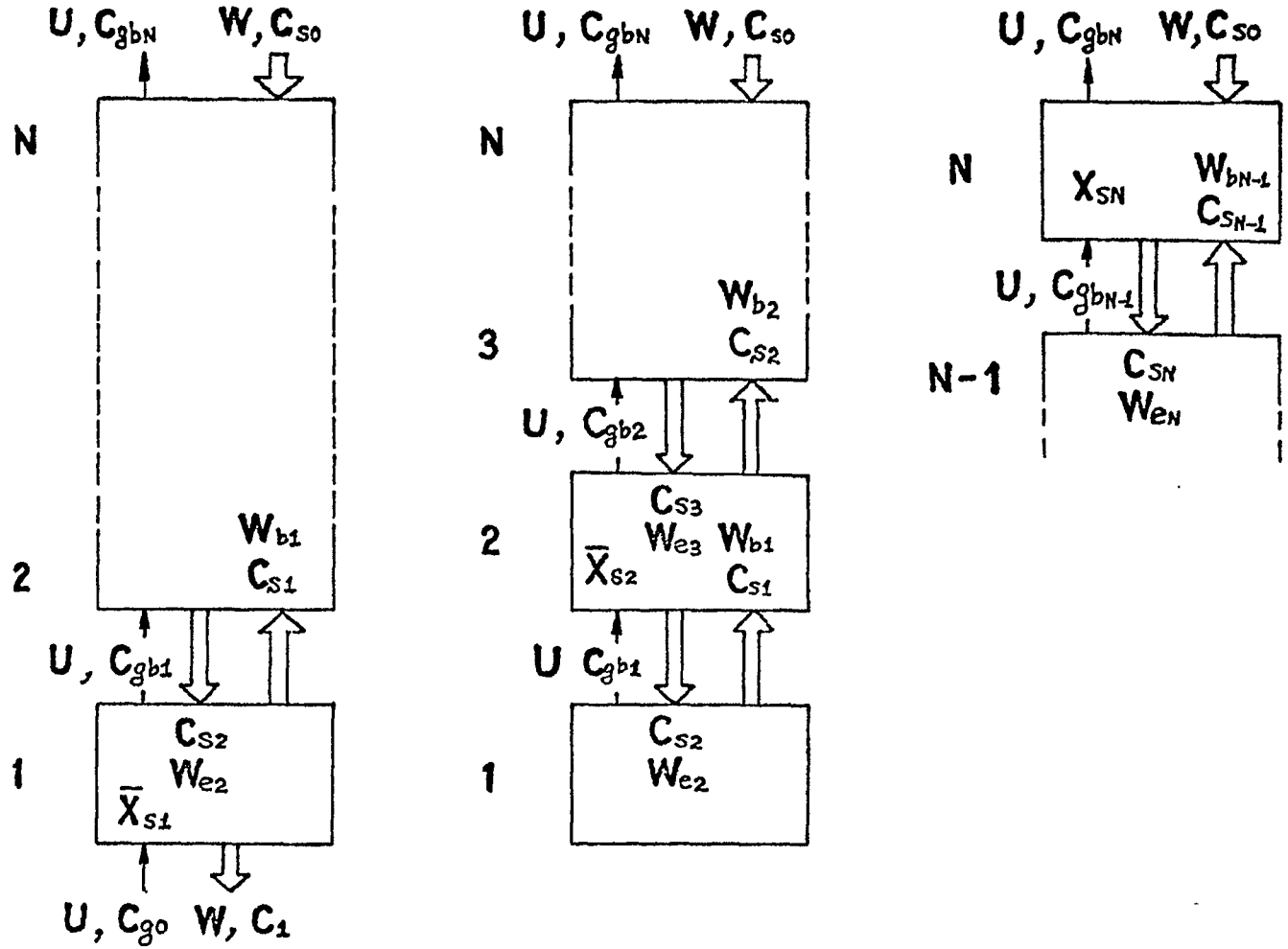

(b) countercurrent feed of solid

Figure A-27 Illustrative computational procedures

to the first, calculate $C_{s(N-2)}$ by the following equation.

$$\frac{1}{a} U (C_{go} - C_{g(N-2)}) = W \cdot C_{so} + W_{e(N-1)} \cdot C_{s(N-1)} - W_{b(N-2)} \cdot C_{s(N-2)}$$

(l) The material balance for both gas and solid streams in the (N-1)-th compartment is

$$\frac{1}{a} U C_{gb(N-2)} \cdot X_{g(N-1)} = U C_{gb(N-2)} \frac{C_{gb(N-2)} - C_{gb(N-1)}}{a C_{gb(N-2)}} = (W_{b(N-2)} \cdot C_{s(N-2)} + W_{eN} C_{sN}) \bar{X}_{sN} \quad (34)$$

(m) Find K_r which satisfies eq. (34). Hence, the values of $C_{gb(N-2)}$ and $C_{s(N-2)}$ can be obtained.

(n) Repeat the same procedures until the second compartment is reached.

Calculation of the first compartment:

(o) Calculate K_r from eq. (28) by using the value C_{go} and C_{gb1} obtained from step (n).

(p) Calculate C_{ge1}, C_{g1} and $\bar{X}_{s1}$, by using K_r obtained in step (o).

(q) Check the material balance in the first compartment.

$$\frac{1}{a} U C_{go} \bar{X}_{g1} = U C_{go} \frac{C_{go} - C_{g1}}{a C_{go}} = (W C_{so} + W_{e2} C_{s2}) \bar{X}_{s1} \quad (35)$$

(r) If eq. (35) is satisfied, the value of C_{gbN} assumed in step (b) is the correct exit gas concentration and the corresponding value of C_{sN} is also the correct exit solid concentration. If eq. (35) does not hold, then the value of C_{gbN} in step (b) is changed and calculations in all steps repeated until the material balance of eq. (35) is satisfied.

An illustrative computational procedure is shown in Fig. A-27(a) and a computor logic diagram corresponding to these steps is shown in Fig. A-28 .

In the case of countercurrent feed of solids, similar steps but in reverse order are followed from the bottom to the top of the reactor. The computational procedure is illustrated in Fig. A-27(b).

The procedure for estimation of C_{gbN} is given below:

First, calculate the theoretical exit gas concentration based on the stoichiometric eq. (1). Use this value as the starting value of C_{gbN}, increase C_{gbN} incrementally until the material balance of eq. (35) is satisfied. By this method the desired condition can be found with a relative ease.

4.6 Results and Discussions

Since most of the experimental data were obtained using porous plates, the bubble diameter d_o just above the distributor is very difficult to estimate. In the analyses of the catalytic reactions, the effect of the height of the first compartment on overall conversion has been examined [3] and the assumption of $\Delta h_1 = 1.0$ cm is found to be reasonable so long as the particle size is comparatively small. Therefore, in the following calculations this assumption is also employed.

In order to demonstrate the validity of the proposed method, the experimental results of the roasting of zinc sulphide obtained by Yagi et al. [10] are analyzed. The essential operating conditions of this experiment are listed in Table A-10(a). The results of calculation are then compared with the actual experimental conversions. The degree of agreement is shown in Table A-10(a). In the book by Kunii and Levenspiel[6] an example was given to show the calculation method based on the bubbling bed model. The operating conditions of the example are listed in Table A-10(b). This example has been recalculated by

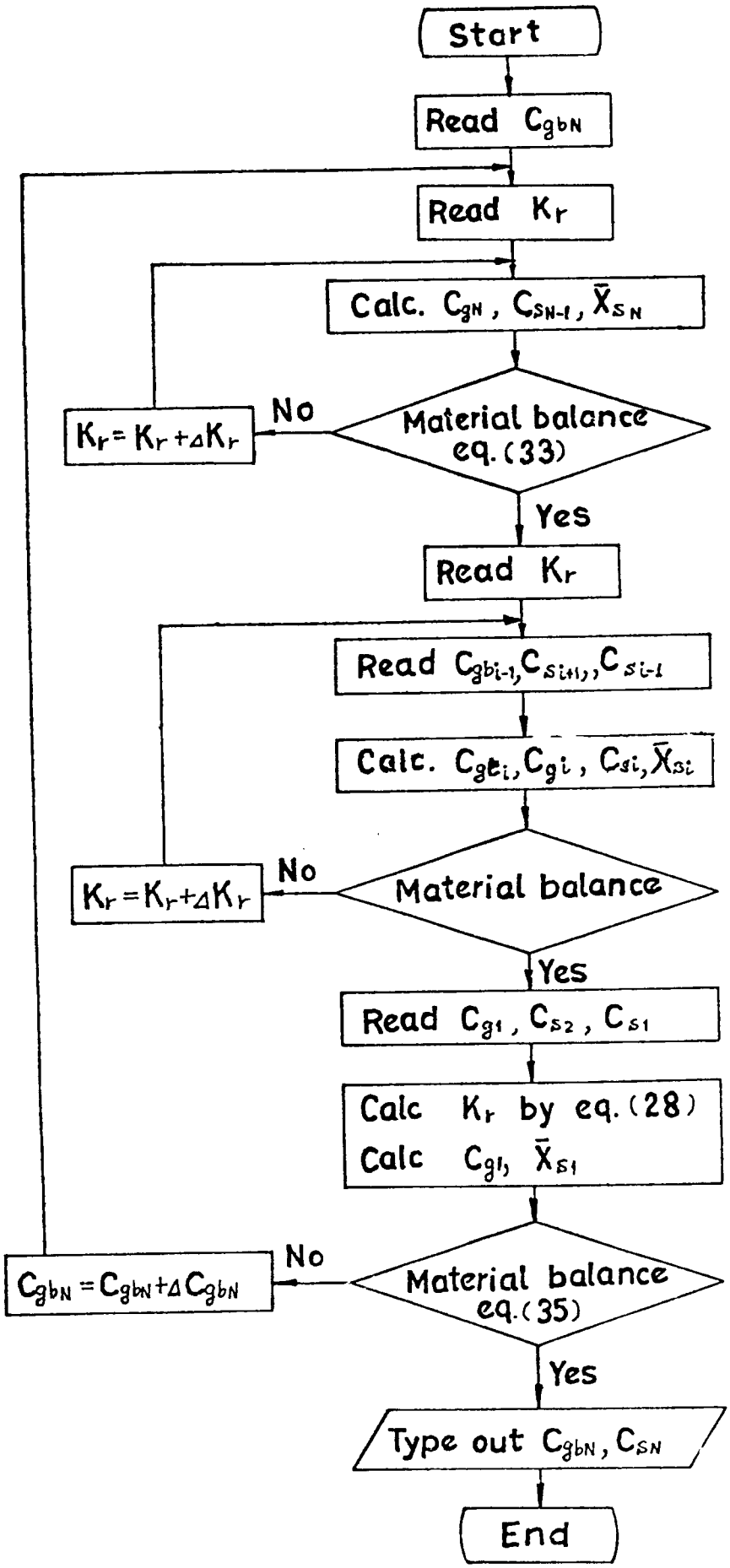

Figure A-28 Logic diagram for computor simulation

Table A-10 Results of Calculation and Pertinent Experimental Data

a) Experiments conducted by Yagi et. al. (10)

Roasting of ZnS: $3O_2 + 2ZnS \longrightarrow 2O_2 + 2ZnO$

d_t = 5.0 cm, cocurrent feed of solids, ρ_p = 6.0 and 7.14 g/cm^3

d_p mm	Bed temp. °C	W cm^3/s	*u_o cm/s	L_{mf} cm	k_c cm/s	*$C_{go} \times 10^{-6}$ g-mol/cm^3	C_{so} g-mol/cm^3	Conversion of solid	Calculated Conversion	
									Solid $\bar{X}_s$	gas X_g
0.11	700	0.00503	20.0	3.8	2.0	2.18	0.0356	0.904	0.998	0.306
0.089	700	0.00233	19.4	3.0	0.1	2.24	0.0573	0.887	0.900	0.188
0.089	750	0.00475	19.4	3.0	0.3	2.50	0.0573	0.910	0.930	0.402
0.089	800	0.00215	22.5	3.0	0.6	2.38	0.0548	0.974	0.964	0.162
0.11	900	0.00755	20.0	4.1	2.0	2.18	0.0356	0.972	0.985	0.451
0.089	750	0.00701	19.4	3.0	0.3	2.50	0.0573	0.869	0.869	0.552
0.089	800	0.00468	19.4	3.0	0.6	2.38	0.0573	0.935	0.950	0.423

* based on the bed temperature

Table A-10 Calculation Results

b) Examples shown in the book by Kunii and Levenspiel (6)

Roasting of ZnS: d_t = 6.7 m, u_o = 60 cm/s, bed temperature 900 °C

d_p = 0.02 cm, ρ_p = 4.13 g/cm^3, ε_{mf} = 0.50, α = 0.1, L_{mf} = 110 cm,

D_{eA} = 0.08 cm^2/s, k_c = 2 cm/s, C_{go} = 2.18 x 10^{-6} g-mol/cm^3,

C_{so} = 0.0424 g-mol/cm^3

Solid feed rate, cm^3/s	Cocurrent feed		Countercurrent feed	
	conversion		conversion	
	gas	solid	gas	solid
484.0	0.664	0.995	0.667	0.999
605.5	0.823	0.987	0.832	0.997
726.0	0.978	0.978	0.988	0.988

the method discussed in this paper. Calculation has been accomplished for the cases of both cocurrent feed and countercurrent feed of solids, the results are shown in Table A-10(b). The concentration profiles of gas and solid for the case of feed rate 726 cm^3/sec in this example, are shown in Fig. A-29. The mean concentration of gas $\bar{C}_g$ has been calculated by the following equation.

$$\bar{C}_g = \frac{L_f - L_{mf}}{L_{mf}} C_{gb} + \frac{L_{mf}}{L_f} C_{ge} \qquad (36)$$

As is seen from Fig. C28concentration changes in the vicinity of feed section are quite remarkable, especially in solids. In the numerical calculation, the interchange of solids between the bubble and the emulsion phase is assumed to be infinite for simplicity. However, the procedure can be extended to include a finite interchange coefficient. This problem will be discussed in more detail in another paper dealing with the effect of solid mixing in fluidized bed reactor.

4.7 Conclusion

This section presents a model for noncatalytic solid-gas reactions taking place in a fluidized bed and a simulation-method for determing the extent of chemical conversions for both reacting gas and solids in continuous flow systems(for both gas and solid). Taking a zinc blende roaster as an example, the adequacy of the proposed procedure is demonstrated.

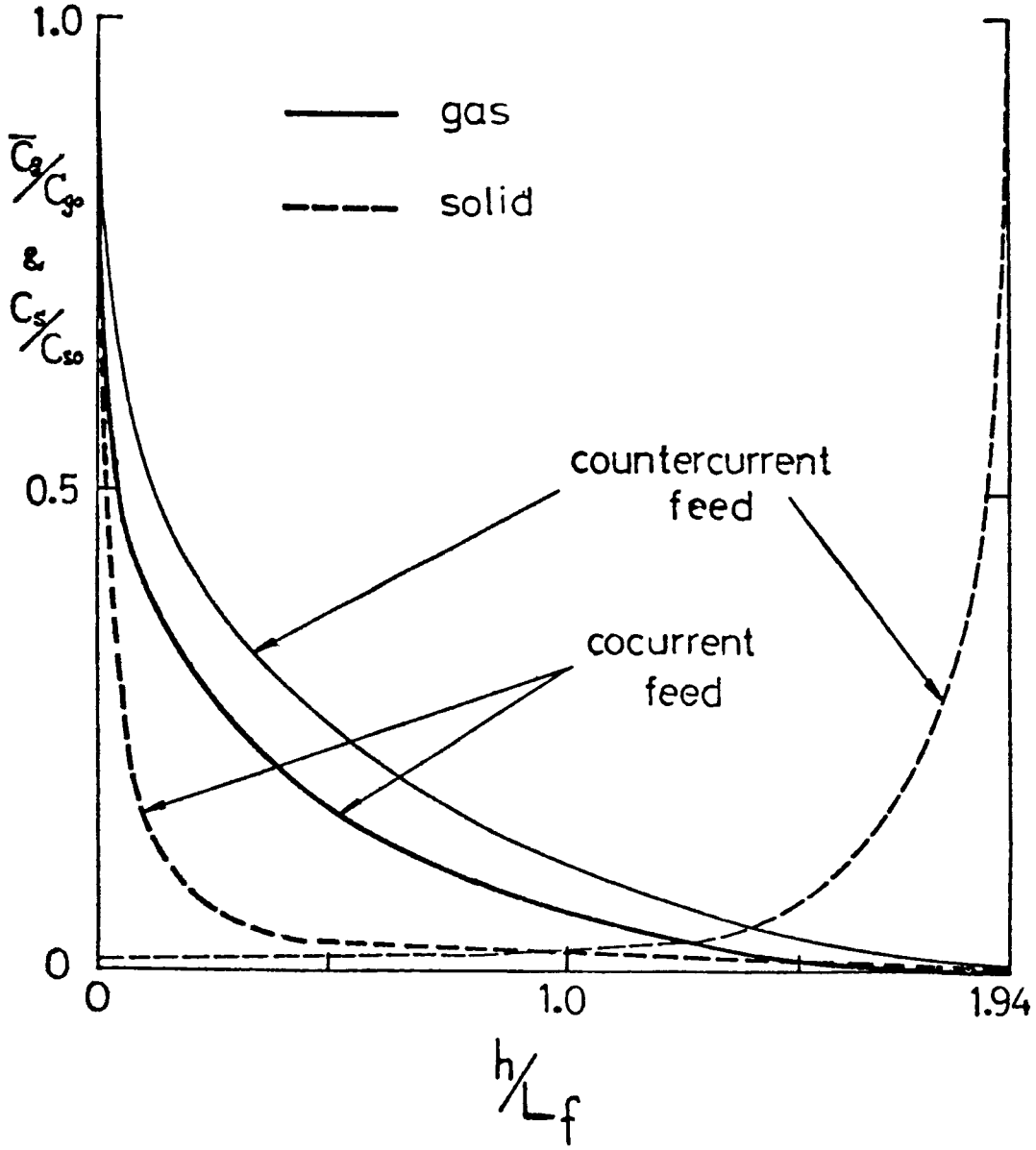

Figure A-29 Concentration profiles of gas and solid

Notation

a = stoichiometric coefficient in eq. (1)

$\bar{C}_g$ = time average concentration of gas which a particle encounters, g-mol/cm^3

C_{gbN} = concentration of gas (or bubble gas) leaving the bed, g-mol/cm^3

C_{gb} = concentration of gas in bubble, g-mol/cm^3

C_{ge} = concentration of gas in emulsion, g-mol/cm^3

C_{go} = concentration of gas (or bubble gas) in the inlet gas stream, g-mol/cm^3

C_s = concentration of solid, g-mol/cm^3

C_{so} = concentration of solid in the inlet stream, g-mol/cm^3

D_{eA} = diffusion coefficient through layer of solid product or ash, cm^2/s

d_b = bubble diameter, cm

d_{bt} = maximum stable bubble diameter, cm

d_c = diameter of cloud, cm

d_o = bubble diameter just above the distributor, cm

d_p = particle diameter, cm

d_t = bed diameter, cm

g = acceleration of gravity, cm^2/s

h = distance from the distributor, cm

Δh_i = height of the i-th compartment, cm

$(K_{be})_b$ = interchange coefficient of gas between bubble and emulsion, s^{-1}

$(K_{be})_{bs}$ = interchange coefficient of solid between bubble and emulsion based on volume of a bubble, s^{-1}

K_r = reaction rate constant defined in eq. (26), s^{-1}

$(K_r)_b$ = overall rate coefficient for reaction, s^{-1}

$\bar{k}$ = overall rate constant, cm/s

k_c = rate constant for surface reaction defined in eq. (2), cm/s

L_f = height of fluidized bed, cm

L_{mf} = bed height at minimum fluidizing conditions, cm

N_A, N_B = gramme moles of A and B

N_o = number of holes per unit surface area of distributor, cm^{-2}

n = number of bubbles in i-th compartment

R = radius of a particle, cm

r_c = radius of a shrinking core, cm

S_t = cross sectional area of the bed, cm^2

S_{bi} = cross sectional area of bubble phase in the i-th compartment, cm^2

$\bar{t}$ = mean residence time of particles, s

U = volumetric gas flow rate based on empty tube, cm^3/s

u_b = velocity of rising bubble, cm/s

u_{br} = velocity of bubble with respect to the emulsion ahead of it, cm/s

u_{mf} = minimum fluidizing velocity, cm/s

u_o = superficial gas velocity, cm/s

u_t = terminal velocity of fluidized particles, cm/s

V_{bi} = volume of bubble phase in the i-th compartment, cm^3

V_{ci} = volume of cloud region in the i-th compartment, cm^3

V_{ei} = volume of emulsion phase in the i-th compartment, cm^3

V_s = volume of solid particles in fluidized bed, cm^3

W = volumetric feed and outflow rate of solids, cm^3/s

W_{bi} = volumetric upward flow rate from the i-th compartment, cm^3/s

W_{ei} = volumetric downward flow rate from the i-th compartment, cm^3/s

X_g = fractional conversion of reactant gas

$\bar{X}_s$ = mean fractional conversion of solid

Greek Letters

γ_c, γ_e = volume fraction of solid as defined by eq. (21)

ε = void fraction in a bed as a whole

ε_{mf} = void fraction in a bed at minimum fluidization

ρ_p = density of solid, g/cm^3

τ = time for complete conversion of a single particle, s

1. Davidson, J. F., Trans. Instn. Chem. Engrs., 39, 230 (1961)

2. Davidson, J. F., "Fluidized Particles", Cambridge Univ. Press, New York (1963)

3. Kato, K. and C. Y. Wen, Chem. Eng. Sci., 24, 1351 (1969)

4. Kobayashi, H., F. Arai and T. Shiba, Kagaku Kogaku (Chem. Eng. Japan), 29, 858 (1965)

5. Kobayashi, H., F. Arai and T. Sunagawa, Kagaku Kogaku (Chem. Eng. Japan), 31, 239 (1967)

6. Kunii, D. and O. Levenspiel, "Fluidization Engineering", John Wiley, New York (1969)

7. Levenspiel, O., "Chemical Reaction Engineering", John Wiley, New York (1962)

8. Rowe, P. N. and B. A. Partridge, Trans. Instn. Chem. Engrs., 43, T55 (1964)

9. Wen, C. Y., I. and E.C. Monthly, 60, 34 (1968)

10. Yagi, S., D. Kunii, T. Nagano and H. Mineta, J. Chem. Soc. (Japan) Ind. Chem. Eng. Sec., 56, 213 (1953)

11. Yoshida, K. and D. Kunii, J. of Chem. Eng. Japan, 1, 11 (1969)